UNIVERSITÉ DE MONTRÉAL

CHEMICAL LOOPING GASIFICATION OF BIOMASS

MILAD AGHABARARNEJAD
DÉPARTEMENT DE GÉNIE CHIMIQUE
ÉCOLE POLYTECHNIQUE DE MONTRÉAL

THÈSE PRÉSENTÉE EN VUE DE L'OBTENTION
DU DIPLÔME DE PHILOSOPHIÆ DOCTOR
(GÉNIE CHIMIQUE)
AOÛT 2014

UNIVERSITÉ DE MONTRÉAL

ÉCOLE POLYTECHNIQUE DE MONTRÉAL

Cette thèse intitulée :

CHEMICAL LOOPING GASIFICATION OF BIOMASS

présentée par : AGHABARARNEJAD Milad

en vue de l'obtention du diplôme de : Philosophiæ Doctor

a été dûment acceptée par le jury d'examen constitué de :

M. STUART Paul, Ph.D., président

M. CHAOUKI Jamal, Ph.D., membre et directeur de recherche

M. PATIENCE Gregory S., Ph.D., membre et codirecteur de recherche

M. LEGROS Robert, Ph.D., membre

Mme ELLIS Naoko, Ph.D., membre

DEDICATION

"To my beloved parents and brothers."

ACKNOWLEDGMENTS

First of all, I would like to express my deep and sincere gratitude to my supervisor, Prof. Jamal Chaouki. His wide knowledge and his logical way of thinking, encouragements, advices, and guidance have been great value for me.

I am deeply grateful to my co-supervisor, Prof. Gregory S. Patience, for his detailed and constructive comments, and for his important support, encouragement, advices throughout this work.

Special thanks to the technical staff of the chemical engineering department, especially Mr. Robert Delisle, Mr. Yazid Belkhir, Mr. Jean Huard and Ms. Martine Lamarche.

I would like to extend my thanks to all my colleagues in Prof. Chaouki group for sharing knowledge and ideas. I am thankful to Ms. Odile Vekemans for translation a part of this thesis to French. Many thanks also to all my friends Mahsa, Majid, Amin, Jaber, Hamed, Pierre-Phillipe, Abbas, Alireza ... for all the unforgettable moments which I had with them.

My special gratitude is due to my father, mother and brothers and their families for their lovely support and encouragement.

RÉSUMÉ

La gazéification à la vapeur de la biomasse est une réaction endothermique dont l'énergie nécessaire peut être fournie soit par une source externe, soit par combustion d'une partie de la biomasse par de l'oxygène. Parmi les différentes sources d'oxygène on trouve l'air, qui entraine la dilution du gaz de synthèse dans l'azote, et l'oxygène pur, qui augmente fortement les coûts totaux de production. Une alternative à l'air et à l'oxygène pur est le procédé de boucle chimique. Dans ledit procédé, l'oxygène est séparé de l'air à haute température à l'aide d'oxydes métalliques. Dans un premier réacteur, appelé réacteur d'oxydation, le métal réduit est oxydé par l'air. Ce métal oxydé est ensuite transféré dans un second réacteur, appelé gazogène, où il libère l'oxygène qui permet la combustion partielle de la biomasse. Ce métal une fois réduit est recyclé vers le réacteur d'oxydation où il est régénéré. Afin d'augmenter la stabilité thermique et mécanique de l'oxyde métallique, il est supporté par un matériau à haute résistance et cette combinaison est appelée transporteur d'oxygène.

Comme dit précédemment, les transporteurs d'oxygène sont capables d'absorber l'oxygène de l'air et ensuite de le désorber dans le gazogène. En se basant sur des données thermodynamiques, les oxydes de cuivre, de manganèse et de cobalt, ont été identifiés comme ayant les capacités les plus élevées de libération de l'oxygène parmi les différents transporteurs d'oxygène potentiels. Ces derniers ont été déposés sur de l'alumine par imprégnation jusqu'à humidité naissante ou "Incipient Wetness Impregnation". Des analyses thermogravimétriques ont permis d'évaluer la perte de poids du couple CuO-Cu_2O à 10 % alors qu'elle n'était que de 7 % pour le couple Co_3O_4-CoO et 3 % pour le couple Mn_2O_3-Mn_3O_4. Néanmoins, la température optimale d'opération de CuO était de 950 °C, soit 100 °C de plus que celle des deux autres transporteurs. Un modèle modifié de croissance de noyau a été utilisé pour caractériser la perte et le gain de masse pendant les cycles d'oxydo-réduction de cobalt. A 875 °C, le taux de réduction est 3 fois supérieur à celui à 825 °C, alors que la vitesse d'oxydation diminue de plus de 10 fois. D'autre part, la surface spécifique du transporteur CuO diminue de 70 % alors qu'elle ne diminue que de 30 % et de 60 % pour les

transporteurs fait de Co_3O_4 et de Mn_2O_3 respectivement. Le cobalt a donc moins tendance à fritter à haute température par rapport au cuivre ou au manganèse, et ce couplé à une bonne capacité de transport d'oxygène et un bon taux d'oxydation-réduction. Par conséquent, en dépit de son coût élevé et de sa toxicité, l'oxyde de cobalt peut être considéré comme un transporteur d'oxygène potentiel pour la gazéification de combustibles solides.

Dans la seconde partie de la thèse, de la biomasse a été gazéifiée dans un lit fluidisé a bulles avec de la vapeur et de l'oxygène. Ce dernier était fourni par la réduction de Co_3O_4 en CoO. L'oxyde de cobalt réduit (CoO) a ensuite été régénéré par substitution de la vapeur par de l'air et ce lors de l'interruption de l'alimentation de la biomasse. En modifiant la température de 825 °C à 875 °C, le rendement de H_2 a augmenté jusqu'à 60 %. En modifiant l'injection de vapeur de 0 à 18 %, le rendement de H_2 a augmenté de 4 fois. En remplaçant 50 % du sable qui constituait le lit avec du Co_3O_4, le rendement de CO a augmenté jusqu'à 45 % et le rapport H_2 :CO a été diminué. Afin de modéliser le réacteur, un modèle à deux phases pour le lit dense et un modèle d'écoulement piston pour la zone de projection ou "freeboard" ont été utilisés. Une des hypothèses adoptées dans ce modèle est que les solides sont bien mélangés. Lors de l'augmentation de température de l'ambiance à 850 °C, le coefficient de dispersion axiale est augmenté de 0.09 à 0.12 m^2/s. De plus, la variation de la composition du gaz dans la direction radiale est négligeable. Ce modèle hydrodynamique couplé à un modèle cinétique disponible dans la littérature caractérise adéquatement la composition des gaz à la sortie du réacteur.

Dans la partie finale de cette thèse, un système de gazéification conventionnel (CG) et un système de gazéification en boucle chimique (CLG) pour le traitement de 86 t/j de biomasse ont été simulés avec Aspen Plus et leurs coûts d'exploitation et de capital ont été comparés. A l'exception de la configuration du réacteur, ces deux systèmes sont identiques. Le réacteur CG est composé d'un lit fluidisé a bulles (ID = 1.8 m, et H = 6.6 m) qui sert de gazogène, dont le lit est composé de sable, et l'oxygène est fourni par l'intermédiaire d'une unité de modulation de pression d'adsorption. Le CLG, quant à lui, se compose d'un gazogène à lit fluidisé dense (ID = 1.8 m, et H = 6.6 m et) travaillant en parallèle avec un réacteur d'oxydation à lit fluidisé rapide (ID = 1 m, et H = 10 m).

Un débit de Co_3O_4(8 %)/Al_2O_3 de 44.6 kg /s passe du gazogène au réacteur d'oxydation, et permet de fournir l'oxygène nécessaire à la gazéification. L'investissement total en capital (ITC) des unités CG et CLG sont estimées à 6.3 et $9.7M respectivement. Cependant, les coûts de production annuels du CLG sont de $0.58M de moins que la CG, permettant de rembourser la différence en capital du TCI en moins de 6 ans.

ABSTRACT

The steam gasification of biomass is endothermic. The energy can be supplied either by an external source or by combusting a part of biomass feed with oxygen. Air dilutes the produced syngas with nitrogen; while, pure oxygen increases the total production cost. Besides air and pure oxygen, the chemical looping process is an alternative to provide the required oxygen. Using the chemical looping system, the produced syngas has a higher calorific value compared to a conventional biomass gasification process with air. The oxygen is separated from air at high temperature using metallic oxides. The reduced metal is oxidized with air and transferred to the reducer where it releases oxygen. The reduced metal oxide is recycled to the oxidizer for regeneration, and the released oxygen in the reducer is available in the gaseous form to combust or gasify the biomass. To increase the thermal and mechanical stability of the metal oxide, it is supported with a high strength material, and in combination is called an oxygen carrier.

Oxygen carriers for biomass gasification are capable of absorbing oxygen from air and desorbing it in the gasifier. Based on thermodynamic equilibrium, copper, manganese and cobalt oxides have the highest oxygen release capacities among the different oxygen carriers. These oxygen carriers were deposited on alumina via incipient wetness impregnation. The weight loss of the CuO-Cu_2O carrier, as measured in a thermo-gravimetric analyzer, was 10 %, while it was 7 %, for the Co_3O_4-CoO couple, and only 3 % for the Mn_2O_3-Mn_3O_4 couple. The optimum operating temperature for the CuO oxygen carrier was 100 °C higher compared to the other two at 950 °C. A modified nuclei growth model (MNG) characterizes the weight loss/gain during the reduction-oxidation cycles. The reduction rate is 3 times higher at 875 °C compared to 825 °C, while, the oxidation rate decreases more than 10 times. The CuO carrier surface area decreased by 70 %, while it was 30 % and 60 % in the Co_3O_4 and Mn_2O_3 carriers, respectively. Cobalt has a lower tendency to sinter at high temperature compared to either copper or manganese and has a higher oxygen transport capacity and oxidation-reduction rates. Therefore, despite its higher cost and toxicity it might be considered as a potential oxygen carrier especially for solid fuel gasification.

As the second part of the thesis, biomass was gasified in a bubbling fluidized bed with steam and oxygen. The oxygen was supplied by reducing Co_3O_4 to CoO. The reduced cobalt oxide (CoO) was regenerated by switching the fluidizing gas to air. This technology known as chemical looping, is to combust or gasify fuels. The effluent gas is free of nitrogen and has a higher calorific value compared to gasification with air. From 825 to 875 °C, H_2 yield increased up to 60 %. From 0 to 18 % of steam, H_2 yield increased 4 times. Substituting 50 % of the sand as bed material with Co_3O_4, increased the CO yield up to 45 %, while lowering the H_2:CO ratio. A two phase model for the dense bed and a plug flow model for the freeboard region were used for reactor modeling. The solids were assumed to be well mixed. From ambient to 850 °C, the axial dispersion coefficient increased from 0.09 to 0.12 m^2/s. Furthermore, the difference between the gas composition in the radial direction was negligible. The presented hydrodynamic model together with the kinetic expression from the literature characterized the transient gas compositions at the reactor outlet very well.

In the final stage of this thesis, a conventional gasification (CG) system and a chemical looping gasification (CLG) system to treat 86 t/d biomass were simulated with Aspen Plus and the operating and capital cost of them were compared. Conventional gasification (CG) systems use air as an oxygen source. Besides air, the chemical looping process is an alternative method to provide the system with the required oxygen. The syngas produced using the chemical looping has a higher calorific value than that produced using a conventional process with air. For comparison purposes, a conventional gasification unit with pure oxygen (CGPO) and a chemical looping gasification (CLG) system were simulated using Aspen Plus to treat 86 t/d biomass, and an economic analysis comparing the operating and capital costs of the two systems was performed. The two systems were identical except for the reactor configuration. The “CGPO” reactor consisted of a bubbling fluidized bed (ID=1.8 m and H=6.6 m) as gasifier and sand as bed material with oxygen supplied via a pressure swing adsorption unit. The CLG consisted of a bubbling fluidized bed gasifier (ID=1.8 m and H=6.6 m) working in parallel with a fast fluidized bed oxidizer (ID=1 m and H=10 m). Co_3O_4(8 %)/Al_2O_3 with a circulation rate of 44.6 kg/s between gasifier and oxidizer supplied the

oxygen for the CLG system. The total capital investment (TCI) of the CGPO and CLG units were $6.3M and $9.7M, respectively. However, the annual operating cost of the CLG was $0.58M less than that of the CGPO which repays the difference in TCI in less than 6 years.

Milad Aghabararnejad

École Polytechnique de Montréal

July 2014

TABLE OF CONTENTS

DEDICATION iii

ACKNOWLEDGMENTS iv

RÉSUMÉ v

ABSTRACT viii

TABLE OF CONTENTS xi

LIST OF TABLES xv

LIST OF FIGURES xvi

CHAPTER 1 INTRODUCTION 1

CHAPTER 2 LITERATURE REVIEW 4

2.1 Introduction 4

2.1.1 Biomass 5

2.2 Biomass conversion 7

2.2.1 Chemical conversion 7

2.2.2 Biochemical conversion 8

2.2.3 Thermal conversion 8

2.3 Syngas cleaning 14

2.4 Air separation units (ASU) 18

2.4.1 Cryogenic systems 18

2.4.2 Adsorption systems 18

2.4.3 Chemical looping process 19

2.5 Preparation of the oxygen carrier 21
2.5.1 Mechanical mixing 21
2.5.2 Wet impregnation 21
2.5.3 Incipient wetness impregnation 21
2.5.4 Co-precipitation 22
2.5.5 Freeze granulation 22
2.6 Chemical looping combustion-CLC 23
2.7 Chemical looping process for H_2 production 26
2.8 Chemical looping Gasification-CLG 29
2.9 Summary 31

CHAPTER 3 COHERENCE OF THE ARTICLES 33

CHAPTER 4 ARTICLE 1: TGA AND KINETIC MODELING OF Co, Mn, AND Cu OXIDES FOR CHEMICAL LOOPING GASIFICATION (CLG) 35
4.1 Introduction 36
4.1.1 Process description 37
4.1.2 Solid fuel gasification in chemical looping systems 39
4.2 Experiment 43
4.2.1 Materials 43
4.2.2 Methods and techniques 44
4.3 Results and discussion 45
4.3.1 Oxygen release capacity by TGA 45
4.3.2 Reduction and oxidation kinetic 49
4.3.3 XRD results 54
4.3.4 Thermal resistance of the oxygen carrier 55
4.3.5 The interaction between Co_3O_4 and biomass 56
4.4 Conclusions 58

References 59

CHAPTER 5 ARTICLE 2: TRANSIENT MODELING OF BIOMASS STEAM GASIFICATION WITH Co_3O_4 62

5.1 Introduction 63

5.2 Materials, methods and experiments 67

5.3 Steam gasification model 71

5.3.1 Oxygen desorption in a bubbling fluidized bed 72

5.3.2 Biomass pyrolysis 75

5.3.3 Steam gasification 76

5.3.4 Homogeneous gas phase reactions 77

5.4 Results and discussion 78

5.4.1 Hydrodynamic model validation 78

5.4.2 Oxygen desorption in a bubbling fluidized bed 81

5.4.3 Effect of temperature 83

5.4.4 Effect of steam 85

5.4.5 Effect of Co_3O_4 86

5.5 Conclusions 88

References 89

CHAPTER 6 ARTICLE 3: TECHNO-ECONOMIC COMPARSION OF A 7 MW_{th} BIOMASS CHEMICAL LOOPING GASIFICATION UNIT WITH CONVENTIONAL SYSTEMS 97

6.1 Introduction 98

6.2 Design and simulation of the CG unit 101

6.3 Design and simulation of the CLG unit 109

6.3.1 Gasifier 111

6.3.2 Oxidizer 112

6.4 Economic analysis of CG, CGPO, and CLG units 114
6.4.1 Capital cost 114
6.4.2 Total production cost (TPC) 115
6.5 Conclusions 118
References 123

CHAPTER 7 GENERAL DISSCUSSION 127

CHAPTER 8 CONCLUSIONS AND RECOMMENDATIONS 134
8.1 Conclusions 134
8.2 Recommendations 137

REFERENCES 139

LIST OF TABLES

Table 2.1 Operating CLC system 27

Table 4.1 Summary of oxygen-carrier particles prepared and tested for CLOU application 42

Table 4.2 Incipient wetness impregnation for preparation of supported oxygen carrier 43

Table 4.3 Biomass elemental and proximate analysis 43

Table 4.4 Activation energy for copper, cobalt and manganese reduction and oxidation 53

Table 5.1 Equilibrium and kinetic models of gasification 66

Table 5.2 Physical properties of Co_3O_4 68

Table 5.3 Biomass elemental and proximate analysis 68

Table 5.4 The experimental plan for the gas phase RTD 70

Table 5.5 Experimental plan for steam gasification of biomass 71

Table 5.6 State equations and hydrodynamic parameter for a two phase model 74

Table 5.7 Kinetic parameter of Sweet Gum pyrolysis, Nunn et al. [29] 75

Table 5.8 Gas solid reactions at the bed surface 77

Table 5.9 Gas phase reaction rate expressions $(mol/m^3.s)$ 78

Table 6.1 Design of the chemical looping processes 100

Table 6.2 Mass balance of the CG unit, Aspen plus V. 7.2 104

Table 6.3 Mass balance of the CGPO unit, Aspen plus V. 7.2 104

Table 6.4 Simulation description of CG and CGPO units 105

Table 6.5 CG and CGPO gasifier design results 108

Table 6.6 Mass balance of the CLG, Aspen plus V. 7.2 110

Table 6.7 Simulation description of CLG system 110

Table 6.8 Oxidizer design results (CLG unit) 114

Table 6.9 Total capital investment (TCI) 115

LIST OF FIGURES

Figure 2.1 Comparison of the world energy resources in 2011 and 2030 4

Figure 2.2 Carbon cycle 6

Figure 2.3 Methods of biomass conversion to fuel, gases and chemicals 7

Figure 2.4 World syngas market in 2004 11

Figure 2.5 Pressure swing adsorption, bed 1 in regeneration, bed 2 in process, P_2>P_1 . 19

Figure 2.6 Chemical looping combustion of gaseous fuels 24

Figure 2.7 in situ gasification-chemical looping combustion process 25

Figure 2.8 Chemical looping oxygen uncoupling process 25

Figure 2.9 Chemical looping water splitting for hydrogen production 28

Figure 2.10 The Fast Internally Circulating Fluidized Bed (FICFB) gasification system, the arrows correspond to the solid circulation between two sections 30

Figure 4.1 Circulating fluidized bed gasifier, the arrows correspond to the solid circulation between two sections 38

Figure 4.2 Mechanisms of iG-CLC and CLOU (Modified from Adanez et al. 40

Figure 4.3 The profile of weight loss and rate with temperature in (0%, 5% and 21% O_2) for a) CuO, b) Co_3O_4, and c) Mn_2O_3 46

Figure 4.4 The initial temperature of reduction in different oxygen concentrations, Experimental data and equilibrium curve by FactSage 6.4 software, Cu (——), Mn (– ·· –), Co (– – –) 48

Figure 4.5 Co_3O_4 reduction in nitrogen, conversion vs time at 825, 850 and 875 °C, the solid line represents the model) 51

Figure 4.6 CoO oxidation in air, conversion vs time at 825, 850 and 875 °C, (- - - -) NG model, (——) MNG model (modified NG model, Equation 4.13) . . . 52

Figure 4.7 Arrhenius relationship of K_{Oxi} (from MNG model) and K_{Red} with temperature) 53

Figure 4.8 XRD pattern of copper, cobalt, and manganese; ⋆ indicates the formation of the reduced metal oxide) 55
Figure 4.9 Pyrolysis of wood sawdust in the presence of Co_3O_4; A: Co_3O_4, B: Co_3O_4 + biomass (2:1), C: Biomass; 1: Drying, 2-5: Pyrolysis + Gasification) . . . 57
Figure 5.1 Schematic of chemical looping gasification (CLG) unit 65
Figure 5.2 Steam bubbling fluidized bed gasifier schematic 69
Figure 5.3 5 step model for biomass steam gasification with Co_3O_4 as the oxygen source 72
Figure 5.4 Schematic of a two phase fluid bed model 73
Figure 5.5 Radial dispersion, H=20 cm, u_0=13 cm/s, T=25 °C, sand as bed material . . 79
Figure 5.6 Modeling versus experimental RTD at T=25 °C, 400±4°C, and 850±8°C, H=20 cm, r/R=0, u_0=13 cm/s, with sand as bed material 80
Figure 5.7 Modeling results for oxygen flow rate (left axes) and cumulative oxygen desorption (right axes) at the bed surface (H=20 cm), T=825 °C, 850 °C, 875 °C, u_0=13 cm/s, 50 % Co_3O_4 82
Figure 5.8 Concentration profiles of the gases versus time for T=825±8 °C, 850±7 °C, and 875±9 °C; H_2O %=18, Co_3O_4 %=50, R^2>0.896, solid line representing the model 84
Figure 5.9 Concentration profiles of the gases versus time for 0, 10, 18 %steam; T=875 ±9 °C, Co_3O_4 %=50, R^2>0.827, solid line representing the model 86
Figure 5.10 Concentration profiles of the gases versus time for Co_3O_4 %=0, 30, 50; H_2O %=18, T=875±9 °C, R^2>0.860, solid line representing the model . . 87
Figure 5.11 WGS and reforming reaction rate constant versus temperature 94
Figure 5.12 Variation of biomass particle temperature upon entering to the bubbling fluidized bed operating at 850 °C 96
Figure 6.1 Gasifier duty vs. ER, 86 t/d biomass, λ=2 102

Figure 6.2 Simulation of the CG unit, GSR: Gasifier, CYC: Cyclone, FIL: Filter, HX: Heat exchanger, SCR: Scrubber, DCR: Decanter, P: Pump, COMP: Compressor 103
Figure 6.3 Particle flux (E_p) versus freeboard height (H) 108
Figure 6.4 Simulation of the CLG unit; oxygen is supplied via transformation of Co_3O_4 to CoO in the gasifier, GSR: Gasifier, OXI: Oxidizer, CYC: Cyclone, FIL: Filter, HX: Heat exchanger, SCR: Scrubber, DCR: Decanter, P: Pump, COMP: Compressor 109
Figure 6.5 Oxidizer design algorithm 113
Figure 6.6 Operating cost breakdown 116
Figure 6.7 Sensitivity analysis of the CLG and CGPO units 118

CHAPTER: 1

INTRODUCTION

Growth in global energy demand on the one hand and declining fossil energy resources on the other hand are forcing countries to look for alternative resources. Renewable energy sources, especially biomass, have the potential to be the primary energy source by 2035 [1]. Biomass is available in abundance, is neutral with respect to CO_2, and does not contribute to global warming. Consumption of biomass in producing electricity and chemicals, especially biofuels, is growing rapidly. For instance, by 2035, biofuel will contribute as much as 8 % of the transport fuels, including jet fuels [1].

Combustion and gasification are the main technologies to convert biomass to energy or other valuable materials. Combustion is more favourable whenever biomass is used to produce energy. Gasification is used to produce syngas, which is a mixture of mostly CO and H_2. Syngas is a building block for various processes including Fischer-Tropsch and methanol production. Syngas from biomass has more impurities and depending on its application, several conditioning and cleaning steps have to be performed prior to utilization.

The oxygen for gasification is 20-30 % of the stoichiometric oxygen required for complete combustion. To avoid the dilution of syngas with nitrogen and also the formation of acid gases (e.g., NO_x), an air separation unit is usually used to separate the oxygen from air. The air separation unit increases the capital and operational costs of the process.

The chemical looping process is a promising technology to separate oxygen from air at high temperature using an oxygen carrier. The oxygen carrier is oxidized with air in an oxidation reactor and transferred to the reduction side. The reduction reactor can serve as the gasifier by supplying the required oxygen from the oxygen carrier. The oxidation and reduction reactions happen at high temperatures (800-900 °C) and, therefore, can be integrated with the gasification which operates at, 800 °C.

The oxygen from the oxygen carrier is in lattice form and not readily available to react with the biomass. A chemical looping oxygen uncoupling (CLOU) oxygen carrier is an alternative to resolve this issue. The oxygen carrier of the CLOU process is able to react with the oxygen in the oxidizer and release oxygen in the gasifier. In other words, the oxygen from the CLOU process is in gaseous form. CLOU has been used to combust solid fuels; however, the application of CLOU in the biomass gasification has not been previously studied.

Copper, manganese, and cobalt are reported in the literature as suitable oxygen carriers for CLOU. Despite the oxygen transport capacity, oxidation-reduction rates, thermal and mechanical strength, and economical and environmental aspects are the main aspects that must be considered for oxygen carrier selection. Copper has the highest oxygen transport capacity; however, it lacks thermal and mechanical strength due to its low melting point. Manganese has the lowest oxygen transport capacity. Cobalt has a moderate oxygen transport capacity and its thermal and mechanical strength is higher than copper. However, it is more expensive and less environmentally friendly.

Although the preparation and characterization of the oxygen carrier, especially for the treatment of gaseous fuels, have been extensively studied in the literature, the CLOU oxygen carrier, especially with the application in gasification has been widely ignored. Furthermore, a kinetic model, which can describe the reduction rate of the oxygen carrier in the CLOU process, has not been reported.

Besides the selection and characterization of the oxygen carrier, its performance in the presence of biomass should be taken into account. During biomass gasification, tar and sticky materials can form and deactivate the oxygen carrier. Furthermore, steam, which is used as the gasification agent, can serve as an oxidizer and, therefore, reduce the oxygen release rate from the oxygen carrier.

Finally, in order to use a chemical looping biomass gasifier, a preliminary design and economic analysis is necessary. The economic analysis reveals and compares the capital and operational costs of a conventional steam gasification unit with a chemical looping gasifier. This thesis consists of three articles, which have been accepted or submitted to scientific journals and includes the following chapters:

– Chapter 2 presents a critical literature review. It starts with general definitions and discusses various technologies to convert biomass to energy. The authors tried to highlight the research gap on the gasification of solid fuels;

– Chapter 3 introduces the coherence of the articles;

– Chapters 4, 5, and 6 contain three articles and principle findings with related discussions;

– Chapter 7 discusses, in general, the results of the papers as well as some critiques and research issues;

– Finally, Chapter 8 presents the main conclusions and some recommendations for future work.

CHAPTER: 2

LITERATURE REVIEW

2.1 Introduction

Energy is the backbone of the modern industrial society. The more industrialized a country is, the more energy it demands. The global energy demand is growing rapidly from 462.4 quadrillion BTU in 2005 to more than 690 quadrillion BTU by 2030 [2]. Decreasing fossil fuel resources as the current primary energy source and increasing pollution from fossil fuels, as well as the global energy growth are persuading industries to consider clean, cheap, and abundant alternative resources. Currently, renewable energies comprise only 9 % of the global energy supply, which is expected to increase to 22 % by 2030 [2] (Figure2.1).

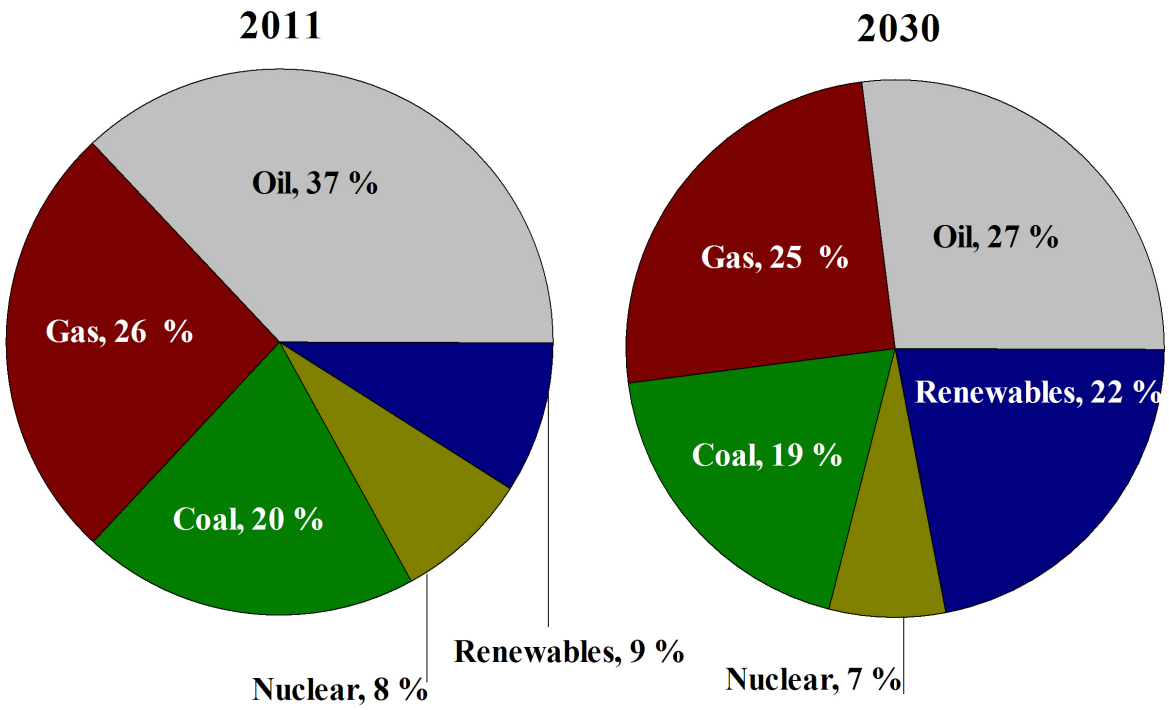

Figure 2.1 Comparison of the world energy resources in 2011 and 2030

Renewable energies include solar energy, wind, biomass, hydro and geothermal (heat from the ground), which are readily available and environmentally friendly. Solar energy and wind require large areas of land to capture their energy and, more importantly, they are not reliable. The installation cost of geothermal facilities is high and it is only suited to particular regions. Hydropower requires expensive facilities and may cause serious geological damage. Also, it is limited to regions with high precipitation rates. Biomass is widely available, and inexpensive, and can be used to produce synthesis fuels, which other renewable sources do not offer. In Canada, biomass is the second largest source of renewable energy after hydroelectricity.

2.1.1 Biomass

Biomass is derived from living or recently living materials. Wood is the largest source of biomass; however, a wide variety of biomass sources include the following:

- Waste from forestry and sawmill operations;
- Wood waste (packing and leftover construction wood);
- Agricultural waste;
- Fast growing plants;
- Organic waste (animal manure and food processing waste); and
- Municipal solid waste.

The plant converts atmospheric CO_2 to organic compounds. By combusting the organic compounds, the same amount of CO_2 is released into the atmosphere. Therefore, converting biomass to energy does not disturb the CO_2 content of the atmosphere. Fossil fuels contain carbon that has been out of the carbon cycle for a very long time. Hence, the combustion of fossil fuels disturbs the carbon cycle (Figure 2.2).

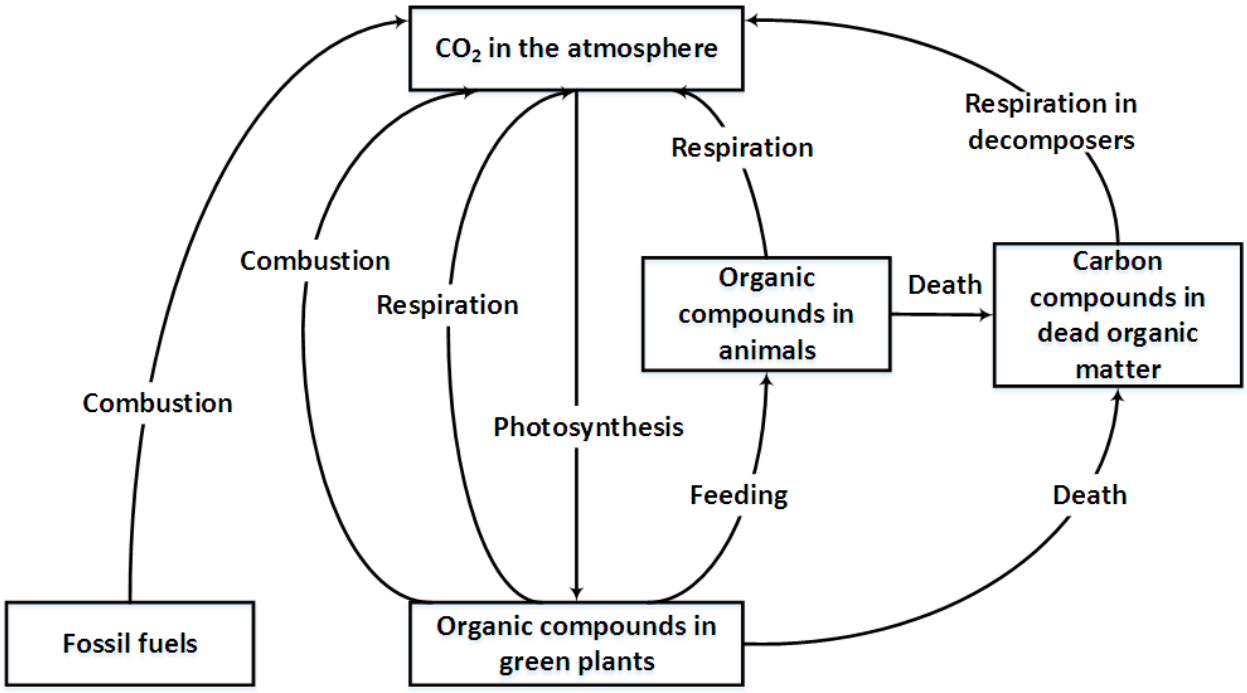

Figure 2.2 Carbon cycle

Biomass is composed of lignin, cellulose, hemicelluloses, lipids, proteins, simple sugars, starches, water, hydrocarbon, and ash. It is characterized by proximate and ultimate analyses. The proximate analysis gives moisture content, volatile content (when heated to 950 °C), char (pure carbon) remaining at that point, ash (mineral) and high heating value (HHV) based on the complete combustion of the sample to carbon dioxide and water. The ultimate analysis gives the percentage of carbon, hydrogen, and oxygen as well as sulfur and nitrogen. Biomass is highly oxygenated compared to conventional fossil fuels [3]. Considering all the advantages, biomass is inefficient and has a low energy density compared to fossil fuels. Furthermore, the pre-treatment of biomass, including harvesting, transportation, crushing, and drying, are energy consuming and costly. Therefore, converting biomass to a convenient energy source is challenging and requires more research and development.

2.2 Biomass conversion

Biomass can be used directly to release energy in the form of heat or electricity, or may be converted to another form, such as liquid (ethanol, biodiesel, methanol, vegetable oil, and pyrolysis oil), gas [biogas (CH_4, CO_2), producer gas (CO, H_2, CH_4, CO_2, H_2), syngas(CO, H_2), substitute natural gas (CH_4)] or solid (charcoal, torrefied biomass) [4]. Conversion of biomass into useful forms of energy or chemical products is categorized into three groups (Figure2.3).

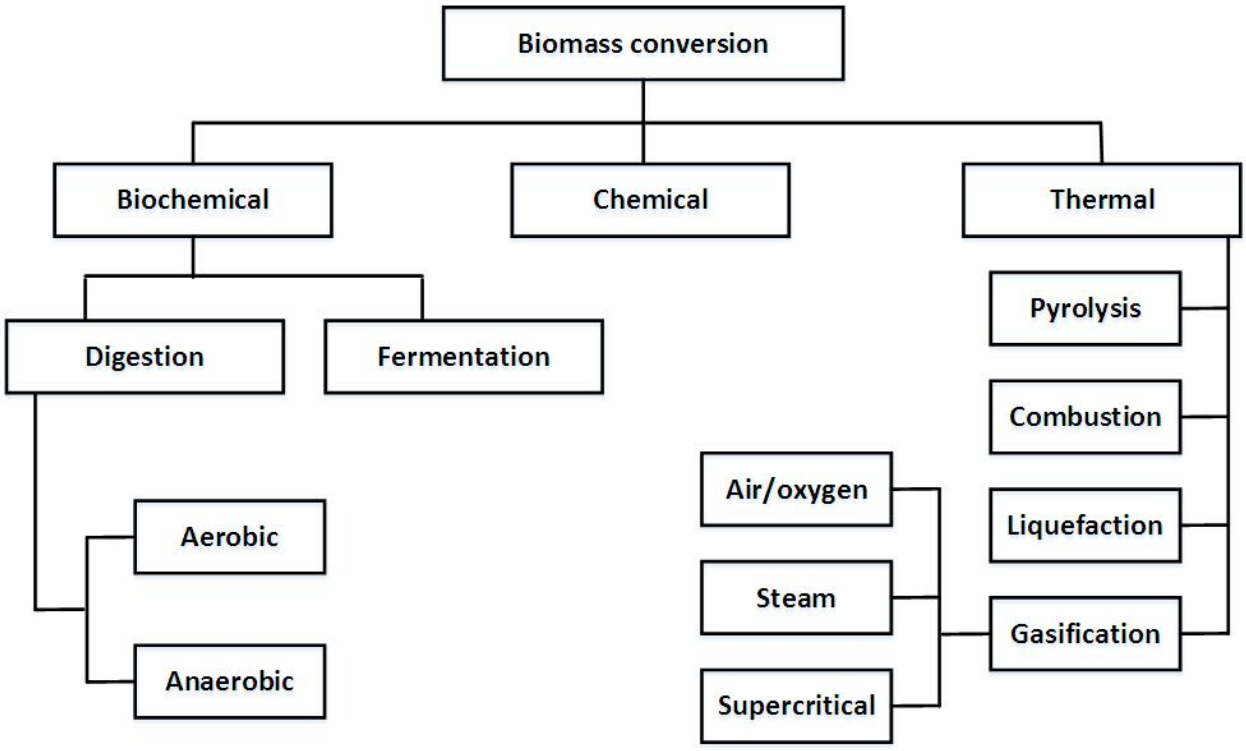

Figure 2.3 Methods of biomass conversion to fuel, gases and chemicals

2.2.1 Chemical conversion

The two principal methods to produce chemicals from biomass are based on sugar and syngas. The final products of sugar based methods include xylose, fructose, glucose, arabinose, lactose, sucrose, and starch [4]. Syngas is a mixture of predominantly H_2 and CO with trace amounts of CH_4, H_2O and CO_2. Syngas is a building block to produce numerous chemicals including hydrogen,

methanol, glycerol (C3), fumaric acid (C4), xylitol (C5), glucaric acid (C6), and gallic acid (Ar) [5]. Each of these components can be an intermediary to produce a large number of chemicals, which can be used in transportation, textile and food industries, the environment, communications, health, housing, and recreation [5]. Although chemical conversion methods result in a value added product, in most cases they cannot use biomass directly and the first step is to convert biomass to sugar or syngas via another process.

2.2.2 Biochemical conversion

In this process biomass components are decomposed to smaller molecules by bacteria, microorganisms and enzymes. Digestion (anaerobic or aerobic) and fermentation are the most popular biochemical technologies. Anaerobic digestion is a biological process, which stabilizes organic materials in the absence of oxygen and transforms it into solid residue (bio-fertilizer) and biogas (mostly CH_4 and CO_2). The bacteria supply the oxygen from the biomass rather than the air. Aerobic digestion uses different types of bacteria that access oxygen from the air, producing carbon dioxide, heat, and a solid residue [6]. The fermentation process is to convert the plant's glucose (or carbohydrate) to an alcohol or acid by yeast or bacteria. In fermentation the bacteria touch only the sugar based materials and the other components in the biomass (e.g., lignin) are left unchanged. Therefore, it is more economical to use a biomass with high sugar content (e.g., sugarcane, corn or sweet potatoes) for fermentation. Biochemical conversion of biomass is inexpensive but the conversion rate is much slower compared to thermal and chemical processes [6].

2.2.3 Thermal conversion

Thermal conversion is one of the most important processes to convert biomass to energy. In all thermal processes heat is the dominant mechanism to convert biomass. Thermal processes are classified into three categories based on the oxygen availability as combustion, pyrolysis and gasification.

Combustion

Combustion is the thermal degradation of hydrocarbons ($C_xH_yO_z$) in the excess air atmosphere. Water vapor, carbon dioxide, and heat are the main products of combustion (Eq. 2.1).

$$aC_xH_yO_z + bO_2 \longrightarrow cCO_2 + dH_2O + Q \tag{2.1}$$

The produced energy can be used to generate electricity or mechanical movement and also for heating purposes. Combustion happens at 700<T(°C)<1400 [7]. In air combustion, the separation of CO_2 from the un-reacted O_2 and N_2 is difficult. Therefore, the CO_2 is released to the atmosphere without separation. Furthermore, combustion in air creates several forms of nitrogen oxide-NO_x, which are not environmentally friendly.

Pyrolysis

Pyrolysis is thermal decomposition of substances by heating them at high temperature and in an oxygen free atmosphere. Pyrolysis occurs at a temperature range of 380-530 °C [7]. As a result, it takes part in all other thermal conversion processes. There is some content of oxygen in biomass or other solid fuels and, therefore, achieving a complete pyrolysis is impossible. This process can be represented by the following general reaction:

$$\text{Biomass} + Q \longrightarrow \text{Char} + \text{Gases} + \text{Vapour or Liquid} \tag{2.2}$$

The produced gases are mostly CO, H_2, CO_2, CH_4, and H_2O and liquid products are water, tar and bio-oil. Tar is a viscous and sticky liquid, which contains heavy organic and inorganic molecules. Tar causes many challenges for downstream facilities, like filters, compressors, etc. Up to 200 °C only water is driven off. Between 200 to 280 °C carbon dioxide, acetic acid and water are reduced. The main step of pyrolysis, which takes place between 280 to 500 °C, produces large quantities of tar and gases, including carbon dioxide. The composition of the pyrolysis products depends on the fuel type, temperature, and heating rate. Increasing the temperature beyond 900 °C

decomposes the tar and increases the gas yield [8]. Pyrolysis is an endothermic process and also 20-40 % of the carbon remains as char [8].

Gasification

Gasification is a flexible, reliable, and clean energy technology that can turn a variety of low-value feed stocks into high-value products. The product of gasification is mostly a gas rich in H_2 and CO, called syngas. Tarry components also might form during gasification but their formation is low due to the presence of oxygen and/or steam and the high temperature of gasification [9]. The H_2/CO ratio and the impurity level of the syngas determine its application. Syngas is a building block in the chemical industry and only a small portion of syngas comes from biomass gasification. The largest part of the syngas is used to synthesize NH_3 (53 %), which is used in the fertilizer industry. H_2 production is the second consumption of syngas by 23 %. The production of liquid fuels via Fisher-Tropsch and methanol comprises about 20 % of syngas consumption and only 4 % of the syngas is used for electricity generation (Figure 2.4). However, it is expected that the syngas applications will shift from the production of ammonia to the synthesis of liquid fuels by 2040 with as much as 40 % of the market [9].

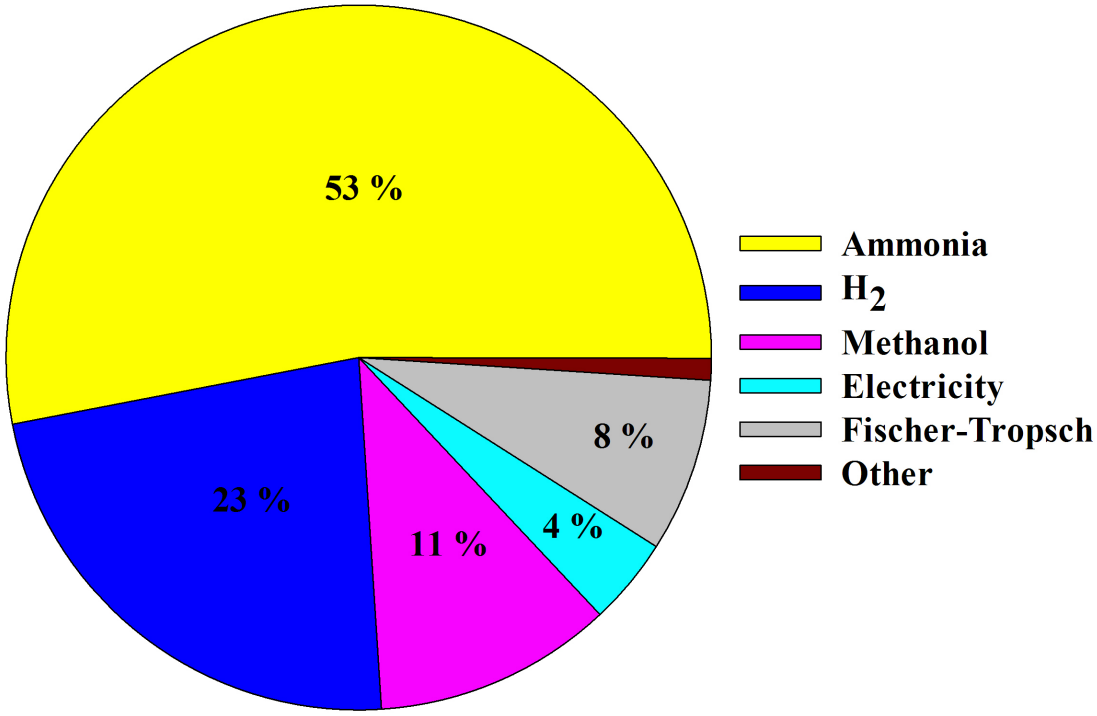

Figure 2.4 World syngas market in 2004 [10]

If power generation is the only desired application, combustion seems preferable and more economical compared to gasification, especially in small to medium-scale plants. However, gasification is the primary step to produce high value liquid fuels, which makes it more favourable compared to combustion. The formation of NO_x in gasification is much less due to the lack of oxygen. Furthermore, the sulfur appears in the form of H_2S during gasification, which is easier to separate from the effluent gas compared to SO_2 formation in combustion. Air (or oxygen), steam, plasma and supercritical are the main gasification technologies.

Air or oxygen gasification

The oxygen required for air gasification is just enough to supply the energy for the entire reaction. In other words, by introducing oxygen to the reactor, the exothermic reactions (Eq. 2.3 and

Eq. 2.4) take place and supply the energy for the endothermic reactions [11].

$$C + 0 \cdot 5\,O_2 \longrightarrow CO + 111 \ \ (kJ/mol) \tag{2.3}$$

$$C + O_2 \longrightarrow CO_2 + 394 \ \ (kJ/mol) \tag{2.4}$$

Reaction 2.4 consumes twice as much O_2 as the Reaction 2.3. Therefore, in an oxygen deficient atmosphere, the first reaction is more likely to take place. The ratio of the oxygen required to gasify the biomass compared to the oxygen required for complete combustion is known as the equivalent ratio (ER):

$$ER = \frac{Required\ O_2\ for\ gasification}{Required\ O_2\ for\ complete\ combustion} \tag{2.5}$$

The ER is normally in the range of 0.2-0.3 [4]. The oxygen content of fuel can affect the ER. The oxygen in biomass (typically 40-60 wt %) is removed by dehydration or decarboxylation (Eq. 2.6and 2.7) and is not available for gasification.

$$C_xH_yO_z \longrightarrow C_xH_{y-2z} + qH_2O \tag{2.6}$$

$$C_xH_yO_z \longrightarrow C_{x-q/2}H_y + qC_2O \tag{2.7}$$

The other reaction which is endothermic and occurs during gasification, is the Boudouard reaction (Eq. 2.8):

$$C + CO_2 \longrightarrow 2\,CO - 162\,(kJ/mol) \tag{2.8}$$

The Boudouard reaction plays an important role in the final gas composition, especially CO and CO_2. Air gasification produces a low heating value of gas (4-6 MJ/m^3) and a high nitrogen content of 45-55 %. A gas with a low nitrogen content and a high heating value (12 MJ/m^3) is produced

with pure oxygen as the gasification agent (the heating value of methane is 40 MJ/m^3) [12].

Steam gasification

The most important reactions during steam gasification are as follows:

$$C + H_2O \longrightarrow CO + H_2 - 161\,(kJ/mol) \tag{2.9}$$

$$CO + H_2O \longrightarrow CO_2 + H_2 - 42\,(kJ/mol) \tag{2.10}$$

Steam gasification is endothermic. Therefore, an external source of energy is required to derive the reactions. The required energy can be provided indirectly by subjecting oxygen to the reactor and deriving exothermic reactions. In this case the ER is more than the air gasification. The H_2O/C molar ratio is a crucial operational parameter during steam gasification. Introducing more steam to the reactor (increasing H_2O/C ratio) increases the H_2 yield and, consequently H_2/CO ratio due to the water-gas shift reaction (Eq. 2.10). The H_2O/C molar ratio depends on the gasification product application, and generally is in the range of 1-3 [8]. The formation of tar during steam gasification is less due to the hydrothermal decomposition of heavy molecules with water.

Supercritical steam gasification

Supercritical gasification is a relatively new technology which uses supercritical water ($T > T_c$=374 ^oC, $P > P_c$=220.64 bar) as the gasification agent. Under supercritical conditions the reaction of organic substances with water is very fast and converts biomass/waste into a medium heating value gas. The syngas from supercritical gasification is rich in hydrogen and is not diluted by nitrogen. More importantly, the produced gas is already at high pressure and can be integrated directly to the Fischer-Tropsch process, which operates at high pressure [13, 14].

Plasma gasification

In plasma gasification, the biomass or solid waste is decomposed to gases and slag using a plasma torch. An inert gas (usually steam) becomes superheated by passing through an electric arc. The electric arc is created by applying a strong electric current under high voltages through two electrodes. The torch temperature ranges from 2200 °C to 13900 °C and can convert any type of waste to gas and solid residue. The produced gas from plasma gasification is cleaner and has no heavy components compared to conventional gasification [15, 16].

2.3 Syngas cleaning

Syngas is mainly produced by partial oxidation or steam reforming of natural gas (Eq. 2.11, 2.12). A small portion of the syngas comes from gasification of coal or biomass. The syngas coming from gasification, especially biomass (referred to as bio-syngas), is highly dirty and has to be cleaned before being sent to other units.

$$CH_4 + \tfrac{1}{2}O_2 \longrightarrow CO + 2H_2 \tag{2.11}$$

$$CH_4 + H_2O \longrightarrow CO + 3H_2 \tag{2.12}$$

The most common impurities of bio-syngas are the following: particulate matter, tar and condensable hydrocarbons, sulfur and CO_2 and N_2. Alkali metals and chlorine are also the other impurities of syngas. However, their quantity is very low, which can be tolerated by most of the syngas applications.

Particulates

Elutriated particles from the gasifier range between $1\mu m$ to over 100 μm [17] are basically ash and un-reacted solid residue. They cause fouling, corrosion, and erosion of the downstream facilities. Therefore, many syngas applications, even combustion processes, require more than 99 % particulate removal [18]. Particulates can be removed by three main technologies: internal

separation, filtering and electrostatic precipitation [19]. The internal separation approach uses the mass difference between particulate and gas. Cyclones and dust agglomerates are the most common devices in this category. Filtering occurs when a gas stream passes around fibers or through a porous solid. Electrostatic separators (ESP) remove the solids and fine particles by applying a strong electric field. The gas stream flows through many wires. A negative voltage of several thousand volts is applied to the wire and the particles became ionized. The charged particles flow with the gas stream through a stack of large flat metal plates, which are connected to a high positive voltage source. The particles stick to the plates and form a layer. The electrostatic separators are very effective in removing particulate matter from gas streams [20].

Tar

Tar is considered the main challenge of the gasification process because it can block filters and lines and damage the downstream processes. The tar content of syngas depends on the operating conditions, gasifier type, and feed. Increasing temperature decreases tar formation [19, 21, 22] but increasing temperature beyond a certain point may cause clogging and the sintering of particles in the gasifier. Ciferno and Marano [23] reported that the tar yield is 10-20 % in an up-draft gasifier where the carrier gas and solids are counter-current while in a down-draft gasifier with a co-current flow of gas and solid, the tar yield is as low as 1 %. The syngas produced from biomass has a higher tar concentration compared to coal or peat gasification [24]. Removing all tar and heavy components from syngas may be expensive and not applicable. However, a practical way is to eliminate a sufficient amount of tar until the dew point of the syngas drops below the minimum temperature experienced by the gas stream [25].

Thermal cracking, catalytic cracking, and physical separations are the main techniques to remove tar from the produced gas [18]. Non-physical methods eliminate tar by increasing the tar decomposition rate. Usually these techniques are applied in a secondary vessel (post-gasifier). However, thermal and catalytic cracking can be applied in-situ with gasification as well. In thermal cracking, large organic compounds are broken down into smaller non-condensable gases at high

temperatures (1100-1300 °C). The higher the temperature is, the less residence time is required [26, 27]. Although thermal cracking seems to be simple in principle, implementing a high temperature gasifier is difficult and expensive. In some cases it is even more economical to have separate tar cleanup equipment and a low temperature gasifier rather than a high temperature gasifier [28–30].

In catalytic cracking, the catalyst increases the tar cracking rate by decreasing the activation energy. Catalytic cracking, unlike thermal cracking, does not suffer from high temperatures. However, catalyst deactivation, especially during the in-situ process, is problematic. Agglomeration, attrition, poisoning with sulfur, and coke formation are the main deactivation mechanisms. Different materials have been reported to have a catalytic effect for the tar decomposition reaction, including nickel, iron, alkali-based metals, activated alumina, FCC, char and less expensive materials, like calcined dolomite, limestone, calcined rocks, olivine and clay minerals [31–35]. The literature in this domain is extensive with a prominent review paper from Woolcock et al. [18].

At temperatures lower than 450 °C tar starts to condense and forms heavy droplets, which resemble the particulate matter [36]. Therefore, they can be removed by the techniques presented for the removal of particulate.

Sulfur and CO_2

Sulfur compounds usually appear in the form of H_2S and COS during gasification. The sulfur content of biomass is significantly less than coal (0.5 g/kg compared to 50 g/kg) [37]. Sulfur causes the corrosion of metal surfaces and also contaminates the metal catalysts in post processing facilities. Furthermore, if the syngas is burned, the sulfur compounds convert to SO_2, which can produce acid gases. Neglecting the green house gas effect of the CO_2, it is considered as a diluent rather than an impurity for the post-processing of syngas. In other words CO_2 does not negatively impact the downstream catalytic processes.

Adsorption and absorption are the two main processes to remove H_2S and CO_2. The adsorption can be applied at high and low temperatures. The high temperature process can be integrated

with the gasification. The adsorbent removes the impurities from the syngas in one vessel and is transferred to another vessel for regeneration. CaO, activated carbon, metal-based adsorber and zeolite are normally used as adsorbers.

Chemical absorption with amine solutions are the most commonly used CO_2-H_2S (acid gases) removal technologies, which rely on the reactions of the acid gas with the solvent to form weakly bonded compounds. The absorbed acid gas can be released by applying heat and the solvent is regenerated [38]. Physical solvent absorption may be competitive with amine processes when the feed gas is available at high pressure (generally P>20 bar) [39]. The Selexol and Rectisol processes are the leading physical absorption technologies to treat feed gas with a high CO_2 concentration [40]. In the Selexol process polyethylene glycol di-methyl ether is used as a solvent, which is able to remove CO_2, H_2S and water simultaneously. The solubility of H_2S in most organic solvents is higher than CO_2, which helps to remove it completely [41]. The solvent can be regenerated by decreasing the pressure in a series of vessels.

Nitrogen

Nitrogen is considered as a diluent and contamination of syngas. Air as the oxygen source of gasification contains 78 % N_2. Therefore, the syngas from air gasification has a considerable amount of nitrogen (30-50 %). This will affect the size and, consequently, the equipment cost of the processes after the gasifier. Also, the presence of nitrogen in the gasifier forms nitrogen compounds, such as NO_x, NH_3 and HCN. NO_x contributes to global warming and affects the environment by producing acid rain. Gas turbines usually demand a syngas with an ammonia concentration less than 50 ppm to control the NO_x emissions [42]. Furthermore, a syngas with an ammonia concentration of 0.05 ppm can deactivate the catalysts used to upgrade syngas [42]. There are two main approaches to remove nitrogen from biomass: to avoid direct contact of air and fuel; and to separate nitrogen from the syngas after gasification. In the latter approach nitrogen has already entered in the gasifier, which may form toxic nitrogen compounds. Therefore, the former technology is of more interest. The direct contact of nitrogen and fuel can be avoided by either

feeding pure oxygen (generated from air separation units-ASU) instead of air or using a chemical looping system for gasification.

2.4 Air separation units (ASU)

Cryogenic and non-cryogenic systems are the main air separation methods. Cryogenic systems are preferable whenever a large capacity with high purity separation is required. Non-cryogenic systems, including adsorption and membrane technologies, are generally for lower product purities.

2.4.1 Cryogenic systems

In cryogenic methods, air is compressed and cooled first. Next the water and carbon dioxide are removed by molecular sieve adsorbers. The air is then cooled by exchanging heat with the cold streams of the gaseous products and afterward liquefied by a refrigeration process. The liquefied air is sent to a set of distillation columns and separated into oxygen, nitrogen and argon. The cryogenic technology consumes a lot of power, specifically in the refrigeration step (0.28-0.3 kWh/Nm^3 [43, 44]). Therefore, it is not economical unless a large capacity of separation is required.

2.4.2 Adsorption systems

Pressure swing adsorption (PSA) and vacuum pressure swing adsorption (VPSA) are the main adsorption technologies to separate oxygen from air. The air is switched periodically between two beds packed with a zeolite molecular sieve. Nitrogen is adsorbed more strongly by zeolite compared to oxygen molecules. Therefore, the outlet stream is concentrated in oxygen. When the adsorbent becomes saturated with nitrogen, the air is switched to the second bed. To increase the adsorption rate, the bed is pressurized. In the case of PSA, the saturated bed is de-pressurized to atmospheric pressure while for VPSA the bed is subjected to vacuum to provide an additional driving force for regeneration. A small portion of produced oxygen is used to flush the adsorbed gas, preparing the bed for another cycle (Figure 2.5).

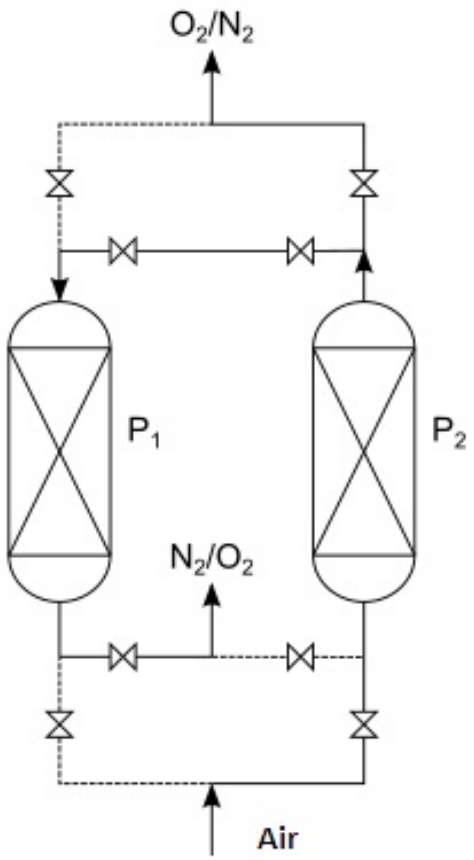

Figure 2.5 Pressure swing adsorption, bed 1 in regeneration, bed 2 in process, $P_2 > P_1$

Each bed is saturated in the order of 10 s [44], and every time the composition of the gas feed changes, it takes on the order of hours to reach steady state conditions [45]. Therefore, adsorption systems compared to cryogenic processes are not flexible. Membrane technology is also another air separation method, which has received substantial attention in recent years. The permeability of oxygen in some materials like polysulphone, is five times more than nitrogen [43]. This property is used to separate two gases. Membrane processes can deliver oxygen with low-medium purity levels; however, clogging is their main challenge.

2.4.3 Chemical looping process

A chemical looping system is a process to supply the required oxygen for oxidation (or partial oxidation) and contains two vessels: oxidation and reduction. A metallic particle (Me) circulates

between two vessels and serves as an oxygen transporter. In an oxidation reactor, which is usually called air reactor, the metallic particles (Me) adsorb oxygen from air at high temperature ($\sim$800 °C) and is converted to metal oxide (MeO). MeO is transferred to the reduction vessel, which is usually called fuel reactor. In a reduction reactor, MeO loses the oxygen that is in contact with a reducing agent. The reducing agent can be a gaseous fuel (CH_4), solid (coal, biomass) or even an inert media, like N_2. The fuel reactor is also working at high temperature ($\sim$800 °C). The reduced particles (Me) are transferred to the air reactor for regeneration. Using this configuration, oxygen is supplied without direct contact of fuel with air. Consequently, the outlet stream from the fuel reactor is free of nitrogen.

The oxides of Ni, Cu, Cd, Mn, and Fe, which have the ability to be reduced and oxidized periodically, have been studied as metal oxides for chemical looping systems. Considering the weight of metal oxide in its fully oxidized and fully reduced forms as m_{Oxi} and m_{Red}, the oxygen transport capacity (R) of a metal oxide is defined as follows:

$$R = \frac{m_{Oxi} - m_{Red}}{m_{Oxi}} \tag{2.13}$$

A higher oxygen carrying capacity results in a lower solid circulation rate. The oxidation-reduction rates are also very important parameters in designing a chemical looping system. A metal oxide with a high oxidation-reduction rate requires less residence time in the oxidizer-reducer to reach a certain conversion, which results in a smaller reactor. The metal oxide is subjected to high mechanical stress due to the intense solid-solid contact. Therefore, to improve its lifetime and durability, it is dispersed on a support (e.g., Al_2O_3, SiO_2). The metal oxide dispersed on the support is referred to as the oxygen carrier. The metal oxide should have a proper heat capacity, as besides carrying oxygen, it can serve as a heat transfer media. Therefore, a metal oxide with a high heat capacity can moderate the heat effect caused by endothermic or exothermic reactions to a greater extent [46]. Cost, resistance to contamination, melting point, physical durability, and environmental impacts are other factors that have to be considered in the selection of metal oxide.

2.5 Preparation of the oxygen carrier

2.5.1 Mechanical mixing

Mechanical mixing is the simplest and less expensive method to prepare a supported oxygen carrier. This process involves mechanically mixing of metal oxide with a support. A binder can be used to reinforce the metal oxide-support bond. Calcination and processing to the desired size are the next steps in mechanical mixing. Calcination persuades interactions between the support and metal and results in an oxygen carrier with a higher mechanical strength [46]. The homogeneity of the oxygen carrier prepared by mechanical mixing is poor, giving the oxygen carrier a metal oxide rich phase and a support rich phase. Therefore, for low melting point metal oxides (e.g., copper), mechanical mixing is not proposed to prepare the oxygen carrier [47].

2.5.2 Wet impregnation

The support is soaked in a metal nitrate solution and after mixing for a certain time, the solution is filtered and dried. Then the powder is calcined in air to decompose the nitrates into non-soluble oxides. The weight difference between the impregnated and fresh support indicates the oxide percentage in the support. This method can be repeated several times to achieve the desire oxide percentage. A part of the active phase forms on the outer layer, which has a weak bond with the support. This layer is attired after initial cycles and therefore, the oxygen carrier does not show the expected performance.

2.5.3 Incipient wetness impregnation

The difference between incipient wetness impregnation (also referred as dry impregnation) and wet impregnation is the volume of metal nitrate solution used. The amount of the metal nitrate solution is equal to the total pore volume of the support. Therefore, no nitrate solution is wasted during preparation. Like wet impregnation, drying and calcination are the next steps in preparation. Adding just enough solution to fill the total pore volume causes poor homogeneity in the final

product.

2.5.4 Co-precipitation

The metal and support sources, which are in liquid form, are mixed together. To precipitate the metal and support, a precipitating agent (e.g., alcohol) is added to the mixture. The precipitated powders are filtered and dried to remove the water. Finally the dried powders are calcined in air at high temperature to remove the impurities. The pH of the solution controls the precipitation rate of the support and metal sources [47]. Co-precipitation results in a more homogeneous mixture compared to impregnation.

2.5.5 Freeze granulation

In freeze granulation, the metal oxide and support are mixed with distilled water. To improve the homogeneity, polyacrylic acid can be added to the mixture as a dispersant. A fine powder slurry is then obtained by grounding the mixture in a milling instrument. Finally, the mixture is dried in a freeze dryer and is calcined at high temperature in air. The oxygen carrier prepared by freeze granulation is very homogenized in size and shape. However, like mechanical mixing, the metal oxide is not well dispersed on the support phase [48]. The metal oxide (MeO) and support (e.g., γ-Al_2O_3) after calcination can form a spinel structure ($MeAl_2O_4$):

$$MeO + Al_2O_3 \xrightarrow{calcination} MeAl_2O_4 \tag{2.14}$$

The spinel structure traps the metal oxide and therefore the oxygen of the oxide is no longer available for the fuel, which affects the performance of the oxygen carrier [49]. To avoid this effect, the spinel structure can be used itself as a support. Chemical looping systems can be used in combustion, H_2 production, gasification, and any other process that requires oxygen.

2.6 Chemical looping combustion-CLC

CLC is the most common application of chemical looping technology. Basically, chemical looping technology has been proposed first to produce pure carbon dioxide from carbon monoxide by copper oxides [50]. CLC of gaseous fuels (Figure 2.6) (e.g., methane or syngas) for power generation have been extensively explored during the last two decades [51, 52]. The possibility of using solid fuels (e.g., biomass or coal) in CLC has received more attention in the past 10 years [53–56]. The general reaction in the reduction reactor is as follows:

$$\textit{Reduction side}: \quad \mathrm{MeO} + \text{Solid or gaseous fuel} \longrightarrow \mathrm{Me} + \mathrm{CO_2} + \mathrm{H_2O} \tag{2.15}$$

H_2O is separated from CO_2 by condensation and CO_2 is sent for sequestration. Reaction 2.15 can be endothermic or exothermic depending on the type of oxygen carrier [46]. The general reaction in the oxidizer is as follow:

$$\textit{Oxidiation side}: \quad \mathrm{Me} + \mathrm{Air} \longrightarrow \mathrm{MeO} + \mathrm{O_2} + \mathrm{N_2} \tag{2.16}$$

Reaction 2.16 is always exothermic and can support some of the energy for the reduction side (if necessary) through sensible heat carried by the oxygen carrier.

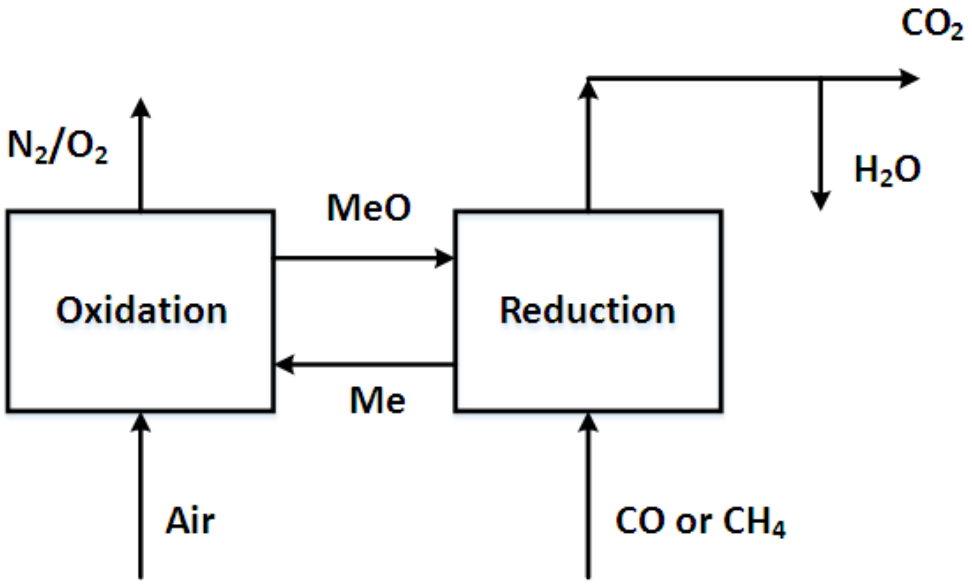

Figure 2.6 Chemical looping combustion of gaseous fuels

The most common configuration of the CLC of gaseous fuels is based on a low velocity bubbling fluidized bed as the reducer and a high velocity riser as the oxidizer [57]. In chemical looping combustion of solid fuels the solid-solid reaction rate between oxygen carrier and solid fuel is low. There are two approaches to this issue: in-situ gasification chemical looping combustion (iG-CLC) process; and chemical looping oxygen uncoupling (CLOU) process. In iG-CLC the solid fuel is first gasified with CO_2 and H_2O to CO and H_2. The released gas then reacts with the oxygen carrier and produces CO_2 and steam (Figure 2.7) [54]. The first step, which is the gasification of solids, is slow, thus a high solid residence time should be applied to reach a high conversion [57].

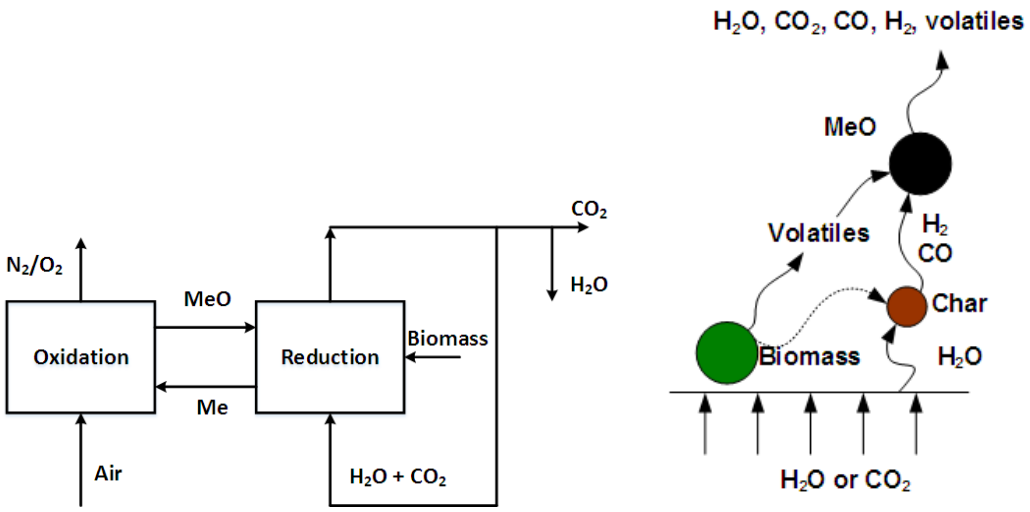

Figure 2.7 in situ gasification-chemical looping combustion process

In the CLOU process, the metal oxide is subjected to a lean oxygen atmosphere and releases (pumps) oxygen to the system. The oxygen reacts directly with solid fuels and volatile gases (Figure 2.8).

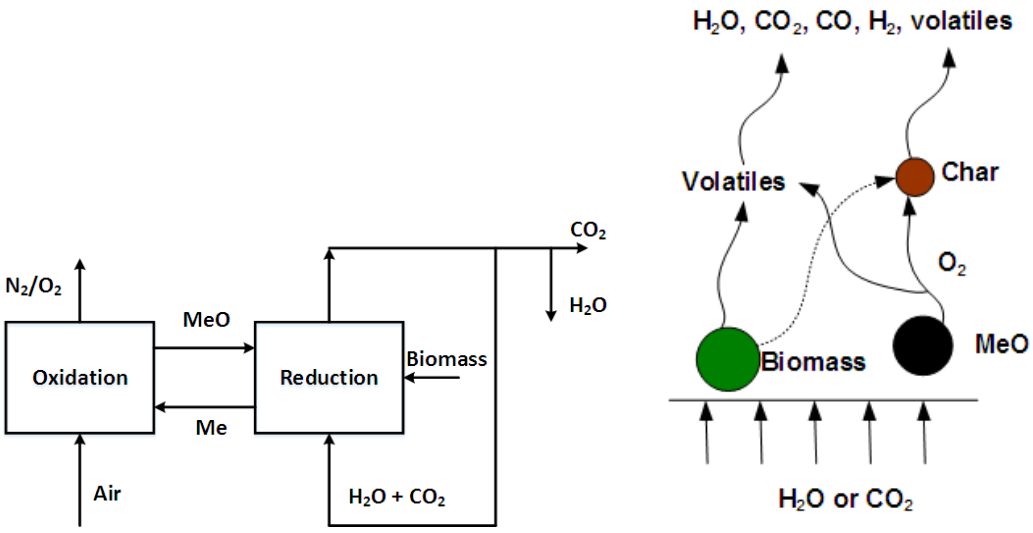

Figure 2.8 Chemical looping oxygen uncoupling process [57]

CLOU does not require the gasification step. However, only a limited number of oxygen carriers are able to release oxygen at high temperatures. CuO/Cu_2O, Mn_2O_3/Mn_3O_4 and Co_3O_4/CoO

systems have been reported as proper oxygen carriers for CLOU with the oxygen transport capacity of 0.1, 0.03 and 0.066 respectively [58].

$$2\,\mathrm{CuO} \longleftrightarrow \mathrm{Cu_2O} + \tfrac{1}{2}\,\mathrm{O_2(g)} \qquad \Delta H_{850} = 263.2\ \ kJ/molO_2 \tag{2.17}$$

$$3\,\mathrm{Mn_2O_3} \longleftrightarrow 2\,\mathrm{Mn_3O_4} + \tfrac{1}{2}\,\mathrm{O_2(g)} \qquad \Delta H_{850} = 193.9\ \ kJ/molO_2 \tag{2.18}$$

$$\mathrm{Co_3O_4} \longleftrightarrow 3\,\mathrm{CoO} + \tfrac{1}{2}\,\mathrm{O_2(g)} \qquad \Delta H_{850} = 408.2\ \ kJ/molO_2 \tag{2.19}$$

Copper is the most studied oxygen carrier for the CLOU process. The agglomeration possibility of copper is less in CLOU compared to the normal CLC process because copper presents as CuO and Cu_2O and it never reduced completely to pure copper. The melting point of CuO and Cu_2O are 1446 and 1235 °C respectively, which are higher than pure copper (1085 °C). A 1.5 KW_{th} ICB-CSIC unit working with copper as the oxygen carrier and bituminous Colombian coal as the fuel is the only proof of concept for CLOU technology, which was developed by Adanez-Rubio et al. [59]. They have reported a 97 % conversion of char at 940 °C with no un-burnt volatile matter at the reactor outlet. Cobalt has a moderate oxygen transport capacity (6.6 %) but it has been researched less due to the high cost and high amount of required energy for decomposition (Equation 2.19). Manganese is also less attractive due to its low oxygen transport capacity.

2.7 Chemical looping process for H_2 production

Chemical looping water splitting (CLWS) is a new technology to produce pure H_2 using the chemical looping concept. The CLWS is exactly like CLC with the difference that in the oxidation reactor steam is used to oxidize (or partially oxidize) the metal oxide. Therefore, water is hydrolysis to H_2 and O_2 and the hydrogen is separated by condensation from water in the outlet stream (Figure 2.9).

Table 2.1 Operating CLC system

Name	Capacity	Fuel	Temperature (^oC)	Oxygen carrier	Reference
CLC of gaseous fuels					
The Chalmers University	10-kW_{th}	Methane	950	$NiO/NiAl_2O_4$	Lyngfelt and Thunman[60]
(CSIC) System	10-kW_{th}	75 %N_2+ 25 % CH_4	700-800	CuO/γ-Al_2O_3	de Diego et al. [61]
VUT CLC System	120-kW_{th}	Natural gas	850-940	$NiO/NiAl_2O_4$ 50 % +	Kolbitsch et al. [62]
					Proll at al. [63]
				$NiO/(NiAl_2O_4$-$MgAl_2O_4)$ 50 %	
KIER CLC System	50-kW_{th}	CH_4	869-890	$NiO/Bentonite$	Ryu et al. [64]
				$Co_xO_y/CoAl_2O_4$	
CLC of solid fuels					
Modified Chalmers University	10-kW_{th}	South African coal	950	Ilmenite	Berguerand and Lyngfelt [65]
		Petroleum coke			Berguerand and Lyngfelt[66]
Southeast University	10-kW_{th}	Coal	960-970	NiO/Al_2O_3	Shen et al. [67, 68]
		Biomass		Fe_2O_3	Shen et al. [69]
ICB-CSIC	1.5-kW_{th}	Bituminous coal	900-960	CuO	Adanez-Rubio et al. [59]

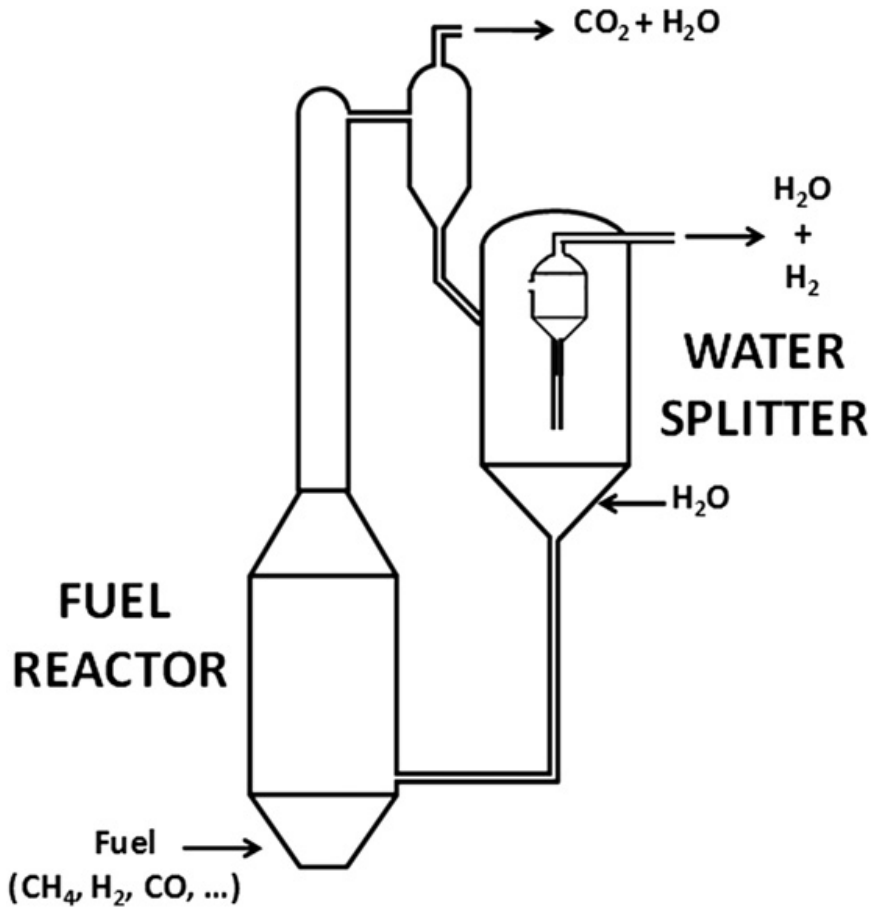

Figure 2.9 Chemical looping water splitting for hydrogen production [70]

The metal oxide used for water splitting should be able to use water as the oxidant, which makes it different from conventional metal oxides for CLC. FeO/Fe_3O_4 is the most studied metal oxide for hydrogen production [70] with the governing equations as follows:

$$\textit{Reduction side}: \quad Fe_3O_4 + CH_4 \longrightarrow 2FeO + CO_2 + 2H_2O \quad \Delta H_{873K} = 325 \ \ kJ/mol \tag{2.20}$$

$$\textit{Oxidation side}: \quad 3FeO + H_2O \longrightarrow Fe_3O_4 + H_2 \quad \Delta H_{873K} = -58 \ \ kJ/mol \tag{2.21}$$

Chiesa and Lozza [71] have shown that water is not able to completely regenerate the metal oxide. Therefore, they proposed a complete oxidation of metal oxides with air in a third reactor before transferring to the reduction reactor.

2.8 Chemical looping Gasification-CLG

Despite all the advantages of gasification over combustion, including the production of liquid fuels and synthetic materials, the application of chemical looping technology in gasification has not been explored extensively in the literature. Hofbauer et al. [72, 73] are among the few researchers who applied chemical looping technology to produce syngas from the gasification of organic material. Basically, they used a chemical looping system working with olivine to supply the required energy for steam gasification. Steam gasification of biomass (reaction 2.9) and water-gas shift reactions (reaction 2.10) are the governing reactions that take place during steam gasification. A part of the un-reacted biomass (char) is transferred to a combustion reactor where it is burned with air. Olivine particles circulate between combustion and gasification sections and transfer produced heat from combustor to gasifier (Figure 2.10).

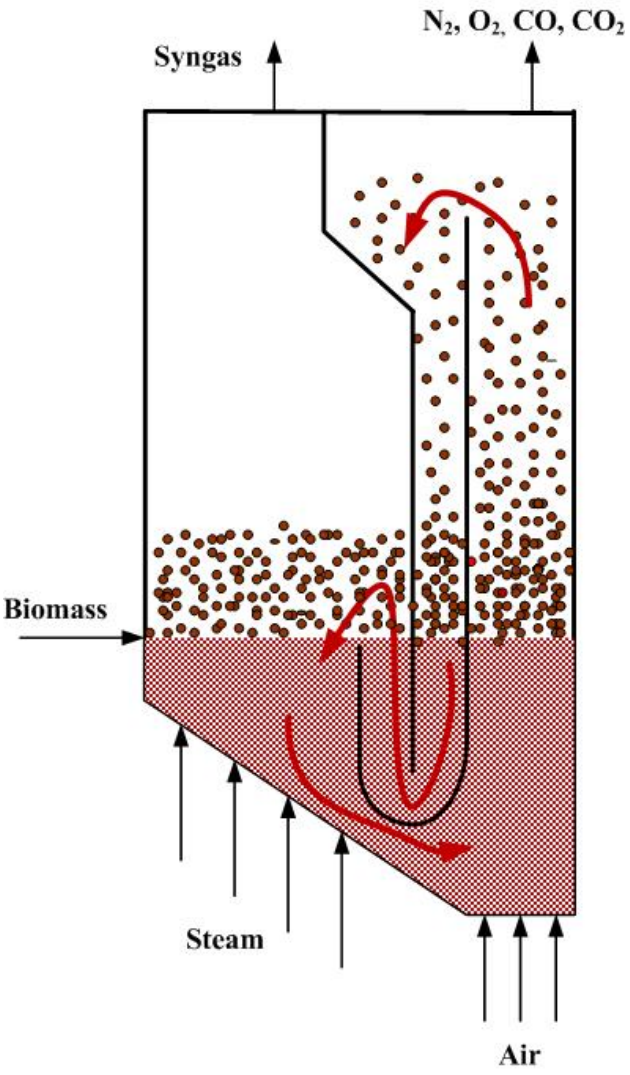

Figure 2.10 The Fast Internally Circulating Fluidized Bed (FICFB) gasification system, the arrows correspond to the solid circulation between two sections

This process was later commercialized by AE&E, Repotec and Ortner Angenbau to produce high purity syngas. The syngas produced using this technology is concentrated in hydrogen and the H_2/CO ratio is >4 [74], which is not suitable for liquid fuel synthesis. Furthermore, the CO_2 from the combustion of un-burnt char in the combustor is sent into the atmosphere. Olivine as a bed material serves as a heat carrier rather than an oxygen carrier. Lancee et al. [75] used the same concept and olivine as bed material for biomass gasification. Besides the heat carriage of olivine, they reported that the iron in the olivine has a catalytic effect on tar cracking. Also, iron

is capable of releasing oxygen to the gasifier, which compensates the endothermicity of the steam gasification. Calcium oxide can be also used as a circulating material instead of olivine. Using calcium oxide not only provides the required energy, it serves to remove the CO_2 and H_2S from the gasifier (Reactions 2.22 and 2.23) and a syngas with high purity [76].

$$CaO + CO_2 \longleftrightarrow CaCO_3 \tag{2.22}$$

$$CaO + H_2S \longrightarrow CaS + H_2O \tag{2.23}$$

2.9 Summary

Solid fuels, especially biomass compared to fossil fuels, are more abundant and inexpensive, which should encourage us to develop a process to utilize them in the industry. Gasification as a tool to convert invaluable solid fuels to syngas has been proven to be more beneficial over combustion if the liquid products were interesting. Using air as a gasifying agent dilutes the produced syngas and for post-processing units the separation of nitrogen is required. The chemical looping concept is a promising technology to supply oxygen indirectly. There is a chance to integrate gasification with the chemical looping concept to produce a high purity syngas free of nitrogen. Chemical looping has been extensively studied for the combustion of gaseous and solid fuels as well as H_2 production. These applications require high amounts of oxygen for complete oxidation. On the other hand chemical looping is not very effective in terms of oxygen supplier. Therefore, it might be asked that why the chemical looping concept has not been used extensively in the literature for gasification, which requires less oxygen (20-30 % of the oxygen required for combustion).

The oxygen uncoupling materials which are able to release oxygen at high temperature have been used in combustion of solid fuel. However, their application for the gasification of solid fuels has never been tried. The proposed biomass gasification process by Hofbauer et al. [72] is very interesting in terms of self producing energy process. However, the H_2/CO ratio is greater than 4 which is not suitable for post syngas processing (Fischer-Tropsch or methanol production).

Keeping the same reactor configuration (as Hofbauer et al. [72]) in this thesis, we have tried to replace the olivine with an uncoupling oxygen carrier. It is predicted that the released oxygen in the gasifier not only will provide required heat for the steam gasification, it will increase the CO yield and consequently lower the H_2/CO ratio.

CHAPTER: 3

COHERENCE OF THE ARTICLES

Chapters 4 to 6 are the main body of this thesis and include, in general, the oxygen carrier selection, the effect of the oxygen carrier on the biomass gasification, and the economic analysis which answer the specific objectives of this research. More specifically, they cover the following topics:

– Chapter 4 includes the first article entitled "TGA and kinetic modeling of Co, Mn and Cu oxides for Chemical Looping Gasification (CLG)". The oxygen carriers were prepared via incipient wetness impregnation. The oxygen transport capacity, the temperature in which the oxygen carrier reacts with oxygen and releases oxygen, and the oxidation-reduction rates of oxygen carriers were compared by the thermo-gravimetric analysis. The total surface area and XRD pattern of the fresh and used oxygen carriers were measured to compare the thermal strength. Finally, a new model was derived to predict the reduction-oxidation rates. The new model takes into account the effect of the reverse reaction in the oxygen release from the oxygen carrier;

– In Chapter 5 the second article, "Transient modeling of biomass steam gasification with Co_3O_4" was presented. After the selection of the oxygen carrier, its performance in the presence of biomass was tested in a 7.8 cm fluidized bed reactor. Tar and sticky liquids form during biomass gasification which can deactivate the oxygen carrier and affect its performance. In addition to the effect of the oxygen carrier, the effects of steam and temperature on the product gas composition have been measured. A two phase model was proposed for the gas phase hydrodynamic in the dense bed region. The hydrodynamic model was verified by performing a residence time distribution test of argon. Using the proposed hydrodynamic

model and the oxygen desorption rate from the first article together with the reaction rate expression from the literature, the CO, CH_4, H_2 and CO_2 composition was calculated along the reactor and the results were compared with the experimental data;

– Chapter 6 includes the third article entitled “Design and economical analysis of a chemical looping gasification process”. Using the kinetic data obtained in the first and second paper, a chemical looping gasifier to treat 86.4 t/d, including a bubbling fluidized bed as the gasifier and a high velocity riser as the oxidizer was designed. The objectives of the preliminary design were to calculate the diameter and height of the gasifier and oxidizer. The height of the gasifier was calculated based on the required steam residence time to reach 90 % biomass conversion. Also, the oxidizer height was calculated based on the required residence time of the oxygen carrier for regeneration. Furthermore, the possibility of an autothermal gasification using a chemical looping system has been studied. Finally, an economical analysis has been performed to compare the feasibility of a chemical looping gasifier and a conventional gasification process.

CHAPTER: 4

ARTICLE 1: TGA AND KINETIC MODELING OF Co, Mn, AND Cu OXIDES FOR CHEMICAL LOOPING GASIFICATION (CLG)

Milad Aghabararnejad, Gregory S. Patience, Jamal Chaouki

Department of Chemical Engineering, Polytechnique Montréal, C.P. 6079, Succ. CV Montréal, H3C 3A7 Québec, Canada

This work is in press in the journal: *The Canadian Journal of Chemical Engineering* (2014)

Abstract

Oxygen carriers for biomass gasification are capable of absorbing oxygen from air and desorbing it in the gasifier. Based on thermodynamic equilibrium, copper, manganese, and cobalt oxides have the highest oxygen release capacities among the different oxygen carriers. These oxygen carriers were deposited on alumina via incipient wetness impregnation. The weight loss of the CuO-Cu_2O carrier, as measured in a thermo-gravimetric analyzer, was 10 % while it was 7 % for the Co_3O_4-CoO couple and only 3 % for the Mn_2O_3-Mn_3O_4 couple. The optimum operating temperature for the CuO oxygen carrier was 100 °C *higher compared to the other two at* 950 °C*. A modified nuclei growth model (MNG) characterizes the weight loss/gain during the reduction-oxidation cycles. The reduction rate is 3 times higher at* 875 °C *compared to* 825 °C *while the oxidation rate decreases more than 10 times. The CuO carrier surface area decreased by 70 %, while it was 30 % and 60 % in the Co_3O_4 and Mn_2O_3 carriers, respectively. Cobalt has a lower tendency to sinter at high temperature compared to either copper or manganese and has a higher oxygen transport capacity and oxidation-reduction rates. Therefore, despite its higher cost and toxicity, it might be considered as a potential oxygen carrier especially for solid fuel gasification.*

Keywords: *Biomass Gasification, Oxygen Carrier, Oxygen Desorption, Kinetic Modeling.*

4.1 Introduction

In recent years, interest in biomass as an energy source has increased considerably due to the elevated price of fossil fuels and a desire to reduce emissions of carbon dioxide since it returns carbon to the atmosphere. Biomass as an energy vector is common for heating applications, power generation, and domestic cooking (particularly in developing countries). Regardless of these advantages, low heating value and transportation logistics impede the use of biomass as a primary energy source.

Gasification is superior, among alternative processes, for converting biomass to energy because

of its excellent efficiency and capability of producing syngas, which is a precursor to synthesis fuels and chemicals [1]. It converts carbon to carbon monoxide and hydrogen. Overall, the gasification reactions are endothermic; therefore, an energy source is required to drive the reaction [2]. One possible energy source is to partially combust biomass with air. However, the resulting product gas has a low calorific value (4-6 MJ/m^3) and a high nitrogen content of 45-55 %. A gas with low nitrogen content and a high calorific value (12 MJ/m^3) is produced with pure oxygen as a gasification agent but oxygen separation is costly [3]. Chemical looping process is an alternative to provide the required oxygen for gasification or any other partial or selective oxidation. Chemical looping technology was first developed as a means to capture CO_2 during combustion, but it has been further developed toward gasification because it requires less oxygen compared to combustion and producing oxygen is limited in chemical looping processes.

4.1.1 Process description

In chemical looping combustion (CLC), CO_2 and water vapour are produced in a concentrated stream ready for sequestration. It is based on circulating an oxygen carrier between a reduction zone, in which the oxygen from the solid reacts with the reducing agent and an oxidation zone where the metal is re-oxidized by air. Figure 4.1 shows the steam gasification of biomass in a circulating fluidized bed [3]. The gasifier consists of two interconnected fluidized beds. In the gasification unit, the biomass is gasified at 850 °C by steam. Non-gasified carbon (charcoal) is transported by olivine from the gasifier into the combustion chamber where it combusts. This exothermic reaction heats the bed material, which is returned to the gasifier, providing energy for the gasification of the biomass.

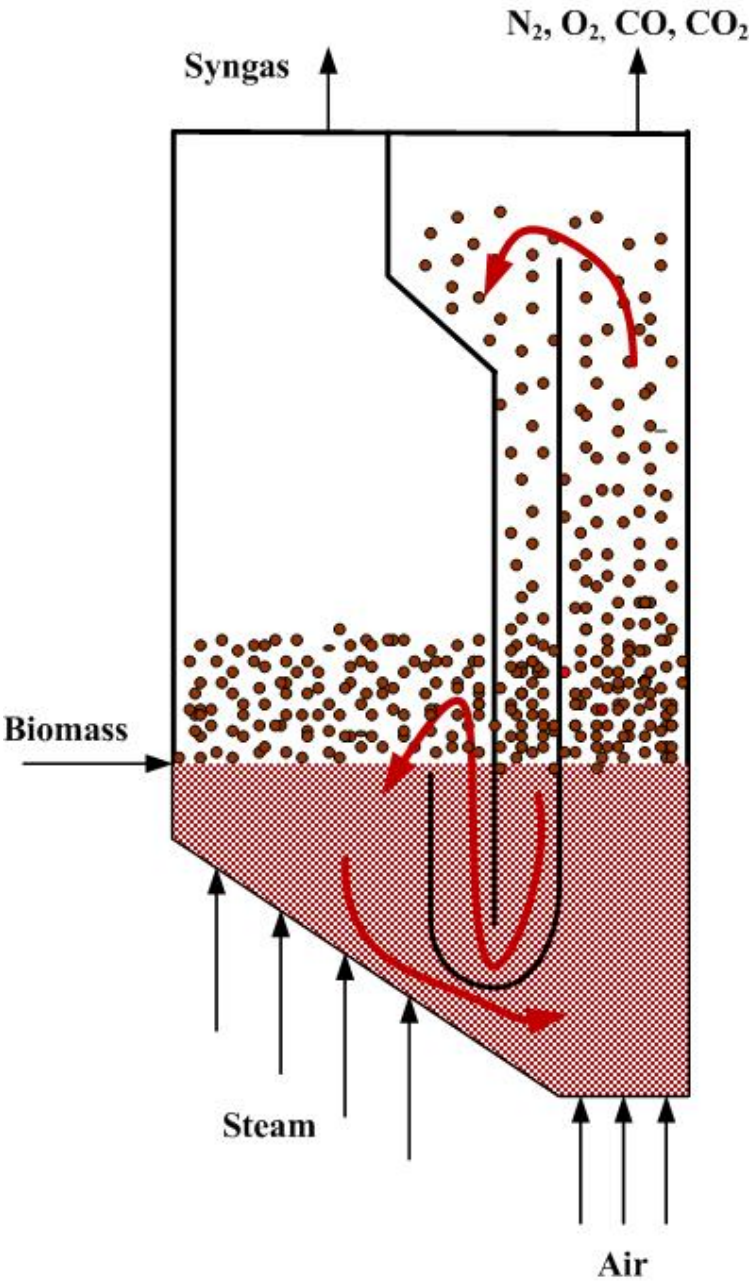

Figure 4.1 Circulating fluidized bed gasifier, the arrows correspond to the solid circulation between two sections

We propose using an oxygen carrier instead of olivine as both a heat source to drive the gasification reactions as well as an oxygen source (replacing or supplementing water vapour). The oxygen carrier is reduced in the gasifier and transferred to the regenerator where it is re-oxidized by air. The flue gas from the regenerator contains predominantly nitrogen and non-reacted oxygen, and a

small amount of carbon dioxide. The flue gas on the fuel side contains mainly CO, hydrogen, and water vapour. With this concept, it is possible to produce a high-grade syngas that is nearly free of nitrogen without using pure oxygen. The required heat for the gasification is supplied by the oxidation of the metal in the air reactor and partial oxidation of biomass by the oxygen carrier in the fuel reactor. The syngas can be burned for energy production or it can be used for synthetic fuels. We anticipate that this concept will have a lower investment cost compared to the current CFB gasification technologies and possibly superior thermal management. Both sides (fuel reactor and oxidation reactor) work at elevated temperatures (850 °C), and solid particles are subjected to high mechanical and thermal stresses. Chemical looping systems were first developed for methane combustion. In recent years, solid fuels have received more attention as feed stock for combustion and gasification. This work highlights the process operation with solid fuels, specifically biomass.

4.1.2 Solid fuel gasification in chemical looping systems

Two processes have been proposed for solid fuel gasification in a chemical looping system:

1. iG-CLC (in-situ gasification chemical looping combustion);
2. CLOU (chemical looping with oxygen uncoupling).

In the former process, biomass reacts with H_2O or CO_2 to form H_2 and CO, and the produced gases react with metal oxide (MeO) as described in Figure 4.2. In the latter process, biomass reacts with steam and gaseous oxygen (Figure 4.1), which is released by the oxygen carrier [4–6].

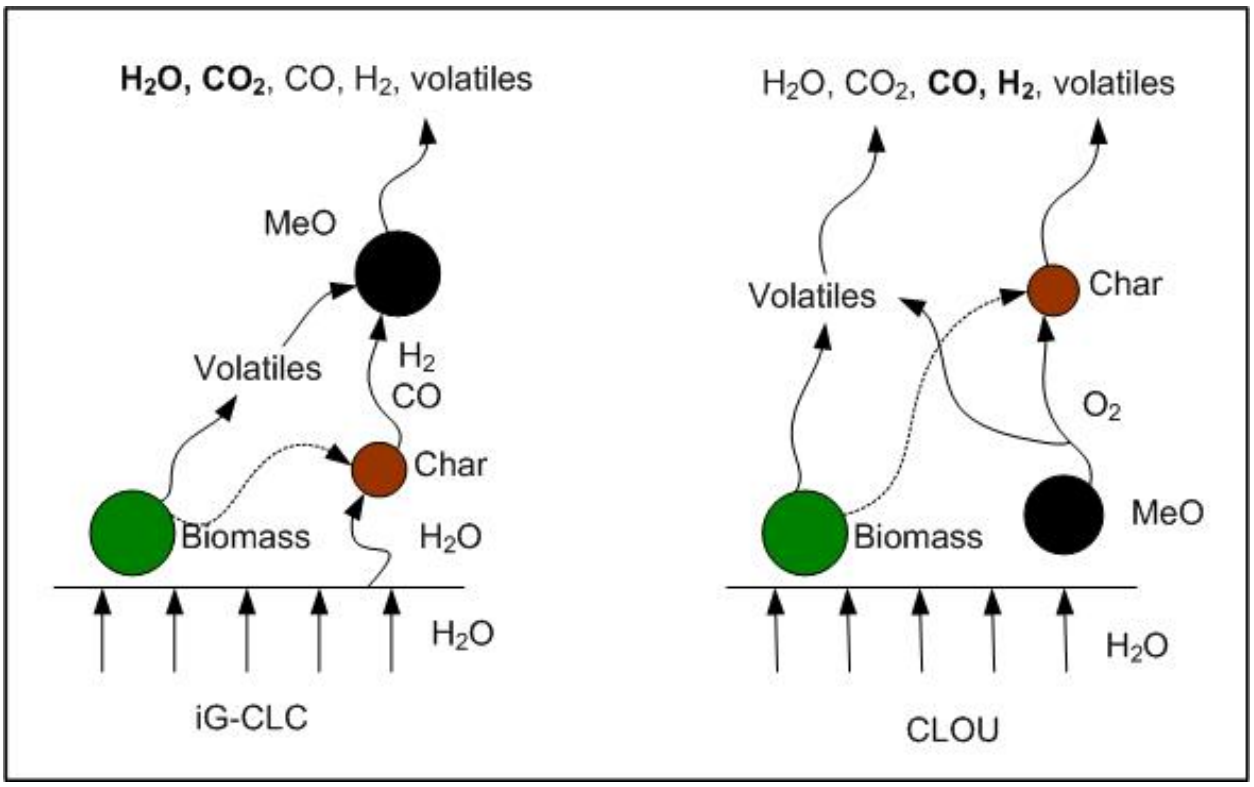

Figure 4.2 Mechanisms of iG-CLC and CLOU (Modified from Adanez et al. [4]

The CLOU process overcomes the low reactivity of the char gasification step of the iG-CLC process. The following reactions occur in the oxidation and fuel reactors:

$$Oxidation\ zone : Me_xO_{y-1}(\mathrm{s}) + 0\cdot 5\,\mathrm{O_2(g)} \longrightarrow Me_xO_y(\mathrm{s}) + \mathrm{Q} \tag{4.1}$$

$$Gasification\ zone : \begin{cases} Me_xO_y(s) + Q \rightarrow Me_xO_{y-1}(s) + \frac{1}{2}O_2(g) \\ biomass + steam + O_2 \rightarrow H_2 + CO + ash + Q \end{cases} \tag{4.2}$$

$$Total\ reaction : biomass + steam + Me_xO_y(s) \rightarrow H_2 + CO + ash + Me_xO_{y-1}(s) \tag{4.3}$$

The steam, biomass, and solid circulation rate is adjusted to minimize the required heat in the gasifier. Releasing oxygen distinguishes CLOU from chemical looping combustion (CLC). Metal oxides containing copper, manganese, and cobalt have this property [7]. Moghtaderi considered the application of the chemical looping process for the separation of oxygen from air [8]. He performed some thermodynamic calculations and preliminary experiments on oxides of Cu(CuO/Cu_2O), Mn (Mn_2O_3/Mn_3O_4), and Co(Co_3O_4/CoO). He reported that a mixture of 50 % Co and 50 % Mn is feasible for a CLC process. Shah et al. tested the performance of 40 different oxygen carriers using thermodynamic calculations [7]. They identified cobalt and copper as superior oxygen carriers for chemical looping air separation. Shah et al. recommended Al_2O_3 and SiO_2 supports for cobalt and copper, respectively, to avoid the mixed oxide phases or the spinel structures [7].

Leion et al. combusted coal with Ni based oxygen carriers [9]. The fuel conversion was slower with increasing sulfur content. Cao et al. investigated the CLC of coal, biomass, and waste solid as solid fuels and CuO as oxygen carrier [10]. They presented the concept of CLC of solid fuels using a circulating fluidized bed with three loop seals: the riser of the circulating fluidized bed as the oxidizer, one of the loop seals as the reducer of the oxygen carrier and the separator for ash and oxygen carrier, and the other loop seal was used for pressure balance in the solid recycle process. Adanez-Rubio et al. developed a CuO oxygen carrier for the combustion of solid fuels [11]. They compared the oxygen transfer capacity of various carriers prepared by incipient wetness impregnation, mechanical mixing, extrusion, and pelletizing by pressure, in a TGA.

Eyring et al. combusted coal with CuO in which oxygen was released during the phase change of cupric oxide (CuO, black) to cuprous oxide (Cu_2O, red) at 950 °C [12]. Their thermo gravimetric analysis showed 10 % weight change from complete oxidation (in air) to complete reduction (in N_2). Also, they reported that raising the temperature favours the reduction of cupric oxide. The most common oxygen carrier for CLUO is CuO followed by Mn_3O_4 (Table 4.1).

Table 4.1 Summary of oxygen-carrier particles prepared and tested for CLOU application

MeO 1 (wt %)	MeO 2 (wt %)	Support	Preparation	Facility	Reacting gas or fuel
CuO					
60		Al_2O_3	FG	bFB	CH_4, coke, air [5, 6]
40		ZrO_2	FG	bFB	Coke, coal, char, air [9]
N.A.		SiO_2	N.A.	TGA, bFB	Coke, N_2, air [12]
15, 33		$\gamma - Al2O3$	IMP	TGA	N_2, CO_2, air [13]
15, 21		$MgAl_2O_4$	IMP	TGA	N_2, CO_2, air [13]
60, 80		Al_2O_3	MM+PE	TGA	N_2, CO_2, air [13]
80		Sepiolite, SiO_2, TiO_2, ZrO_2	MM+PE	TGA	N_2, CO_2, air [13]
60		$MgAl_2O_4$, Sepiolite, MgO	MM+PP	TGA, bFB	N_2, CO_2, air [13]
40		ZrO_2	MM+PP	TGA, bFB	N_2, CO_2, air [13]
60		$MgAl_2O_4$	SD	1500 W	Coal [14]
Mn_3O_4					
80		SiO_2	FG	bFB	CH_4, air [15]
60, 63		ZrO_2	FG	bFB	5 % O_2, 50 % CH_4 [16]
65.4		MgO	FG	bFB	N_2, 10 % O_2, CH_4 [17]
80-60	Fe_2O_3(20-40)		FG	bFB	CH_4, air [15]
80-20	Fe_2O_3(20-80)		SD	bFB	CH_4, Coke, coal [18]
79.3-19.3	Fe_2O_3(20-80)		SD	bFB	N_2, CH_4, Char, 5 %O_2 [18]
80	NiO(20)		FG	bFB	CH_4, air [15]

FG: Freeze granulation, IMP: Impregnation, N.A.: Not applicable, bFB: Bubbling fluidized bed,
MM: Mechanical mixing, PE: Pelletizing by extrusion, PP: Pelletizing by pressure, SD: Spray drying,
TGA: Thermo-gravimetric analysis, CLOU: Chemical looping oxygen uncoupling, N.A.: Not applicable

The solid circulation rate between the fuel reactor and regenerator depends on the oxygen carrying capacity (OXO capacity). On the other hand, solid inventory depends on the oxygen carrying capacity as well as oxidation-reduction rates. As a consequence, the oxygen carrier has a direct impact on capital and variable costs. Developing an oxygen carrier with an elevated OXO capacity is essential for an economically feasible process. Copper and manganese or a combination of these metals have been used as oxygen carriers while cobalt has been largely ignored. Copper releases oxygen at 950 °C [12] and has a tendency to agglomerate. Manganese has a very low oxygen transport capacity (3 % of its initial mass), which is three times less than copper. Cobalt is more expensive and has a higher toxicity compared to Cu or Mn. In this study, the oxygen release capacity of copper, manganese, and cobalt were measured in a TGA by alternating the gas phase between air and nitrogen. We propose using Co_3O_4/Al_2O_3 for biomass gasification to supply both heat and oxygen, which has not been described in the literature. Furthermore, a kinetic model was derived for both the CoO oxidation and Co_3O_4 reduction. The thermal stability was also evaluated by measuring the change in surface area before and after the reaction.

4.2 Experiment

4.2.1 Materials

Copper, manganese and cobalt oxides were prepared by incipient wetness impregnation. The nitrate hydrate was used as a precursor (Table 4.2).

Table 4.2 Incipient wetness impregnation for preparation of supported oxygen carrier

Oxygen carrier	Precursor	Solubility g/100 ml	g of salt
Copper	$Cu(NO_3)_2.\ 2.5H_2O$	138 at 0 ^oC	18.3
Manganese	$Mn(NO_3)_2.\ 4H_2O$	380 at 20 ^oC	22.8
Cobalt	$Co(NO_3)_2.\ 6H_2O$	134 at 0 ^oC	25

The precursor was dissolved in 50 ml of deionized water. Next, 10 g of activated alumina with an average size of 130 μm was gradually added as a binder to the solution. The solution was filtered after 30 min of mixing. The filtrate was dried at 140 °C for 12 hours. In each impregnation step, a portion of the active phase settles on the support. The impregnation step was repeated to reach the desired concentration of the active phase (around 25 % in this case). Finally, the powders were calcined at 850 °C for 5 hours in air. During the calcinations, the reaction between metal and support to form a spinel structure is possible. This will decrease the available metal content for the oxidation and reduction and, therefore, decrease the oxygen transport capacity of the oxygen carrier. To avoid this issue some authors proposed to use the spinel structure itself as the support. For instance, Mattisson et al. [19] used $NiAl_2O_3$ as support for NiO oxygen carrier.

Wood sawdust with an average particle size of 200 μm was used as the biomass source. It was 48 % carbon with 81 % volatile matter, 16 % char, and 3 % ash (Table 4.3).

Table 4.3 Biomass elemental and proximate analysis

Elemental (wt %)		Proximate (wt %)	
C	48	Char	16
H	6.2	Volatile	81
O	45	Ash	3
N	0.2		
S	0.6		

4.2.2 Methods and techniques

Thermo-gravimetric analysis was performed in a Mettler Toledo (TGA/SDT A851) analyzer working at atmospheric pressure. Thirty milligrams of oxygen carrier was loaded to a 70 μl (inside diameter of 6 mm and height of 4.5 mm) alumina crucible, and the weight changes were monitored at a frequency of 1 Hz. The oxygen release temperature of the oxygen carrier was determined by raising the temperature from 25-1100 °C at a rate of 10 °C/min. Three gases were used: air (21 % O_2), 5 % O_2 (balance argon) and pure nitrogen. To simulate the chemical looping cycles, the temperature was raised from 25 to 825, 850 °C, and 875 °C at 10 °C/min in nitrogen. Then, the oxygen carrier was cycled between air and nitrogen alternatively for 30 min. Preliminary experiments have shown that the oxidation-reduction reactions are the rate limiting steps and gas flow, and sample loading and particle size have insignificant effects on the reaction rate at the studied operating conditions. The gas flow was maintained at 50 ml/min in all experiments, which minimized the external mass and heat transfer resistances from the bulk of the gas to the surface of the particles. Furthermore, intra-particle diffusion effects were minimized using small quantities of particles (30 mg) and moderate packing. The heating rate was minimized to achieve equilibrium at each temperature so that oxygen has sufficient time to react with the oxygen carrier. The weight loss data corresponds to a sample containing only 25 % of the active phase. Most literature data report weight loss based on 100 % of the active phase. Therefore, we have multiplied our experimental results by a factor of 4 to put it on the same basis.

The XRD pattern was measured with a Bruker AXS X-ray goniometer equipped with a Hi-STAR two-dimensional area detector. The generator was set at 50 kV and 40 mA and the copper CuK radiation (λ = 1.542 A) was selected using a graphite crystal mono-chromator. The surface area of the particles was measured before and after the reaction with adsorption of nitrogen in an autosorb-1 BET instrument from Quantachrome. Before the measurements, samples were degassed at 250 °C for three hours. The particle size distribution of the samples was measured by a Horiba particle size analyzer.

4.3 Results and discussion

The suitability of a metal oxide as an oxygen carrier for biomass gasification depends on its oxygen release capacity, rate of oxygen desorption and adsorption, thermal resistance, and resistance to poisoning due to NH_3, chlorine, and especially sulfur species.

4.3.1 Oxygen release capacity by TGA

The temperature at which oxygen carriers begin to release oxygen depends on the partial pressure of oxygen in the reaction atmosphere. To see this effect, 30 mg of metallic oxide was placed in TGA and the temperature was raised from ambient to 1100 °C. In a nitrogen atmosphere, the CuO begins to lose weight at about 850 °C and by 950 °C it loses 10 % (Figure 4.3-a). In a 5 % O_2 atmosphere it releases oxygen at 950 °C and at 990 °C the weight loss is complete. In air oxygen release began at 1050 °C and at 1070 °C it reduces the same load as the other two conditions.

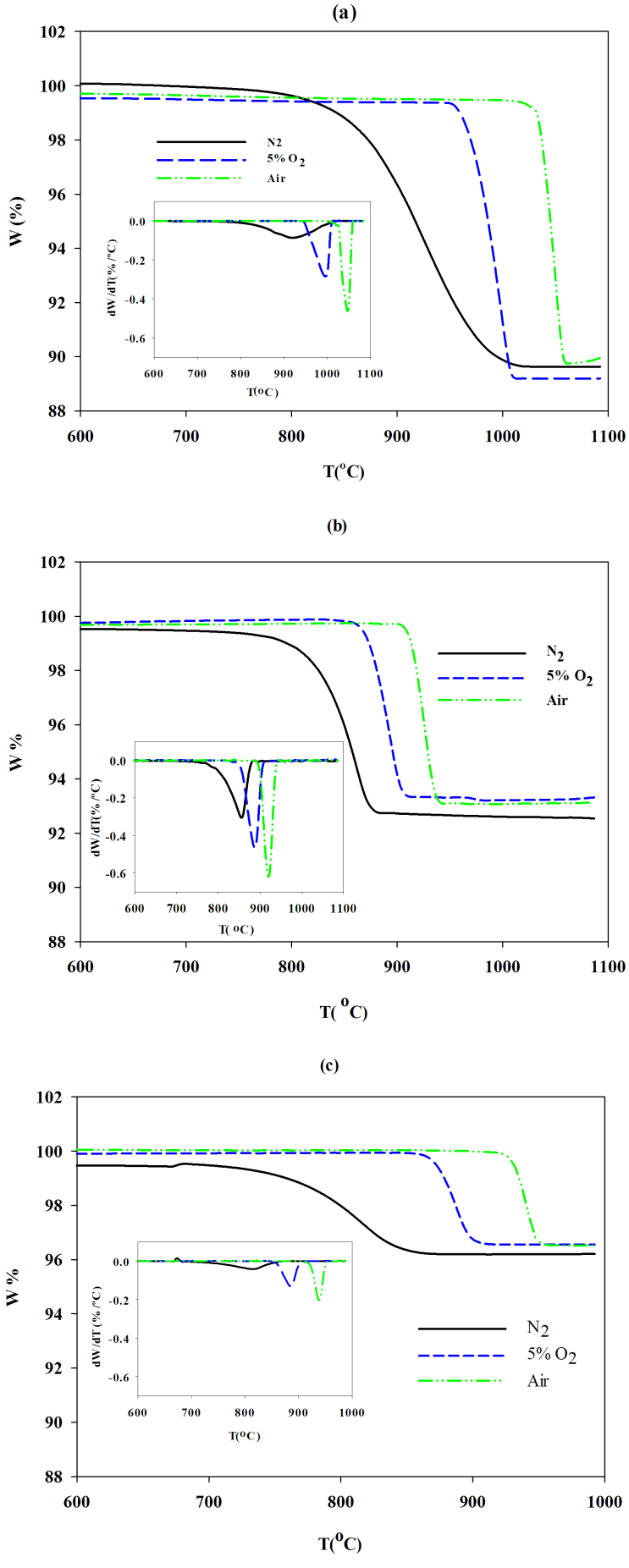

Figure 4.3 The profile of weight loss and rate with temperature in (0%, 5% and 21% O_2) for a)

The Co_3O_4 starts to release oxygen at about 750 °C and by 860 °C, it loses 7 % (Figure 4.3-b) in nitrogen. In a 5 % O_2 atmosphere, the oxygen desorption happens at 850 °C, and at 900 °C, the weight lost is complete. In air, weight lost began at 920 °C, and at 950 °C, it completes. For Mn_2O_3, the weight lost starts and completes at lower temperatures compared to cobalt and copper (Figure 4.3-c).

The weight of CuO, Co_3O_4, and Mn_2O_3 dropped by 10, 7, and 3 %, respectively, which is in agreement with the expectation based on the stoichiometry.

$$2\,CuO \longleftrightarrow Cu_2O + \tfrac{1}{2}\,O_2 \tag{4.4}$$

$$Co_3O_4 \longleftrightarrow 3\,CoO + \tfrac{1}{2}\,O_2 \tag{4.5}$$

$$3\,Mn_2O_3 \longleftrightarrow 2\,Mn_3O_4 + \tfrac{1}{2}\,O_2 \tag{4.6}$$

The temperature at which the MeO releases oxygen increases with increasing oxygen concentration. The trend was confirmed by thermodynamics using Factsage 6.4 (Figure 4.4) by considering the reactions as equilibrium at different temperatures. The relative error between simulation and experimental data for Mn, Co, and Cu, are respectively: 4.7, 3.8, and 2.5 %.

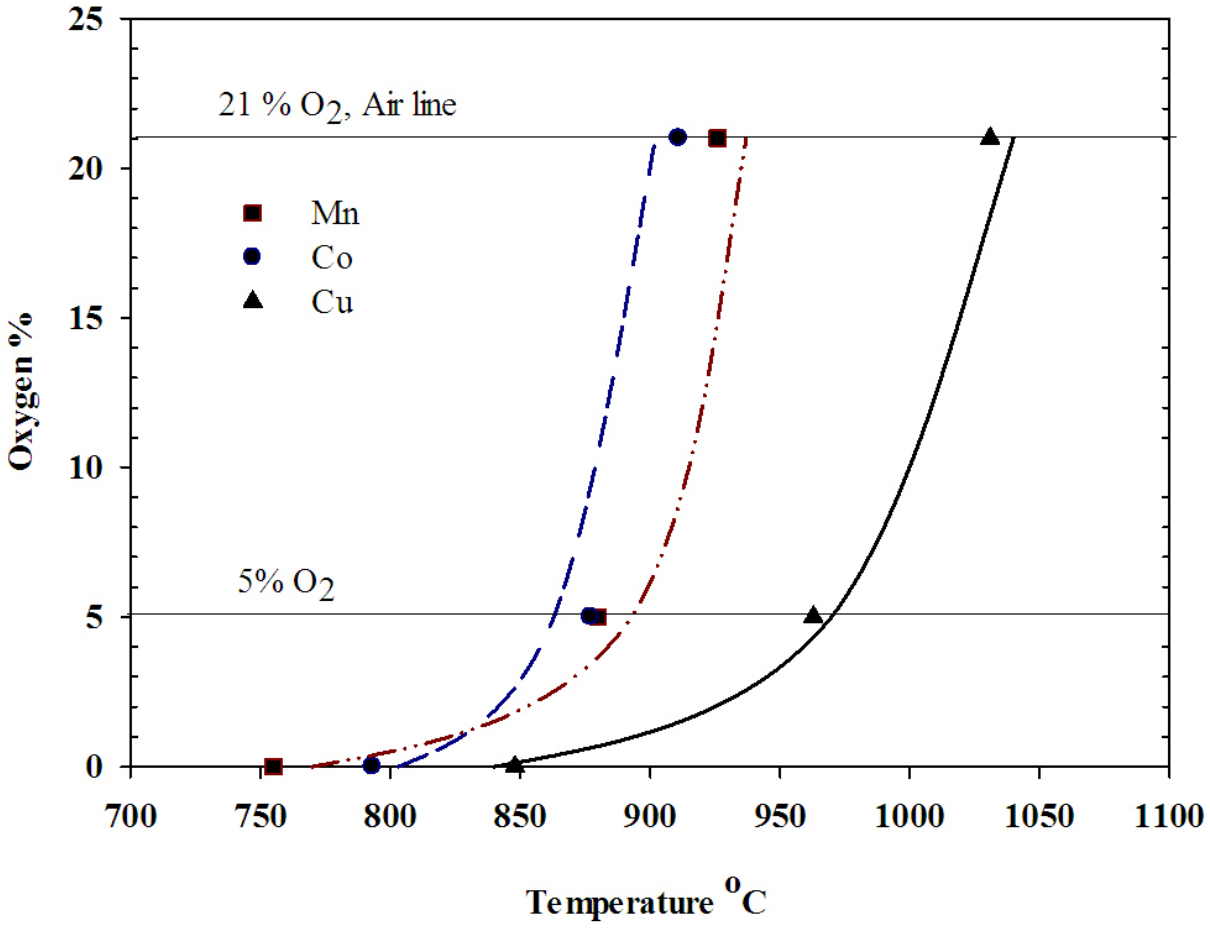

Figure 4.4 The initial temperature of reduction in different oxygen concentrations, Experimental data and equilibrium curve by FactSage 6.4 software, Cu (——), Mn (– ·· –), Co (– – –)

The left side of each curve represents the situation in which the oxidized phase of metal is stable while the right side corresponds to the reduced phase. Cobalt and manganese release oxygen at a lower temperature compared to copper; while, copper, has the highest amount of available oxygen (10 % compared to 7 % for Co_3O_4 and 3 % for Mn_2O_3). A high temperature is unfavourable for oxidation, especially for manganese and cobalt.

4.3.2 Reduction and oxidation kinetic

The oxygen carrier oxidation and reduction rates along with the oxygen transport capacity play an important role in designing a chemical looping process. The oxidation-reduction rate decreases with time parabolically due to diffusion resistance from the unreacted core and the bulk phase. In the case of fine particles or highly porous surface layer, this resistance is negligible and the entire particle takes part in the reaction, and a nuclei growth model (NG) is recommended. Transformations obeying this model are often seen to follow a characteristic s-shaped profile where the reaction rates are low at the beginning and the end of the transformation but rapid in between.

$$ln(-ln(1-X(t))) = lnK + nlnt \tag{4.7}$$

where “K” and “n” are the model constants and “X(t)” is the fractional conversion:

$$X(t) = \frac{W_0 - W}{W_0 - W_f} \tag{4.8}$$

This model is known as nuclei growth (NG) model [21, 39] and assumes that:

1. nucleation occurs randomly and homogeneously over the entire non-reacted portion of the material;
2. the growth rate does not depend on the extent of transformation; and
3. growth occurs at the same rate in all directions.

Many researchers have used this model for the oxidation-reduction kinetics of metals. Chiron and Patience summarized various existing models. All of them are applicable for irreversible reactions [22]. Sedor et al. modeled the reduction of NiO with CH_4 in a fluidized bed riser simulator [23]. They compared the experimental results with power law, nuclei growth model and shrinking core model. They concluded that the nuclei growth model describe the experimental data adequately.

During the reduction of oxygen carrier, the released oxygen is purged by a carrier gas and is

inaccessible to re-oxidize the metal. Therefore, we can assume the reduction is irreversible and use directly the NG model. However, when air is fed to the TGA, the metal is reduced and the model has to be modified. Whenever the particle size is smaller than 200 microns, the temperature profile inside the particle can be neglected during the oxidation and reduction [24]. Consider the general oxidation of metal:

$$\mathrm{Me} + \tfrac{1}{2}\,\mathrm{O}_2 \longleftrightarrow \mathrm{MeO} \tag{4.9}$$

The NG model is applicable for each individual reaction when considered as irreversible.

$$ln(-ln(1-X_{Oxi}(t))) = lnK_{Oxi} + n_{Oxi}lnt \tag{4.10}$$

$$ln(-ln(1-X_{Red}(t))) = lnK_{Red} + n_{Red}lnt \tag{4.11}$$

where X_{Oxi} and X_{Red} are the hypothetical conversions for the forward and reverse reactions, considering them as irreversible. The actual conversion "X" is given by

$$X = X_{Oxi}(1-X_{Red}) \tag{4.12}$$

Rearranging Equations 4.10, 4.11 and 4.12:

$$lnX = ln(1 - \frac{1}{exp(K_{Oxi}t^{n_{Oxi}})}) - K_{Red}t^{n_{Red}} \tag{4.13}$$

K_{Red} and n_{Red} are determined from reduction data and Equations 4.7. Figures 4.5 and 4.6 show the difference between the model prediction and the experimental data for reduction and oxidation of cobalt oxide at 825, 850, and 875 °C.

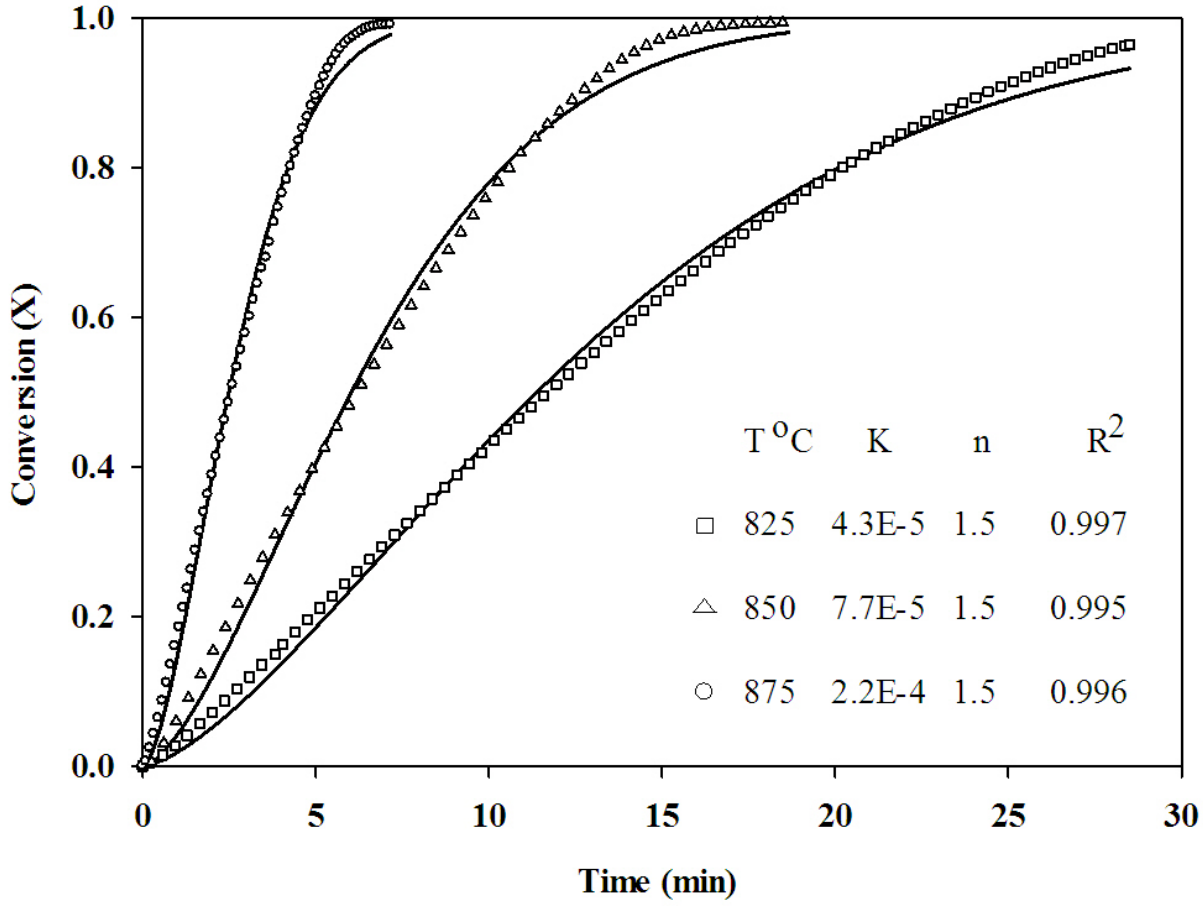

Figure 4.5 Co_3O_4 reduction in nitrogen, conversion vs time at 825, 850 and 875 °C, the solid line represents the model)

The agreement between the model and experimental data for cobalt is good (Figure 4.5, R^2>0.995). At 875 °C the conversion approaches 100 % at 5 min and 30 min at 825 °C. With increasing temperature, the reduction of all three oxygen carriers happens farther from the equilibrium line (Figure 4.4). Therefore, the reaction rate is faster which is in agreement with the data in Figure 4.5.

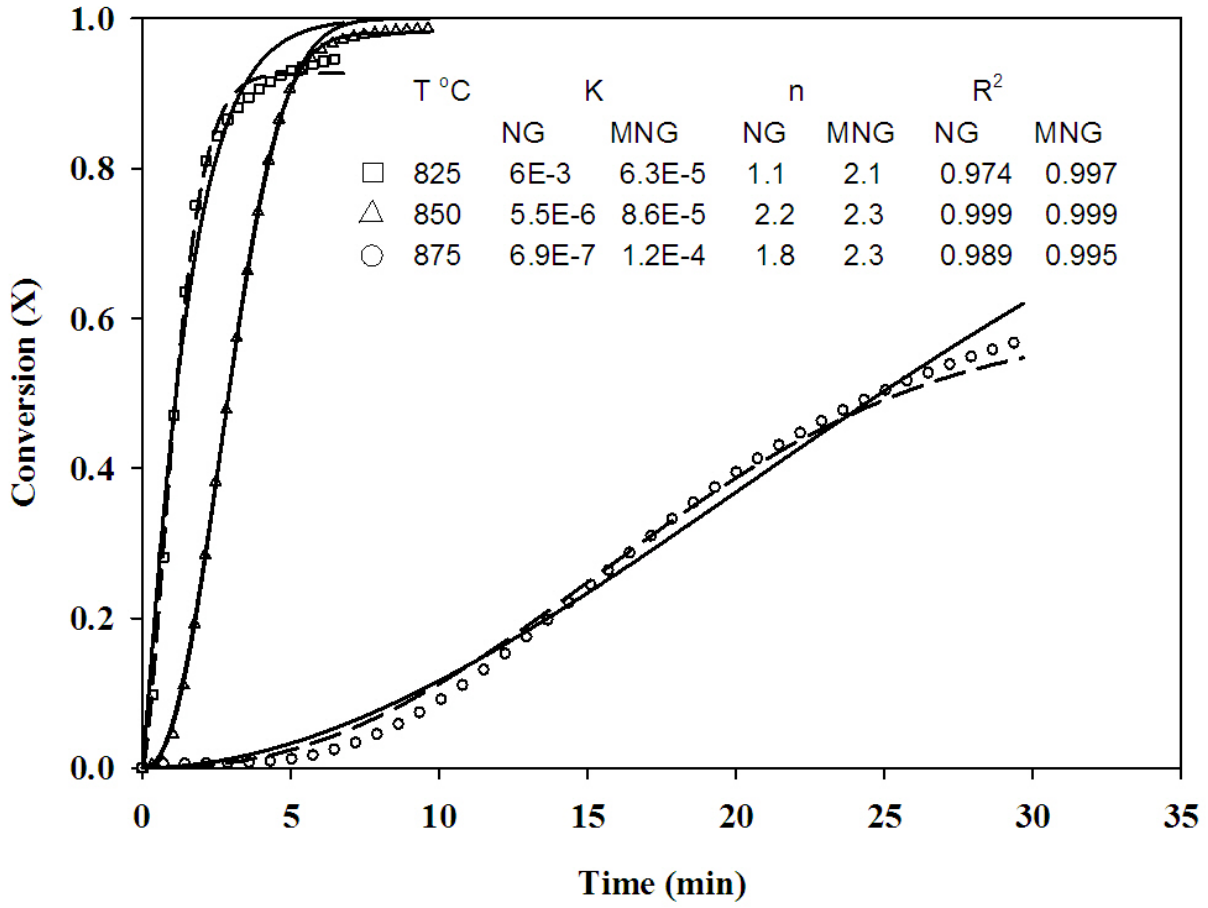

Figure 4.6 CoO oxidation in air, conversion vs time at 825, 850 and 875 °C, (- - - -) NG model, (——) MNG model (modified NG model, Equation 4.13)

At 825 °C, the conversion approaches 100 % at 2 min, and 4 min at 850 °C (Figure 4.6). Further increase to 875 °C never completes the reaction during the operation time. According to Equation 4.12, the metal oxidation conversion is affected by the reduction reaction. By increasing temperature, the reduction rate increases (Figure 4.5), and it has a negative effect on oxidation rate (Figure 4.6). This agrees with the equilibrium results shown in Figure 4.4. As temperature increases, the oxidation of all three oxygen carriers approaches to the equilibrium line. Although the NG model fits the oxidation experimental data well, the calculated K_{Oxi} is meaningless because it decreases with temperature. K_{Oxi} and K_{Red} vary with temperature according to an Arrhenius type

relationship (Figure 4.7)

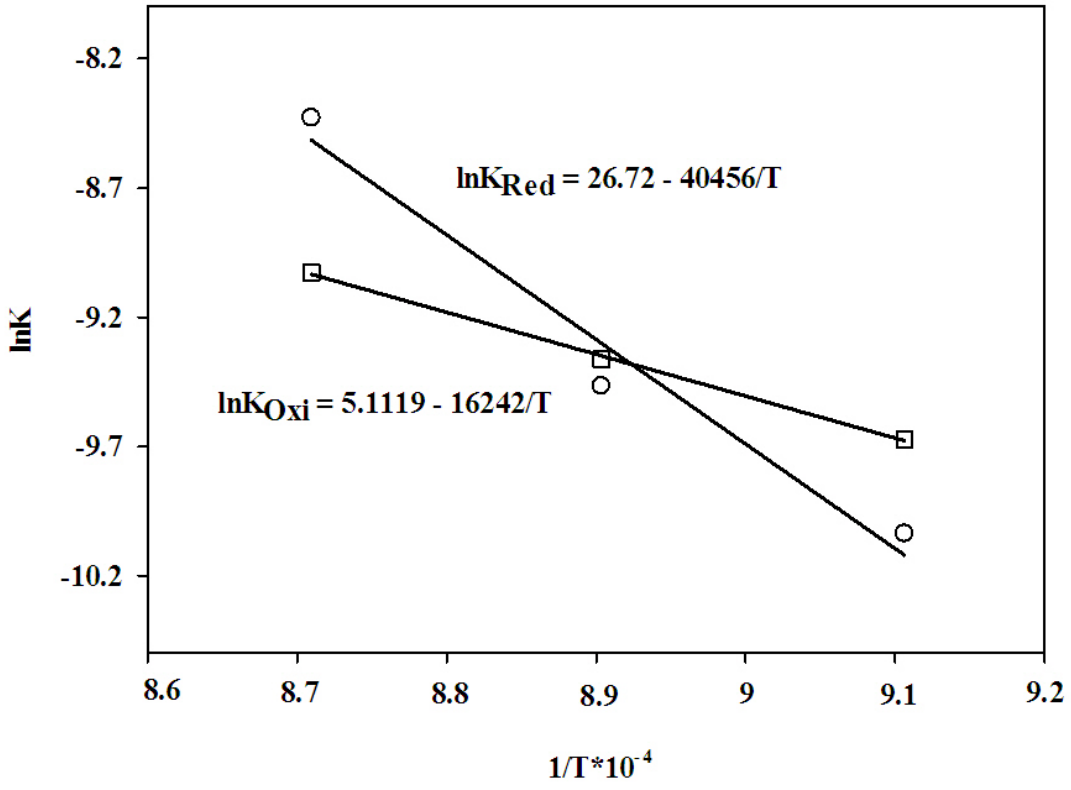

Figure 4.7 Arrhenius relationship of K_{Oxi} (from MNG model) and K_{Red} with temperature)

The activation energy for oxidation is less than that of reduction, which means that the oxidation is faster than the reduction. Furthermore, the activation energy for the reduction of Mn_2O_3 and Co_3O_4 is less than CuO, which make it easier to reduce the manganese and cobalt oxides than copper (Table 4.4).

Table 4.4 Activation energy for copper, cobalt and manganese reduction and oxidation

Reaction	$E_{Red(KJ/mol)}$	$E_{Oxi(KJ/mol)}$	$T\ ^oC$
$2\,CuO \longleftrightarrow Cu_2O + \frac{1}{2}O_2$	54 ± 5	12 ± 1	825-875
$Co_3O_4 \longleftrightarrow 3\,CoO + \frac{1}{2}O_2$	40 ± 3	16 ± 2	825-875
$3\,Mn_2O_3 \longleftrightarrow 2\,Mn_3O_4 + \frac{1}{2}O_2$	37 ± 2	13 ± 1	825-875

4.3.3 XRD results

The XRD patterns of the fresh and reduced oxygen carriers (Figure 4.8) confirm the phase change of the oxygen carriers according to reactions 4.4-4.6. Since the reduction of the oxygen carrier in the furnace is incomplete, some peaks of fresh MeO are noticeable in the reduced pattern (e.g., CuO and Cu_2O patterns). The dominant phase of the copper oxide after reduction is Cu_2O and its melting point is higher than copper (1235 °C vs. 1085 °C, [25]). As a result, the sintering possibility in CLOU working with copper oxide as the oxygen carrier is lower. The formation of $CuAl_2O_4$ reported in the literature during calcination [9], was absent in the XRD spectrums.

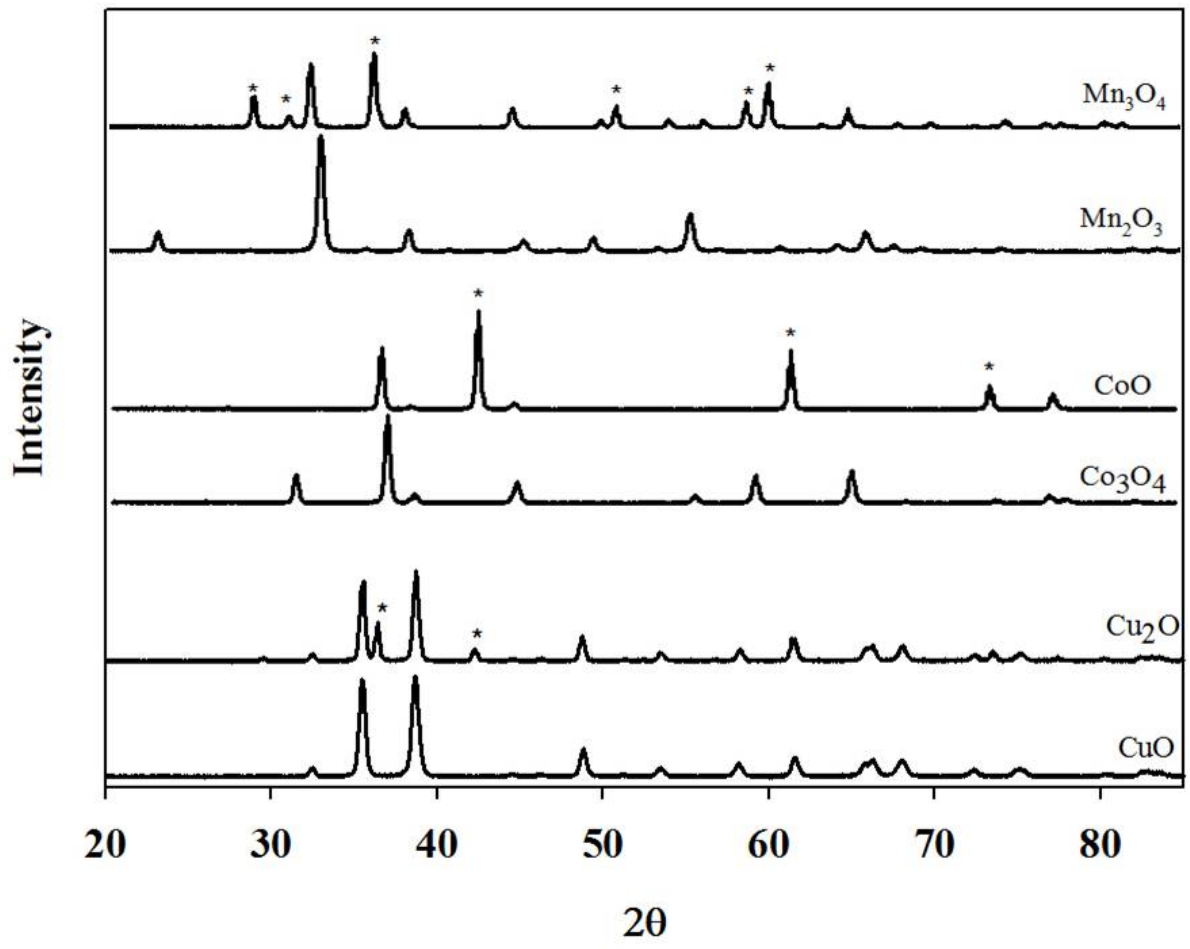

Figure 4.8 XRD pattern of copper, cobalt, and manganese; ⋆ indicates the formation of the reduced metal oxide)

4.3.4 Thermal resistance of the oxygen carrier

Sintering affects the oxygen transport capacity of the oxygen carrier and must be considered in designing a chemical looping process. Scanning electron microscopy (SEM) together with BET analysis are two techniques commonly used to assess oxygen carrier's resistance to sintering. SEM imaging is reliable when a specific particle is tracked before and after a heat treatment, which is inapplicable in our studied temperature range (850 °C). Particles tend to form agglomerates at

higher temperature, with a subsequent loss in the internal pores. To demonstrate this effect, 1 g of fresh oxygen carrier was placed in the furnace and the temperature was raised up to 850 °C in N_2, and then the reacting gas was switched to air; this cycle was repeated 10 times. The specific surface area of fresh and heated powder was subsequently measured. The specific surface area decreased by 77, 32, and 61 % for copper, cobalt, and manganese, respectively, after 10 oxidation-reduction cycles. For all three metals, the decrease in surface area was very sharp for the first couple of cycles, and reached a constant value after the 5^{th} cycle. This data signifies that cobalt has a higher thermal stability compared to other candidates. Even though the surface area decreases with the cycles, the OXO capacity is basically constant. This implies that the reaction is the limiting step, and particle sintering has a minimal effect on the oxygen carrier performance.

Co_3O_4 has the highest OXO capacity among the three oxides with respect to the oxygen desorption and adsorption rate and a superior thermal stability. Therefore, the effect of impurities-sulfur species, for example, must be tested to evaluate its feasibility.

4.3.5 The interaction between Co_3O_4 and biomass

The biomass reduction atmosphere is a complex mixture of steam, hydrogen, CO, CO_2, CH_4, char, ashes, tars, olefins, and many other impurities, such as NH_3, chlorine, and sulfur species. The oxygen carrier stability in such an environment may be problematic. Solunke et al. [26] and Pecho et al. [27] showed that sulfur changes the performance of the oxygen carriers. As a first step in the evaluation of chemical stability, carriers were tested in a TGA in the presence of wood sawdust.

Figure 4.9 shows the thermogravimetric analysis of Co_3O_4, wood and a mixture of both components with the mass ratio of 2:1 (Co_3O_4/Biomass).

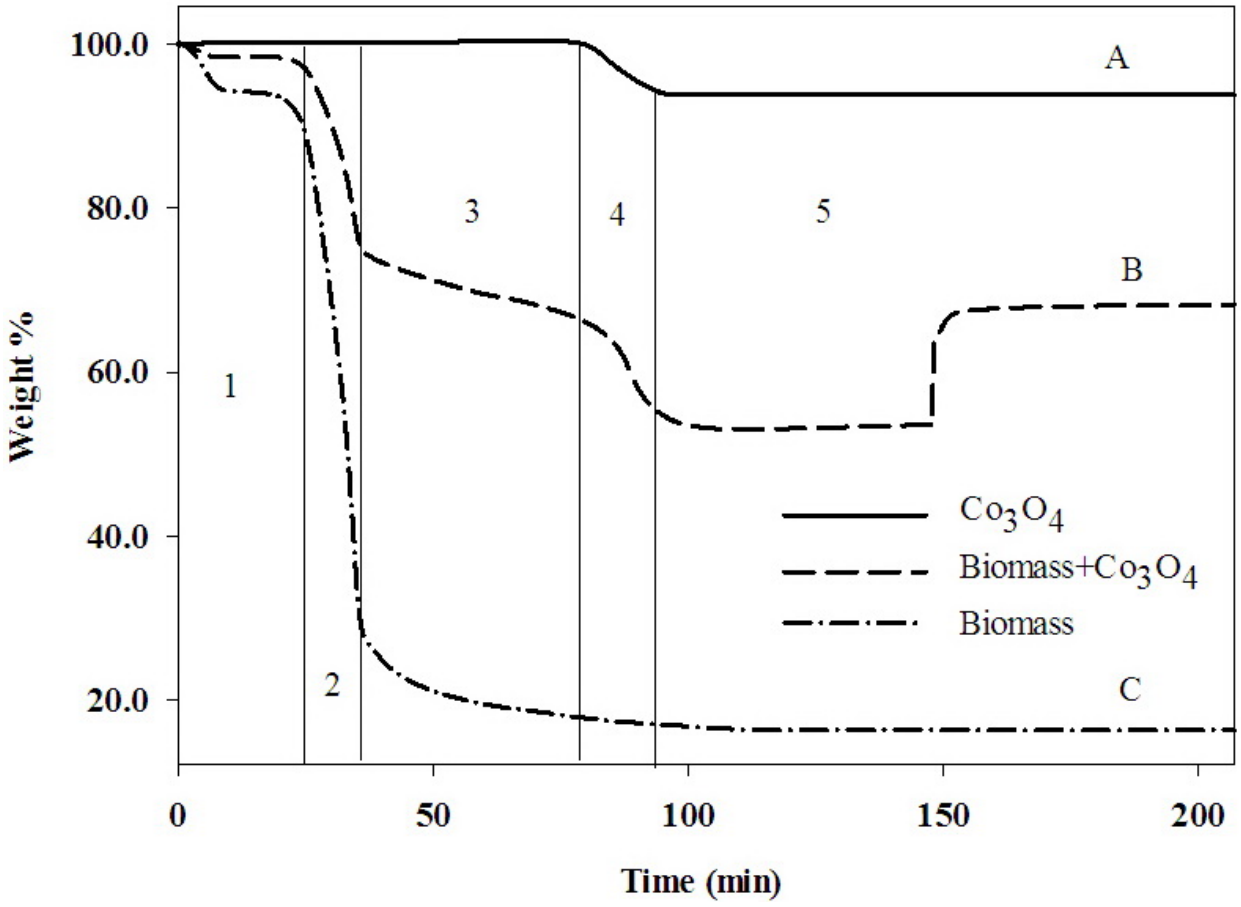

Figure 4.9 Pyrolysis of wood sawdust in the presence of Co_3O_4; A: Co_3O_4, B: Co_3O_4 + biomass (2:1), C: Biomass; 1: Drying, 2-5: Pyrolysis + Gasification)

The temperature was raised from ambient to 900 °C at a heating rate of 10 °C/min in 50 ml/min of nitrogen. Subsequently, the temperature was kept constant for one hour. This step was followed by one-hour air treatment at 900 °C. CoO and Co are oxidized to Co_3O_4 according to the following reactions:

$$3CoO + \frac{1}{2}O_2 \xrightarrow{6.64\ \%wt} Co_3O_4 \tag{4.14}$$

$$3Co + 2O_2 \xrightarrow{26.59\ \%wt} Co_3O_4 \tag{4.15}$$

In plot B (Figure 4.9), a 15 % weight gain after switching nitrogen to air confirms that both reactions 4.14 and 4.15 took part in the oxidation reaction. As a result, the presence of wood provides a reduction media that reduces Co_3O_4 to CoO and then Co. To indicate the occurrence period of this reaction, we divided the graph into five regions. Plot C (pure wood) contains 2 times more biomass compared to plot B (a mixture of wood and Co_3O_4). Therefore, the slope corresponding to each plot has to follow the same order. However, this issue has not been observed in the third region because the cobalt oxide participated in the pyrolysis of biomass by releasing oxygen and converting to CoO and Co. The reduction of Co_3O_4 continued in the fourth region and converted the residual char to ash. As depicted in the fifth region, cobalt is regenerated to its initial phase (Co_3O_4) and the presence of biomass had no effect on its re-oxidation and oxygen release performance.

4.4 Conclusions

Cobalt oxide is an excellent oxygen carrier for chemical looping biomass gasification. Its elevated oxygen release capacity and thermal stability make it a superior carrier compared to the oxides of manganese and copper. Consistent with observations of other systems, oxidizing CoO to Co_3O_4, is much faster than reducing Co_3O_4 to CoO. Therefore, the solids inventory required on the oxidation side is much lower compared to the reduction side. Manganese and cobalt oxides release oxygen at temperatures 100 °C lower than copper oxide. Cobalt has the best oxygen release capability at 850 °C. Based on the nuclei growth model, increasing temperature favours reduction (endothermic); whereas, lower temperatures favour oxidation (exothermic). The activation energy was 40±3 kJ/mol for Co_3O_4 reduction, and 16± kJ/mol for CoO oxidation. The total pore volume of the cobalt oxide before and after heat treatment dropped less than manganese and copper oxides, indicating that it has superior thermal stability. The oxygen-released by Co_3O_4 increased in the presence of biomass at 800 °C. Furthermore, Co is readily re-oxidized to its initial state, indicating that biomass has a negligible deleterious effect on its performance under the conditions tested. Despite the superior performance and thermal stability of cobalt oxide, its high cost and toxicity

reduce its likelihood as a candidate for commercial applications.

Notation

E	Activation energy, $KJmol^{-1}$
K_0	Nuclie growth model parameter
N	Nuclie growth model parameter
R	Gas constant, $KJmol^{-1}K^{-1}$
t	Time, s
T	Temperature, ^oC
W	Mass, kg
X	Conversion
Subscript	
0	Initial conditions
f	Final conditions
Me	Metal
MeO	Metal oxide
Oxi	Oxidation
Red	Reduction

References

[1] S. Consonni, R. E. Katofsky, E. D. Larson, Chem. Eng. Res. Des. 2009, 87, **1293**.

[2] J. Rezaiyan, N. P. Cheremisinoff, Gasification technologies: A Primer for Engineers and Scientists, Taylor & Francis, Boca Raton, USA **2005**.

[3] H. Hofbauer, G. Veronik, T. Fleck, R. Rauch, H. Mackinger, E. Fercher, The FICFB - Gasification Process, Banff, Canada **1997**, 1016.

[4] J. Adanez, A. Abad, F. Garcia-Labiano, P. Gayan, L. F. de Diego, Prog. Energ. Combust. **2012**, 38, 215.

[5] T. Mattisson, H. Leion, A. Lyngfelt, Fuel **2009a**, 88, 683.

[6] T. Mattisson, A. Lyngfelt, H. Leion, Int. J. Greenhouse Gas Control **2009b**, 3, 11.

[7] K. Shah, B. Moghtaderi, T. Wall, Energy Fuels **2012**, 26, 2038.

[8] B. Moghtaderi, Energy Fuels **2009**, 24, 190.

[9] H. Leion, A. Lyngfelt, T. Mattisson, Chem. Eng. Res. Des. **2009**, 87, 1543.

[10] Y. Cao, B. Casenas, W. P. Pan, Energy Fuels **2006**, 20, 1845.

[11] I. Adanez-Rubio, P. Gayan, F. Garcia-Labiano, L. F. de Diego, J. Adanez, A. Abad, Energy Procedia **2011**, 4, 417.

[12] E. M. Eyring, G. Konya, J. S. Lighty, A. H. Sahir, A. F. Sarofim, K. Whitty, Oil Gas Sci. Technol. **2011**, 66, 209.

[13] P. Gayan, I. Adanez-Rubio, A. Abad, L. F. de Diego, F. Garcia-Labiano, J. Adanez, Fuel **2012**, 96, 226.

[14] A. Abad, I. Adanez-Rubio, P. Gayan, F. Garcia-Labiano, L. F. de Diego, J. Adanez, Int. J. Greenh. Gas Control **2012**, 6, 189.

[15] A. Shulman, E. Cleverstam, T. Mattisson, A. Lyngfelt, Energy Fuels **2009**, 23, 5269.

[16] M. Johansson, T. Mattisson, A. Lyngfelt, Chem. Eng. Res. Des. **2006**, 84, 807.

[17] A. Shulman, E. Cleverstam, T. Mattisson, A. Lyngfelt, Fuel **2011**, 90, 941.

[18] G. Azimi, H. Leion, T. Mattisson, A. Lyngfelt, Energy Procedia **2011**, 4, 370.

[19] T. Mattisson, M. Johansson, E. Jerndal, A. Lyngfelt, Can. J. Chem. Eng. **2008**, 86, 756.

[20] M. Avrami, Chem. Phys. **1939**, 7, 1103.

[21] M. Avrami, Chem. Phys. **1940**, 8, 212.

[22] F.-X. Chiron, G. S. Patience, Int. J. Hydrogen Energy **2012**, 37, 10526.

[23] K. E. Sedor, M. M. Hossain, H. I. de Lasa, Can. J. Chem. Eng. **2008**, 86, 323.

[24] F. Garcia-Labiano, L. F. de Diego, J. Adanez, A. Abad, P. Gayan. Chem. Eng. Sci. **2005**, 60, 851.

[25] R. A. Robie, B. S. Hemingway, J. R. Fisher, Thermodynamic properties of minerals and related substances at 298.15 K and 1 bar (105 kPa) pressure and at higher temperatures: a summary of the thermodynamic data for minerals at 298.15 K, Department of the Interior, US Geological Survey, Washington, DC **1978**.

[26] R. Solunke, G. Veser, Fuel **2011**, 90, 608.

[27] J. Pecho, T. J. Schildhauer, M. Sturzenegger, S. Biollaz, A. Wokaun, Chem. Eng. Sci. **2008**, 63, 2465.

CHAPTER: 5

ARTICLE 2: TRANSIENT MODELING OF BIOMASS STEAM GASIFICATION WITH Co_3O_4

Milad Aghabararnejad, Gregory S. Patience, Jamal Chaouki

Department of Chemical Engineering, Polytechnique Montréal, C.P. 6079, Succ. CV Montréal, H3C 3A7 Québec, Canada

This work was submitted to the journal: *Fuel* (2014)

Abstract

Co_3O_4 was subjected alternatively to argon/steam as reducing and air/steam as oxidizing agents in a bubbling fluidized bed reactor. Ten grams of biomass was injected to the reactor at the beginning of the reduction interval. Oxygen was released from Co_3O_4 in the reduction period and together with the steam gasified the biomass. The reduced cobalt oxide (CoO) was regenerated to Co_3O_4 during the oxidation stage. The produced gas is free of nitrogen and has a higher calorific value compared to gasification with air. From 825 to 875 °C, H_2 yield increased up to 60 %. From 0 to 18 % of steam, H_2 yield increased 4 times. Substituting 50 % of the sand as bed material with Co_3O_4, increased the CO yield up to 45 %, lowering the H_2:CO ratio. For reactor modeling, a two phase model for the dense bed and a plug flow model for the freeboard region were used. The presented hydrodynamic model together with the kinetic expression from the literature characterized the transient gas compositions at the reactor outlet very well.

Keywords: *Chemical Looping, Oxygen Carrier, Transient Modeling, Bubbling Fluidized Bed, Biomass Gasification.*

5.1 Introduction

The growth in the world economy and the shift toward clean energies, persuade industries to consider alternative resources. Renewable energies have a potential as a primary energy source in the near future. In 2011 renewable energies contributed as much as 9.7 % of the global energy consumption and it is growing rapidly, especially for industrialized countries, like Germany, which plans to be independent of fossil fuels and atomic energy by 2050 [1]. Currently, biomass comprises only 8 % of the renewable energy world wide. Biomass can be used to produce synthesis fuels, which other renewable sources do not offer. Synthesis fuel from biomass is produced via two processes:

1. Pyrolysis: Biomass pyrolysis at 200<T(°C)<500 in an oxygen free media and produces oil, gas and char. Although this process is very simple, biomass conversion to oil is less than

60 % [2] (depending on the process and type of biomass) and un-reacted char needs further processing to be useful. In addition, since pyrolysis is endothermic, an external source of energy is required;

2. Gasification: Gasification produces synthesis gas, which is a mixture of predominantly H_2 and CO. Synthesis gas is a building block for the production of NH_3, ethanol, methanol and the Fischer-Tropsch (F-T) process. To achieve auto-thermal gasification, part of the biomass is combusted to supply the required heat [2]. Air is usually used as the oxygen source, which dilutes the syngas with nitrogen requiring further separation. Therefore, it is recommended to separate the oxygen from the air and introduce it to the gasifier. This process is costly and increases the capital and variable costs.

Chemical looping is an alternative process to supply oxygen. In this process oxygen reacts with a reduced metal (Me) to form the oxide (MeO). The oxide is transferred to another vessel maintained by a reducing environment (oxygen deficient) (Figure 5.1). Because of the low thermal resistance of the metals, they are dispersed on Al_2O_3 or SiO_2 supports. The metal oxide over the support is referred as the oxygen carrier.

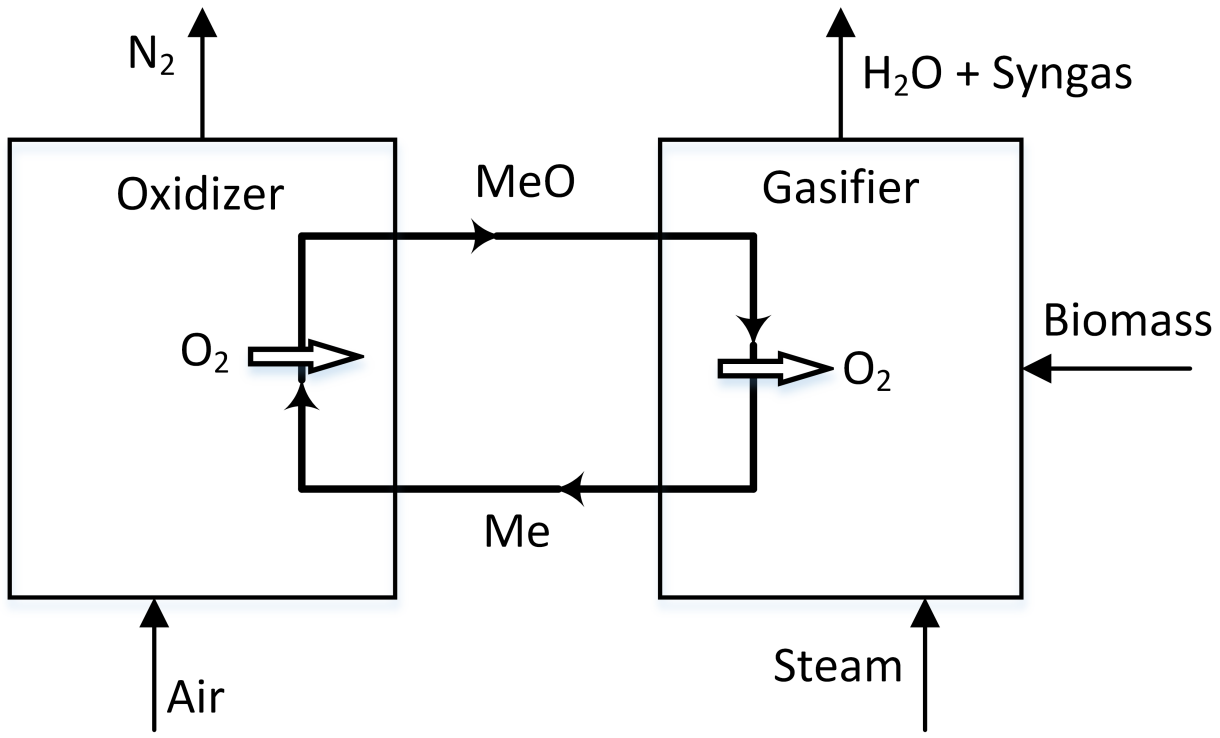

Figure 5.1 Schematic of chemical looping gasification (CLG) unit

To treat solid fuels such as biomass using the chemical looping concept, two processes have been proposed: in-situ gasification coupled with chemical looping combustion (iG-CLC); and chemical looping oxygen uncoupling (CLOU) process. In iG-CLC, the biomass is gasified with steam and/or CO_2 in the first step and the produced syngas is combusted with the lattice oxygen from oxygen carrier. The reduced oxygen carrier is transferred to the oxidation site for regeneration. The syngas-oxygen carrier interaction is a gas-solid reaction. Therefore, there is no difference between the oxygen carrier used in iG-CLC and a gaseous fuel CLC. The iG-CLC is basically for power generation rather than syngas production. In CLOU process the oxygen carrier releases the gaseous oxygen to the gasifier which is available to combust (or partially combust) the biomass. The reduced oxygen carrier is regenerated in the oxidation reactor. The oxygen carrier used in CLOU process should be able to react with oxygen in the oxidizer and releases oxygen in gasifier which distinguishes it from the conventional oxygen carrier of CLC. Among different types

of metal which have been proposed for CLC, only manganese, copper and cobalt can be served for CLOU. We have tested the oxygen transport capacity, oxidation-reduction rates and thermal stability of manganese, cobalt, and copper. Cobalt has a moderate oxygen carrying capacity (7 % of its weight) but the oxidation-reduction rates are 3 times greater and the thermal stability is superior compared to manganese and copper. Furthermore, experiments in a TGA in the presence of biomass have shown that, sulfur has little effect on the cobalt oxide performance [3].

Current gasification models are based on either equilibrium or reaction kinetics. Equilibrium models over predict the production of carbon monoxide and hydrogen, and under predict the formation of hydrocarbons [4]. The kinetic approach models predict well but require reaction rate parameters and a proper hydrodynamic model, which makes them more complex. Achieving steady-state conditions in lab-scale reactors especially with solid injection is troublesome. However, most of the gasification models are dedicated to steady-state conditions (Table 5.1) since the modeling of a steady state process is easier than the transition process.

Table 5.1 Equilibrium and kinetic models of gasification

#	Gasifier	Hydrodynamic model	Feed	Gasifing agent	Reference
Steady state kinetic approach models					
1	BFB	Two phase + CCBM	Sawdust	Steam	Radmanesh et al. [5]
2	CFB	One dimensional plug flow	Biomass	Air/Steam	Corella and Sanz [6]
3	BFB	Two phase+CSTR	Sawdust	Air	Fiaschi et al. [7]
4	PBFB	n-CSTR	Biomass	Air	Evans et al. [4]
5	BFB	Two fluid model	Coal	Air and steam	Yu et al. [8]
6	MB	n-CSTR	Biomass	Air and steam	Hernandez et al. [9]
7	SB	Two plug flow in parallel	Coal	Air/Steam	Lucas et al. [10]
Steady state equilibrium approach models					
8	CFB		Coal	Air	Li et al. [11]
9	EF		Coal	Steam/Oxygen	Kong et al. [12]
Unsteady state models					
10	Batch	Equilibrium	Char	Steam	Inayat et al. [13]
11	FB	N.A.	Char	Steam	Woodruff and Weimer [14]
12	Batch		Cellulose	Steam	Salaices et al. [15, 16]

BFB: Bubbling fluidized bed, CFB: Circulating fluidized bed, PBFB: Pressurized BFB,
MB: Moving bed, SB: Spouted bed, EF: Entrained flow, FB: Fixed bed, N.A.: Not applicable

Woodruff and Weimer [14] studied transient char steam gasification in a fixed bed reactor. Steam was fed continuously over char; while, and the overall conversion was calculated by mea-

suring the total molar flow rate. The reaction rate was modeled using the Langmuir-Hinshelwood type expression. Although measuring the total molar flow rate has a faster response time than measuring the outlet gas composition, it only presents the total reaction conversion and is not able to predict the individual conversion of reactions involved in the gasification. Salaices et al. [15, 16] studied the kinetics of cellulose gasification in a batch fluidized bed reactor. They calculated the overall conversion by measuring the total pressure in the reactor, and were able to sample at several times and determine the production rate of each individual gas. Yazdanpanah et al. [17] modeled CH_4 combustion with $NiO/NiAl_2O_4$ in a chemical looping combustion (CLC) bubbling fluidized bed. A two phase bubble-emulsion model was considered as the hydrodynamic model. They used a plug flow model for the bubble phase, and a plug flow with axial dispersion for the emulsion phase. Also, a perfectly mixed flow reactor for the solid behaviour in the emulsion phase was considered. Their assumptions were substantiated by residence time analysis of helium as a tracer.

In the present paper biomass is gasified with steam and oxygen in a bubbling fluidized bed reactor. The oxygen is provided from cobalt oxide by reduction of Co_3O_4 to CoO. A mass spectrometer (MS) monitored and recorded the gas composition at the reactor outlet. The experimental data were used to validate a kinetic based approach model. The fluidized bed consists of two regions: a dense bubbling bed and a freeboard. A two phase model for the bubbling bed and a plug flow model for the freeboard region were considered to describe the gas flow. The proposed hydrodynamic was validated by residence time analysis.

5.2 Materials, methods and experiments

The Co_3O_4(25 %)/Al_2O_3 was prepared by incipient wetness impregnation. The detail preparation method was discussed in an earlier study [3]. The surface area was 98 ± 2 (m^2/g) and the particle diameter was 138 ± 3 μm (Table 5.2). Hereinafter Co_3O_4(25 %)/Al_2O_3 is referred as Co_3O_4 for simplicity.

Table 5.2 Physical properties of Co_3O_4

Property	Value
Active phase loading (wt%)	25
d_p (μm)	138 ± 3
Surface area (m^2/g)	98 ± 2
Bulk density (kg/m^3)	990
Particle density (kg/m^3)	3300

Silica sand with $d_p = 145 \pm 11$ μm and $u_{mf} = 0.045$ m/s was used as the inert material for non-catalytic tests (bulk density-1430 kg/m^3). The volatile fraction of the saw dust was 81 % wt with 16 % wt char and 3 % wt ash (Table 5.3). To facilitate the solid injection, the biomass pellets with 10 mm length and 6 mm diameter were used.

Table 5.3 Biomass elemental and proximate analysis

Elemental (wt %)		Proximate (wt %)	
C	48	Char	16
H	6.2	Volatile	81
O	45	Ash	3
N	0.2		
S	0.6		

The stainless steel fluidized bed consists of three zones (Figure 5.2). The first zone which is a preheated section, has a 20 cm long and 7.8 cm ID and heats the inlet gas to the operating temperature before entering the bed. The second zone is 76 cm in length and 7.8 cm ID. Distributor plate is located between zone 1 and 2. The distributor is a perforated plate with 42×0.12 cm ID holes (1 % open surface). To return the particles to the bed, there is a disengagement zone 91 cm in length and 15 cm ID. All three sections were covered by a 3 cm layer of insulation to minimize heat loss. An external cyclone is located at the reactor outlet to collect the fine particles and condensates. Biomass was injected through a 1" ID tube, which was located 20 cm above the distributor. The pressure drop across the distributor and fluidized bed was negligible. Steam was generated by atomizing water and argon mixture in an evaporator operating at 300 °C and atmospheric pressure. The gas flow rate was metered using a rotameter (Figure 5.2).

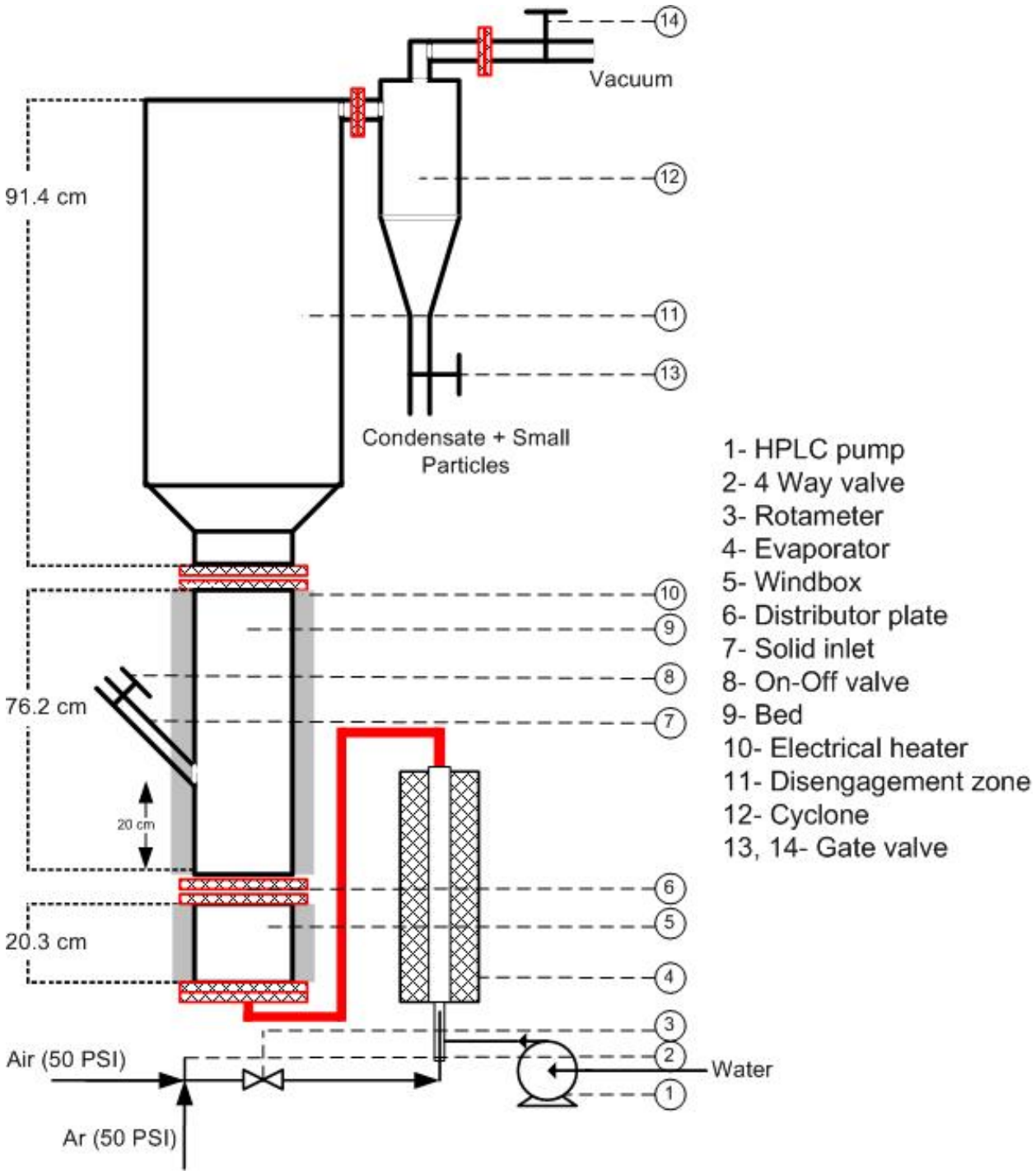

Figure 5.2 Steam bubbling fluidized bed gasifier schematic

Thirteen thermocouples recorded the axial temperature every 10 cm in zones 1 and 2, and every 20 cm in zone 3. The axial temperature profile was constant in zones 1 and 2. However, the

temperature decays in the disengagement zone due to lack of heaters. The tip of the thermocouples were located in the center of the reactor. The bed loading was 15 cm (L/D=2). The gas residence time with sand as bed material was measured by a stimulus-response technique. After reaching the desired temperature, the system was purged with argon at a superficial velocity of 13 cm/s and the gas composition was monitored with a Pfeiffer Thermostar MS. To evaluate the radial dispersion, the MS sampled the gas at r/R=0, 0.5, and 1 and for axial dispersion at H_1=0 cm, and H_2=20 cm (bed surface-considering 5 cm as bed expansion). Furthermore, to find out the effect of temperature on the gas residence time, tests were carried out at ambient conditions, 400 and 850 °C. The experimental design for the gas phase RTD consisted of eight experiments: three temperatures between two axial positions; and three radial positions at H_2=20 cm (Table 5.4).

Table 5.4 The experimental plan for the gas phase RTD

Exp.#	r/R	T ^oC	H(cm)
1	1	25	20
2	0.5	25	20
3	0	25	20
4	0	400	20
5	0	850	20
6	0	25	0
7	0	400	0
8	0	850	0

For the steam gasification tests, a mixture of cobalt oxide and sand was loaded into the reactor and heated to the desired temperature in air/steam agent. The MS sampled the gas at 76 cm above the distributor and r/R=0. When the reactor achieved a steady temperature and concentration (based on the MS trace), air was substituted by argon/steam mixture (t=0 s). At t=20 s, 10 g of biomass was injected into the reactor. The gas velocity remained constant at 13 cm/s in all experiments. Three temperature levels (825, 850, 875 °C) and three steam levels (0, 10, 18 %) were selected as operating conditions (Table 5.5). The temperature deviation from the set point was no more than 10 °C. The argon flow rate was changed in each run to maintain a constant gas velocity.

Table 5.5 Experimental plan for steam gasification of biomass

Exp.#	T ^oC	Steam %	Water (ml/min)	Sand %-Co_3O_4 %	Ar (ml_{STP}/min)
1	825	0	0	100-0	113
2	825	10	0.008	100-0	102
3	825	18	0.015	100-0	93
4	850	0	0	100-0	108
5	850	10	0.008	100-0	97
6	850	18	0.015	100-0	87
7	875	0	0	100-0	103
8	875	10	0.008	100-0	92
9	875	18	0.015	100-0	84
10	875	18	0.015	70-30	84
11	875	18	0.015	50-50	84

When the composition of the gas stream dropped (indicating the completion of the reaction), the gas was switched to air to re-oxidize the oxygen carrier for the next injection. To ensure the data repeatability, each run (Tables 5.4 and 5.5) was repeated three times. After 10 biomass injections, the bed and cyclone were depleted to prevent the ash and condensate accumulation.

5.3 Steam gasification model

Biomass steam gasification with Co_3O_4 as the oxygen source in a bubbling fluidized bed takes place in five steps (Figure 5.3). In the first step, Co_3O_4 releases oxygen to the gas phase. Pyrolysis, the second step, decomposes the biomass to permanent gases, tar and char. The char reacts with steam and oxygen (step 3) and, finally, the produced gases from pyrolysis and gasification react together in the freeboard region (step 4). The temperature was maintained constant in the dense bed and freeboard regions, however, it decayed exponentially in the disengagement zone with the maximum temperature in this region recorded as 230 °C. The homogeneous gas phase reactions can be neglected at these conditions (see Appendix A).

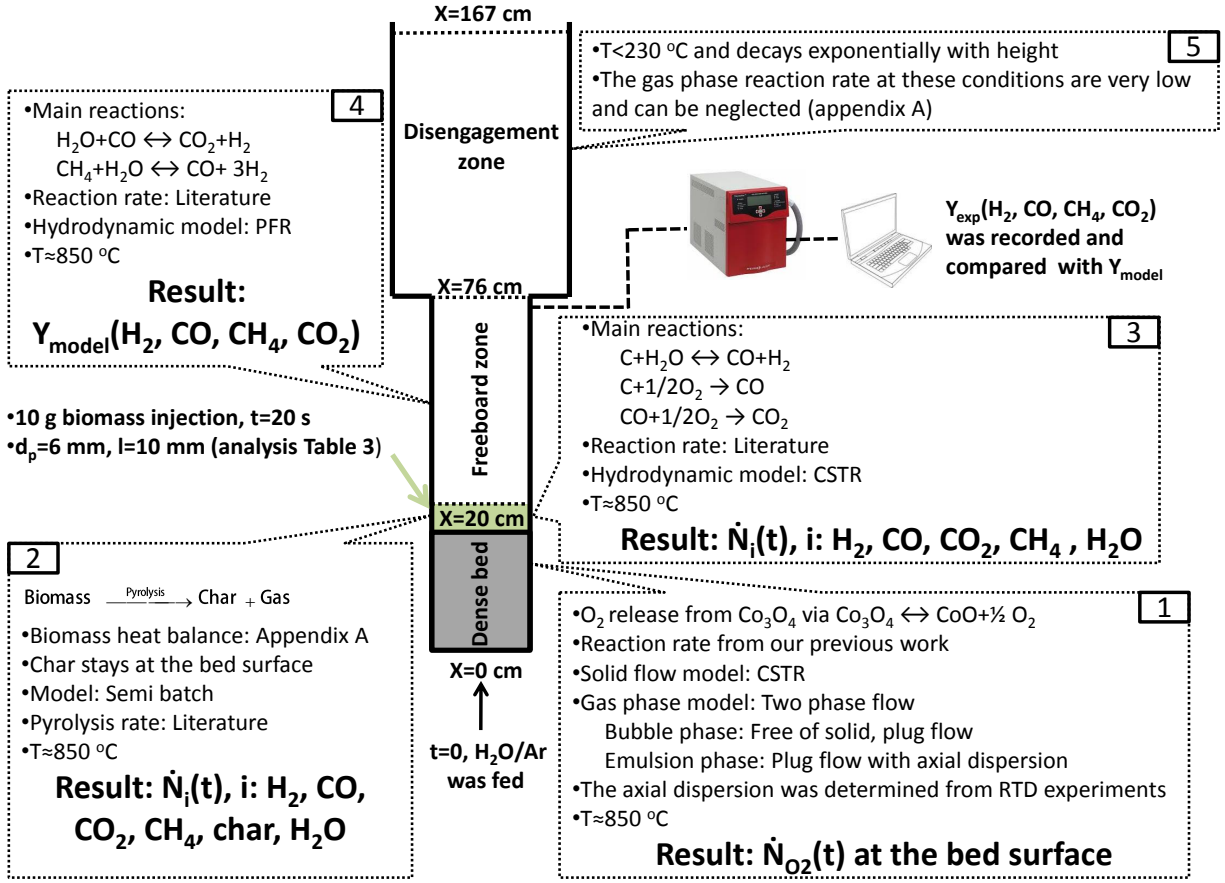

Figure 5.3 5 step model for biomass steam gasification with Co_3O_4 as the oxygen source

5.3.1 Oxygen desorption in a bubbling fluidized bed

The maximum segregation of biomass-Co_3O_4 in the bed occurs at a velocity so-called fully fluidized velocity-u_{ff} (Fotovat et al. [18]). Since the biomass weight fraction in the bed is very low (less than 5 %), the u_{ff} is so close to the u_{mf} of Co_3O_4. Increasing u_0 beyond u_{ff}, causes mixing of two solids in the bed and consequently transferring un-reacted biomass to the oxidizer via L-valve. Since the operating velocity in the present work was close to the u_{mf} of Co_3O_4, it can be assumed that biomass did not sink into the bed and remains at the bed surface.

By switching the fluidizing gas from air/steam to argon/steam, cobalt oxide is subjected to a reducing atmosphere and starts releasing oxygen into the gas phase. In the model, the inlet gas is

split in two phases (bubble and emulsion) upon entering the bed. The emulsion gas is sufficient to fluidize the bed and the excess gas appears as bubbles. The emulsion stays at minimum fluidization conditions and the bubbles are essentially free of solids [19, 20] (Figure 5.4). Therefore, reactions occur only in the emulsion phase but the products can transfer between the phases.

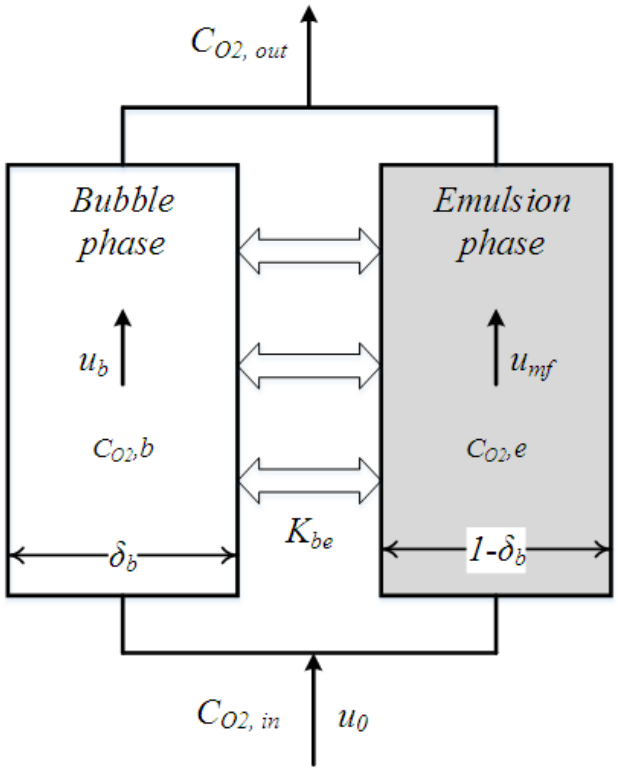

Figure 5.4 Schematic of a two phase fluid bed model

Many authors assume a plug flow model for the bubble phase because of the high bubble rise velocity [21, 22]. On the other hand, the gas velocity in the emulsion phase is an order of magnitude lower. Solid mixing in the emulsion phase may induce mixing of the gas [23, 24]. Emulsion gas phase models vary from perfectly mixed flow to plug flow (or plug flow with axial dispersion) [17]. Considering plug flow for the bubble phase and plug flow with axial dispersion for dense phase, and neglecting the increase in gas velocity along with the bed length (due to the oxygen release from oxygen carrier), the state equations together with model parameters are listed in Table 5.6:

Table 5.6 State equations and hydrodynamic parameter for a two phase model

#	Parameter	Correlation	Ref.
1	O_2 mass balance in emulsion phase	$\frac{\partial C_{O_2,e}}{\partial t} = D_{ax}\frac{\partial^2 C_{O_2,e}}{\partial z^2} - u_{mf}\frac{\partial C_{O_2,e}}{\partial z}$ $-\frac{\rho_p(1-\varepsilon_{mf})}{2W_0} \times r_{Co_3O_4} + \frac{K_{be}\delta(C_{O_2,b}-C_{O_2,e})}{1-\delta}$	
2	O_2 mass balance in bubble phase	$\frac{\partial C_{O_2,b}}{\partial t} = -u_b\frac{\partial C_{O_2,b}}{\partial z} - K_{be}(C_{O_2,b} - C_{O_2,e})$	
3	Mean O_2 concentration	$C_{O_2} = \frac{u_{mf}(1-\delta)}{u_0}C_{O_2,e} + \frac{u_b\delta}{u_0}C_{O_2,b}$	
4	u_{mf}	$Re_{mf} = \sqrt{27.2^2 + 0.0408Ar} - 27.2$	[25]
5	u_b	$u_b = u_0 - u_{mf} + u_{br}$	[26]
6	u_{br}	$u_{br} = 0.711(gd_b)^{0.5}$	
7	d_b	$d_b = d_{bm} + (d_{b0} - d_{bm})e^{-0.3z/D_t}$	[19]
		$d_{bm} = 0.65[\frac{\pi}{4}D_t^2(u_0 - u_{mf})]^{0.4}$	
		$d_{b0} = \frac{1.3}{g^{0.2}}(\frac{u_0-u_{mf}}{N_{or}})^{0.4}$	
		$N_{or} = \frac{1}{l_{or}^2}$	
8	Fraction of bed in bubbles	$\delta = \frac{u_0-u_{mf}}{u_b-u_{mf}}$	[19]
9	Bubble-cloud transfer coefficient	$K_{bc} = 4.5(\frac{u_{mf}}{d_b}) + \frac{5.85D_{O_2,m}^{0.5}g^{0.25}}{d_b^{1.25}}$	[19]
10	Cloud emulsion transfer coefficient	$K_{ce} = (\frac{D_{O_2,m}\varepsilon_{mf}u_{br}}{d_b^3})^{0.5}$	[19]
11	Bubble-emulsion transfer coefficient	$\frac{1}{K_{be}} = \frac{1}{K_{bc}} + \frac{1}{K_{ce}}$	[19]

$D_{O_2,m}$ is the oxygen diffusivity in the mixture and $r_{Co_3O_4}$, refers to the reduction rate of Co_3O_4 to CoO [3]:

$$r_{Co_3O_4} = 1.5Kt^{0.5}exp(-Kt^{1.5})\,[n_{Co_3O_4}]_{in} \tag{5.1}$$

$$K = 4 \times 10^{11}exp(-\frac{40400}{T_p}) \tag{5.2}$$

Where $[n_{Co_3O_4}]_{in}$ is the initial moles of Co_3O_4. Bubble motions agitate the bed and mix the

solid phase close to perfect mixing [27]. Therefore, $r_{Co_3O_4}$ (solid conversion) is only a function of time, and is the same throughout the bed. Axial dispersion coefficient, D_{ax}, was derived from a blank test in which the feed gas was switched from air to argon. Except the axial dispersion term, all other parameters remained constant (Table 5.6).

5.3.2 Biomass pyrolysis

Biomass pyrolysis starts at T=200 °C, and, as the temperature increases, the reaction rate increases. At very high temperatures (e.g., 800 °C), it is instantaneous [28]. The heat balance of a single biomass particle shows that it reaches the reactor temperature in 2 s which can be neglected compared to the gasification reaction time (see Appendix B). Different kinetic models have been presented in the literature for biomass pyrolysis. Among them Nunn et al. [29] developed a model for wood pyrolysis at a high heating rate of 1000 K/s, which is close to the conditions in the present study. The reaction rates of all products are first order with respect to the un-reacted volatile matter:

$$\frac{dV_i}{dt} = k_{0,i} e^{(\frac{-E_i}{RT_P})} (V_i^* - V_i) \tag{5.3}$$

Where V_i and V_i^* are the instantaneous and total amount of volatile matter. According to Nunns model [29], the activation energy vary from 11 (for H_2O) to 27 kcal/mol (for H_2) (Table 5.7).

Table 5.7 Kinetic parameter of Sweet Gum pyrolysis, Nunn et al. [29]

Component	$Log[k_{0,i}]$	$E_i[kcal/mol]$	$V_i^*[g/100g\ biomass]$
Total devolatilization	4.53	16.5	81
Total gas	2.88	11.8	35.7
H_2	6.7	27	1.66
CH_4	3.79	16.6	1.91
CO	3.36	14.6	14.85
CO_2	3.77	14.3	5.2
H_2O	3.35	11.5	4.48
Char=100-total devolatilization-ash			
Tar=Total devolatilization-total gas release			

Tar decomposes via secondary pyrolysis and converts to stable gases and inert tar according

to [30]:

$$\text{tar} \longrightarrow 0\cdot01\,\text{H}_2 + 0\cdot09\,\text{CH}_4 + 0\cdot56\,\text{CO} + 0\cdot11\,\text{CO}_2 + 0\cdot22\ tar_{inert} \tag{5.4}$$

$$\frac{d[tar]}{dt} = 10^{4.98} e^{(-\frac{11222}{T_p})}[tar] \tag{5.5}$$

Higher paraffins, such as ethane or propane is lumped into the methane formation.

5.3.3 Steam gasification

It is assumed that the char from the injected biomass remains at the bed surface and forms a thin layer. Considering the CSTR model for the char layer at the bed surface, the mole balance is:

$$\frac{d}{dt}(\frac{\delta_V}{Q}\dot{N}_{i,out}) = \dot{N}_{i,in} - \dot{N}_{i,out} \pm r_i \tag{5.6}$$

$$Q = \frac{RT}{P}\sum_i \dot{N}_{i,out} \tag{5.7}$$

Where "i" refers to component H_2, CH_4, CO_2, O_2, CO, H_2O and "r" is the reaction rate (mol/s). δ_V is the volume occupied by the char layer, and is a function of time. However, it is negligible compared to the bed volume and can be considered as constant. The inlet conditions are determined from pyrolysis. Gasification contains a complex serious of reactions and considering all of them was not on the scope of this paper and also impossible. A logical strategy to simplify the reaction network, is to consider those whom the reactants are fed to the reactor. For instance, the Boudouard reaction ($CO_2 + C \rightarrow 2CO$) was not considered in the modeling since CO_2 was not fed directly to the reactor. Consequently the main reactions which are likely to take place at the bed surface are reduced to steam-char and oxygen-char reactions (Table 5.8). The same strategy has been applied to simplify the homogeneous gas phase reactions in the freeboard region.

Table 5.8 Gas solid reactions at the bed surface

	Reaction	Kinetic rate	Reference
R_1	$C+H_2O \leftrightarrow CO+H_2$	$\frac{dX_c}{dt} = \frac{k_1 p_{H_2O}}{1+k_2 p_{H_2O}+k_3 p_{H_2}}$	Muhlen et al. [31]
		$k_1 = 4.93 \times 10^3 e^{(\frac{-18522}{T_p})}$	
		$k_2 = 1.11 \times 10 e^{(\frac{-3548}{T_p})}$	
		$k_3 = 1.53 \times 10^{-9} e^{(\frac{25161}{T_p})}$	
R_2	$2\frac{\eta+1}{\eta+2}C+O_2 \rightarrow \frac{2\eta}{\eta+2}CO+\frac{2}{\eta+2}CO_2$	$\frac{dX_c}{dt} = k_4 p_{O_2}(1-X_c)^{1.2}$	Di Blasi et al. [32]
		$k_4 = 1.5 \times 10^6 e^{(\frac{-13078}{T_p})}$	
		$\eta = 3 \times 10^8 e^{(\frac{-30178}{T_p})}$	Monson et al. [33]

Oxygen reacts with char and produces CO and CO_2. Increasing temperature favours CO production. Furthermore, the O_2 % is less than the stoichiometric value. Therefore, the CO production at these conditions is more favourable.

5.3.4 Homogeneous gas phase reactions

The produced gases from pyrolysis together with gasification undergo further homogeneous reactions in the freeboard. Considering a plug flow model, the material balance in the axial direction is:

$$\frac{\partial}{\partial t}(\frac{\dot{N}_i}{Q_f}) = \pm r_i' - \frac{1}{A}\frac{\partial \dot{N}_i}{\partial z} \tag{5.8}$$

$$Q_f = \frac{RT}{P}\sum_i \dot{N}_i \tag{5.9}$$

Deriving the kinetic of each individual reaction is out of the scope of this paper. Also, there are numerous publications dedicated to the kinetics of these reactions. Therefore, the reaction rates were used from the literature as listed in Table 5.9.

Table 5.9 Gas phase reaction rate expressions $(mol/m^3.s)$

	Reaction	Kinetic rate	Reference
R_3	$CO+H_2O \leftrightarrow CO_2+H_2$	$r'_3 = 10^6 e^{(\frac{-6370}{T})}\left[[CO][H_2O] - (\frac{[CO_2][H_2]}{520e^{(\frac{-7230}{T})}})\right]$	Inayat et al. [13]
R_4	$CH_4+H_2O \rightarrow CO+3H_2$	$r'_4 = 3\times 10^6 e^{(\frac{-15000}{T})}[CH_4][H_2O]$	Inayat et al. [13]

To obtain the oxygen concentration at various times and vertical positions in the bubbling bed, the two differential equations of the material balance (Table 5.6) together with the oxygen desorption rates were solved by the explicit finite difference method using MATLAB (R2012a). Time (t) and vertical position (x) are the variables and oxygen concentration in the bubble ($C_{O_2,b}$) and emulsion ($C_{O_2,e}$) are the unknowns. The axial dispersion coefficient (D_{ax}), is the only parameter of these equations which was obtained from RTD measurements. Biomass pyrolysis (steps 2) were solved independently from oxygen desorption (step 1). Eq. 5.3 was applied for all the spices listed in Table 5.7.

Oxygen concentration at the bed surface ($C_{O_2}(t, x = 20cm)$)) and the pyrolysis products compositions ($C_i(t), i : H_2, CH_4, CO, CO_2, H_2O, Char$) was used as the initial conditions for char gasification (step 3). Gas composition calculated at $H=H_{bed}$ provides the boundary condition for the freeboard section where the homogeneous reactions take place (step 4). The time and length intervals of 0.1 s and 1 cm was considered to solve the partial and ordinary differential equations and the gas composition at the end of the reacting media for the first 250 s of reaction time was plotted and compared with the experimental data.

5.4 Results and discussion

5.4.1 Hydrodynamic model validation

Considering the perforated plate distributes well the inlet gas, the radial concentration profile at H=0 is flat. A higher gas residence time close to the reactor wall (r/R=1) was expected due to the

lower gas velocity. However, the difference between the argon concentration at r/R=0, r/R=0.5 and r/R=1; was negligible at H=20 cm (Figure 5.5). This is due to the gas mixing in radial direction and low D_t. At bubbling regime, the radial dispersion is high because of the bubble movement [34]. Another reason for limited radial dispersion could be the low gas velocity. Therefore, the radial concentration profile was considered to be flat and the central position (r/R=0) was selected as the reference point for further analysis.

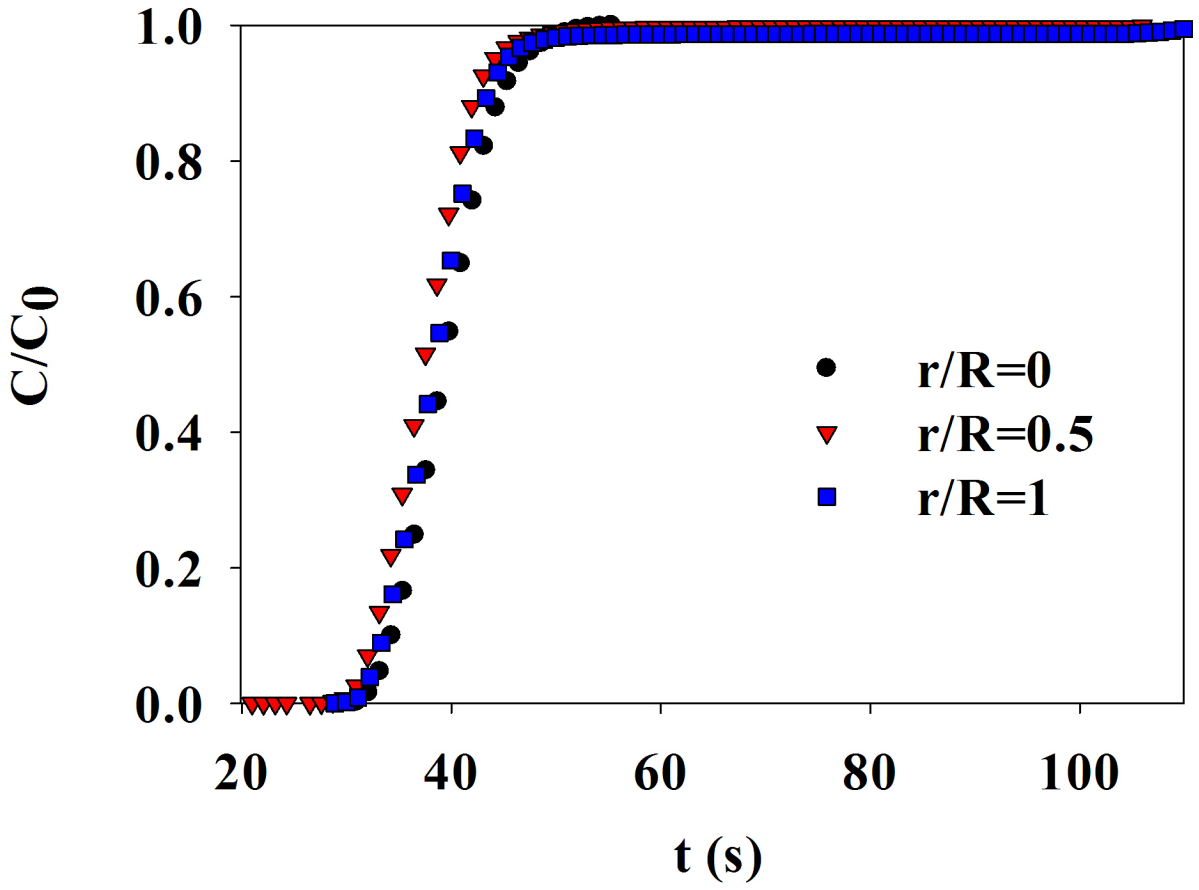

Figure 5.5 Radial dispersion, H=20 cm, u_0=13 cm/s, T=25 °C, sand as bed material

The hydrodynamic model-plug flow of the bubble phase and axial dispersion of the emulsion phase- together with related correlations presented in Table 5.6, was fitted with the axial residence time distribution data (Figure 5.6). The agreement between the model prediction and experimental

data validated the introduced hydrodynamic model for the bubbling fluidized bed (Figure 5.4).

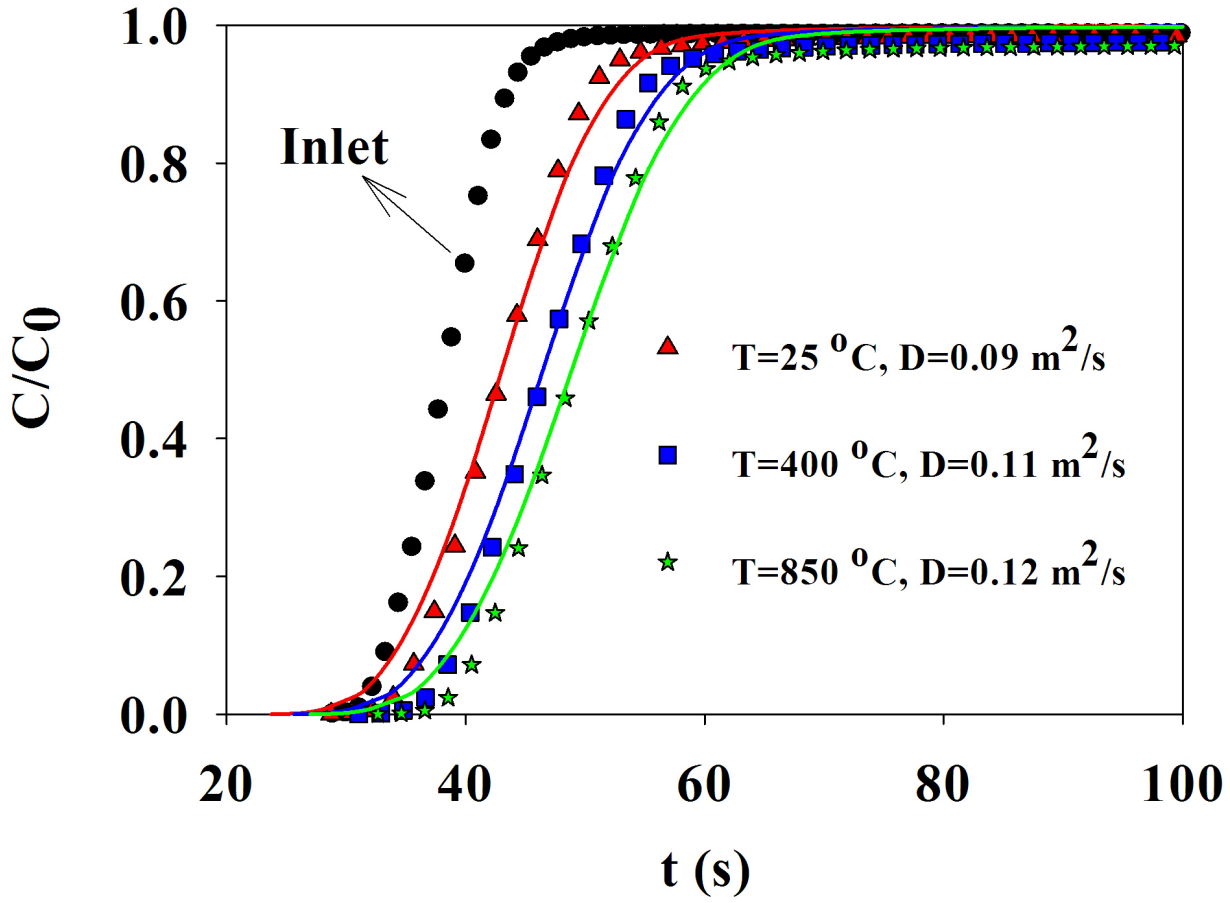

Figure 5.6 Modeling versus experimental RTD at T=25 °C, 400±4°C, and 850±8°C, H=20 cm, r/R=0, u_0=13 cm/s, with sand as bed material

Increasing temperature decreases the minimum fluidization velocity [35, 36]. Therefore, in a bubbling regime (u_0-u_{mf}) increases with temperature and smaller bubbles form, which result in more turbulence and mixing [37]. Therefore, it is expected that the dispersion coefficient increases with temperature. From ambient temperature to 850 °C, the axial dispersion coefficient increases from 0.092 ± 0.002 to 0.124 ± 0.002 m^2/s (Figure 5.6). On the other hand, the inter-particle forces (IPFs) increases with temperature, especially for fine particles with low melting points. Increasing IPFs affect the fluidization behavior and might increase the minimum fluidization velocity [38].

Consequently dispersion coefficient decreases because of lowering the bed turbulency. However, the “IPF” for cobalt oxide particles were negligible because the operating temperature was way lower than the transition temperature of bed materials.

5.4.2 Oxygen desorption in a bubbling fluidized bed

The oxygen desorption rate follows the nucleation growth model which is low at the beginning and the end of oxidation but fast in between. The low reaction rate at the beginning is attributed to the required time for formation and growing of the nuclei of the new phase. Once the initial nuclei have been formed, the reaction proceeds fastly. At the end of the transformation, the reaction rate slows down because there is little untransformed particles [3, 39]. Accordingly, the oxygen concentration is low at the beginning and the end of the reaction but maximum in between (Figure 5.7).

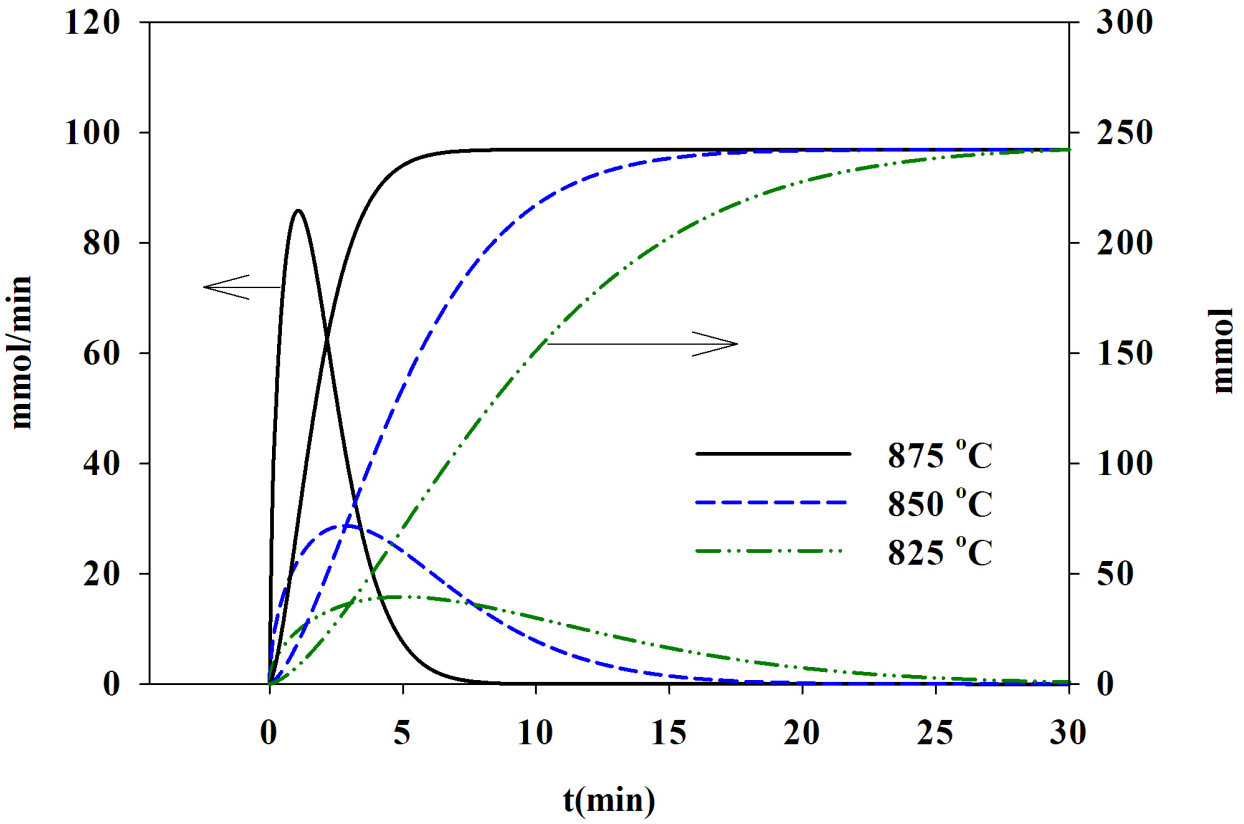

Figure 5.7 Modeling results for oxygen flow rate (left axes) and cumulative oxygen desorption (right axes) at the bed surface (H=20 cm), T=825 °C, 850 °C, 875 °C, u_0=13 cm/s, 50 % Co_3O_4

At $t = 0$ the gas feed switched from air/steam to Ar/steam. The maximum oxygen flow rate at the surface is 85 mmol/min, which was achieved at T=875 °C after 1 min. The peak decreased to 28 mmol/min at T=850 °C, t=3 min and 16 mmol/min at T=825 °C, t=5 min. Moreover, the reaction was complete after 30, 20 and 9 min when increasing the temperature from 825 °C to 875 °C because the oxygen desorption rate increases with temperature according to Eqs. 5.5 and 5.8. The total available oxygen from 421 g Co_3O_4 (bed quantity) is 259 mmol, which means that 93 % of the oxygen was released from cobalt oxide. The oxygen was released to the emulsion phase in the first step and then it diffused to the bubble phase. Therefore, the emulsion phase was richer in O_2 than the bubble phase. As the gas passed through the fluidized bed, it became richer in

oxygen. This may affect the oxygen release rate. Furthermore, the average O_2 quantity increases depending on the temperature because the reduction rate increases with the temperature.

5.4.3 Effect of temperature

For reversible endothermic reactions, increasing temperature favours the forward reaction. The reactions involved in steam gasification are all endothermic except the water gas shift reaction (R_4). Therefore, increasing temperature improves the gas production rate and total carbon conversion. The activation energy of pyrolysis toward hydrogen production is 27 kcal/mol compared to 14-17 kcal/mol for the rest of the gases. Therefore, temperature had more effect on the H_2 yield compared to other gases. Figures 5.8 to 5.10 show that, the presented model can satisfactorily predict the product gas composition versus time.

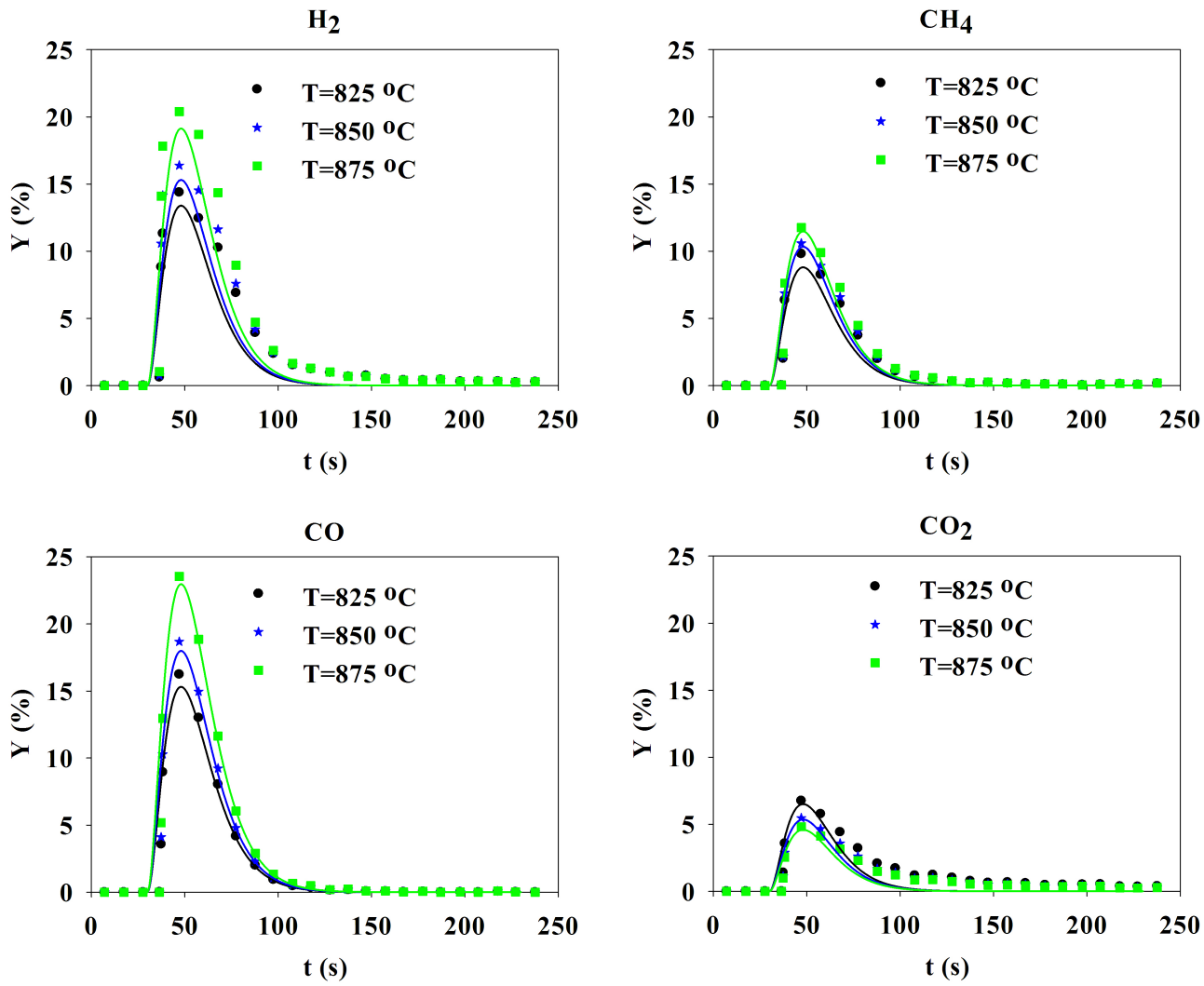

Figure 5.8 Concentration profiles of the gases versus time for T=825±8 °C, 850±7 °C, and 875±9 °C; H_2O %=18, Co_3O_4 %=50, R^2>0.896, solid line representing the model

From 825 to 875 °C the oxygen desorption rate from the oxygen carrier increased up to 500 % [3]. The released oxygen increased the CO production rate. However, the CO_2 composition remained steady because the available oxygen is less than the stoichiometric value for complete combustion. In addition, increasing the temperature increased the CO selectivity rather than CO_2 [32].

5.4.4 Effect of steam

Increasing steam concentration favours the production of H_2 and CO. Also, increasing the steam concentration will favours the water gas shift reaction, which consumes CO. These two effects neutralize each other; consequently, steam has a negligible effect on CO yield (Figure 5.9). CH_4 yield varies little with steam concentration. Increasing the steam concentration displaces the CH_4 reforming reaction (R_4) to the right (forward reaction) to produce more syngas. On the other hand, steam has a positive effect on the production of syngas according to R_1. From 0 up to 50 % steam, the hydrogen yield increased four times (Figure 5.9). The increase in H_2 yield from 0 % to 10 % steam was considerable, 3.2 times, while from 10 % up to 18 % steam it changed slightly, 1.8 times.

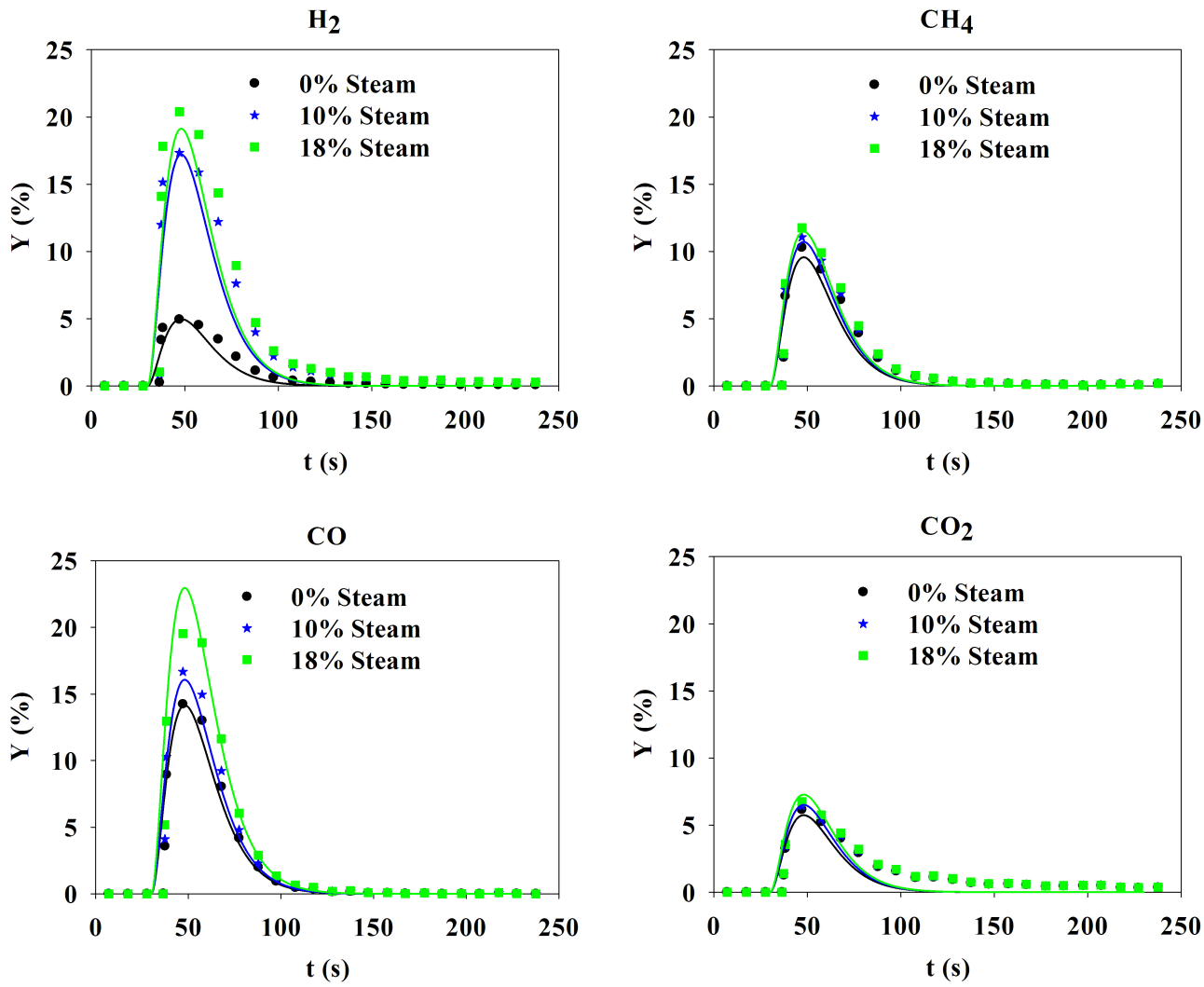

Figure 5.9 Concentration profiles of the gases versus time for 0, 10, 18 %steam; T=875 ±9 °C, Co_3O_4 %=50, R^2>0.827, solid line representing the model

Steam reacts with char to produce hydrogen and carbon monoxide. Excess steam favors hydrogen production rather than CO because of the water-gas shift reaction.

5.4.5 Effect of Co_3O_4

The oxygen carrier contributes to the reaction in two ways: First one is to supply oxygen for the partial oxidation of carbon; and, second to provide energy for steam gasification. Energy is delivered by the metallic oxide through sensible heat from the oxidation reactor and from the partial

combustion of biomass with the oxygen. The released oxygen is insufficient to completely oxidize the char; therefore, the CO production increased (by approximately 25 %) when 50 % of the sand was substituted with Co_3O_4 while the yield of the other gases remained essentially constant (Figure 5.10). The oxygen desorbed from the metal oxide and initiated the exothermic reactions (R_2). This phenomenon decreased the H_2:CO ratio. Furthermore, adding Co_3O_4 increased the total carbon conversion to some extent because of the catalytic effect of the cobalt on the steam gasification reactions. Cobalt promotes gasification especially tar cracking reactions [40, 41]. Therefore, it had opposite effect on the total carbon conversion.

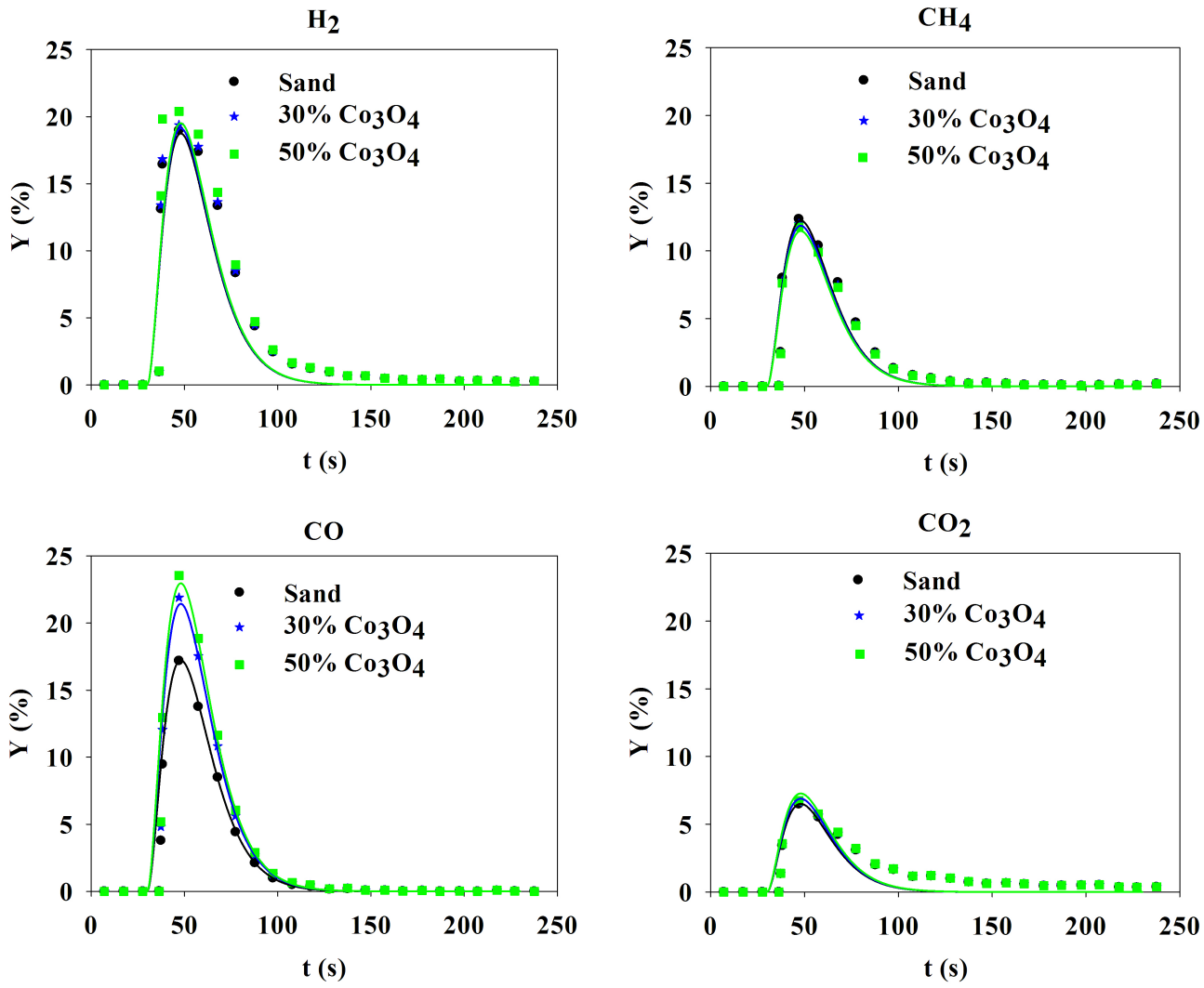

Figure 5.10 Concentration profiles of the gases versus time for Co_3O_4 %=0, 30, 50; H_2O %=18, T=875±9 °C, R^2>0.860, solid line representing the model

The model accounts for more than 90 % of the variance for most of the experimental data. However, the model accuracy for some cases (e.g., "CO" at T=875 °C, Co_3O_4 %=50 and H_2O %=18) is relatively low (R^2=0.83, Figure 5.9-b). The error might be due to of the accuracy of the correlations listed in Table 5.6 for the hydrodynamic parameters. Although the true reaction rates have been chosen, the operating system and conditions in which the reaction rates have been derived are basically not identical to this work.

5.5 Conclusions

Energy to gasify biomass with steam comes from either an external source or by combusting a portion of the biomass with molecular oxygen. We propose a chemical looping process with Co_3O_4-CoO couple to supply oxygen. The produced syngas from this process, has a higher calorific valueas it is not diluted by nitrogen, and, is more concentrated by H_2 and CO. Adding oxygen to the steam gasifier not only provides the required energy but also decreases the H_2/CO ratio which favours F-T synthesis or methanol production. Steam % and temperature both had a positive effect on the total biomass conversion as well as H_2 yield. Total biomass conversion was unaffected by substituting Co_3O_4 with sand; in fact CO yield increased by 45 %. A two phase model for the bubbling bed and a plug flow model for the freeboard region was derived as the gas phase hydrodynamic whereas a CSTR model was applied for the solid mixing in the bubbling bed. The gasification reactions and oxygen release rates were selected from the literature and our previous work. The biomass pyrolysis was completed in less than 10 s under the gasification conditions and can be considered as instantaneous upon injection to the reactor. The difference in gas composition in the radial direction was negligible which is due to the solid mixing in the bed. The bubble phase behaviour was close to a plug flow reactor while the emulsion phase deviated from plug flow. Increasing the temperature, the axial dispersion coefficient corresponding to the emulsion phase increased, which could be due to the higher mixing in the bed. The model accounted for 83% of the variance in the experimental data.

Notation

Ar	Archimedes number, $\frac{d_p^3 g(\rho_p - \rho_g)\rho_g}{\mu^2}$
C	Molar concentration, $molm^{-3}$
C_p	Particle heat capacity, $Wkg^{-1}K^{-1}$
d_b	Bubble diameter, m
d_p	Particle diameter, m
D_{ax}	Axial dispersion coefficient, m^2s^{-1}
$D_{O_2,m}$	Oxygen diffusivity in the mixture, m^2s^{-1}
D_t	Vessel diameter, m
E	Activation Energy, $kJmol^{-1}$
H	Axial position, m
K_{be}	Bubble to emulsion mass transfer coefficient, s^{-1}
k_g	Gas thermal conductivity, $Wm^{-1}K^{-1}$
l_{or}	Spacing between adjacent holes of orifice, m
$\dot{N}$	Molar flowrate, $mols^{-1}$
Q	Volumetric flowrate, m^3
r_i	Reaction rate of component i, $mols^{-1}$
r_i'	Reaction rate of component i, $molm^{-3}s^{-1}$
r/R	Radial position
Re_{mf}	Reynolds number at minimum fluidization velocity, $\frac{\rho_g u_0 d_p}{\mu}$
R^2	Coefficient of determination
u_0	Superficial gas velocity, ms^{-1}
u_b	Bubble velocity, ms^{-1}
u_{br}	Single bubble rise velocity, ms^{-1}
u_{mf}	minimum fluidization velocity, ms^{-1}
u_{ff}	Fully fluidized velocity, ms^{-1}
W_0	Initial weight of oxygen carrier, g
X	Conversion
δ	Fraction of bed in bubbles
ε_{mf}	Voidage at minimum fluidization velocity
ρ_p	Particle density, kgm^{-3}

Subscript

b	Bubble
e	Emulsion
f	Freeboard
oxi	Oxidation
red	Reduction
g	gas

References

[1] Renewables 2013 global status report: Ren21, 2013.

[2] Basu P. Biomass gasification and pyrolysis: Practical design and theory. Academic press; 2010.

[3] Aghabararnejad M, Patience GS, Chaouki J. TGA and kinetic modeling of Co, Mn and Cu oxides for Chemical Looping Gasification (CLG). Can J Chem Eng 2014; DOI: 10.1002/cjce.22046

[4] Evans P, Paskach T, Reardon J. Detailed kinetic modeling to predict syngas composition from biomass gasification in a PBFB reactor. Environ Prog 2010;29(2):184-92.

[5] Radmanesh R. Fluidized bed biomass gasification. Ph.D. thesis, Ecole Polytechnique Montreal, Canada; 2006.

[6] Corella J, Sanz A. Modeling circulating fluidized bed biomass gasifiers. A pseudo-rigorous model for stationary state. Fuel Process Technol 2005;86(9):1021-53.

[7] Fiaschi D, Michelini M. A two-phase one-dimensional biomass gasification kinetics model. Biomass Bioenergy 2001;21(2):121-32.

[8] Yu L, Lu J, Zhang X, Zhang S. Numerical simulation of the bubbling fluidized bed coal gasification by the kinetic theory of granular flow (KTGF). Fuel 2007;86(5-6):722-34.

[9] Badillo-Hernandez U, Alvarez-Icaza L, Alvarez J. Model design of a class of moving-bed tubular gasification reactors. Chem Eng Sci 2013;101:674-85.

[10] Lucas JP, Lim CJ, Watkinson AP. A nonisothermal model of a spouted bed gasifier. Fuel 1998;77(7):683-694.

[11] Li X, Grace JR, Watkinson AP, Lim CJ, Ergüdenler A. Equilibrium modeling of gasification: a free energy minimization approach and its application to a circulating fluidized bed coal gasifier. Fuel 2001;80(2):195-207.

[12] Kong X, Zhong W, Du W, Qian F. Three stage equilibrium model for coal gasification in entrained flow gasifiers based on aspen plus. Chinese J Chem Eng 2013;21(1):79-84.

[13] Inayat A, Ahmad MM, Yusup S, Mutalib MIA. Biomass steam gasification with in-situ CO_2 capture for enriched hydrogen gas production: a reaction kinetics modeling approach Energies 2010;3(8):1472-84.

[14] Woodruff RB, Weimer AW. A novel technique for measuring the kinetics of high-temperature gasification of biomass char with steam. Fuel 2013;103:749-57.

[15] Salaices E, de Lasa H, Serrano B. Steam gasification of a cellulose surrogate over a fluidizable Ni/α-alumina catalyst: A kinetic model. AIChE J 2012;58(5):1588-99.

[16] de Lasa H, Salaices E, Mazumder J, Lucky R. Catalytic steam gasification of biomass: catalysts, thermodynamics and kinetics. Chem Rev 2011;111(9):5404-33.

[17] Yazdanpanah MM, Forret A, Gauthier T, Delebarre A. Modeling of CH_4 combustion with NiO/$NiAl_2O_4$ in a 10 kW_{th} CLC pilot plant. Appl Energ 2014;113(c):1933-44.

[18] Fotovat F, Chaouki J, Bergthorson J. The effect of biomass particles on the gas distribution and dilute phase characteristics of sand-biomass mixtures fluidized in the bubbling regime. Che Eng Sci 2013;102:129-38.

[19] Kunii D, Levenspiel O. Fluidization engineering. Butterworth-Heinemann; 1991.

[20] Mostoufi N, Cui H, Chaouki J. A comparison of two- and single-phase models for fluidized bed reactors. Ind Eng Chem Res 2001;40(23):5526-32.

[21] Werther J. Modeling and scale-up of industrial fluidized bed reactors. Chem Eng Sci 1980;35(1-2):372-9.

[22] Kunii D, Levenspiel O. Bubbling bed model for kinetic processes in fluidized beds. Ind Eng Chem Res Dev 1968;7(4):481-92.

[23] Kato K, Wen CY. Bubble assemblage model for fluidized bed catalytic reactors. Chem Eng Sci 1969;24(8):1351-69.

[24] Wen CY, Yu YH. A generalized method for predicting the minimum fluidization velocity. AIChE J 1966;12(3):610-2.

[25] Hetsroni G. Handbook of multiphase systems. New York: Mcgraw-Hill Book Company; 1982.

[26] Gilliland ER. Fluidized particles. AIChE J 1964;10(5):783-5.

[27] Abad A, Adanez J, Garcia-Labiano F, de Diego LF, Gayan P. Modeling of the chemical-looping combustion of methane using a Cu-based oxygen-carrier. Energy Procedia 2009;1:391-8.

[28] Radmanesh R, Chaouki J, Guy C, Biomass gasification in a bubbling fluidized bed reactor: experiments and modeling. AIChE J 2006;52(12):4258-72.

[29] Nunn TR, Howard JB, Longwell JP, Peters WA, Product compositions and kinetics in the rapid pyrolysis of sweet gum hardwood. Ind Eng Chem Res Dev 1985;24(3):836-44.

[30] Boroson ML, Howard JB, Longwell JP, Peters WA. Product yields and kinetics from the vapor phase cracking of wood pyrolysis tars. AIChE J 1989;35(1):120-8.

[31] Muhlen HJ, van Heek KH, Juntgen H. Kinetic studies of steam gasification of char in the presence of H_2, CO_2 and CO. Fuel 1985;64(7):944-9.

[32] Blasi CD, Buonanno F, Branca C. Reactivities of some biomass chars in air. Carbon 1999;37(8):1227-38.

[33] Monson CR, Germane GJ, Blackham AU, Smoot LD. Char oxidation at elevated pressures. Combust Flame 1995;100(4):669-83.

[34] Hebert Weinsten JL. An experimental comparison of gas backmixing in fluidized beds across the regime spectrum. Chem Ing Sci 1989;44(8):1697-705.

[35] Botterill JSM, Teoman Y, Yuregir KR. The effect of operating temperature on the velocity of minimum fluidization, bed voidage and general behaviour. Powder Technol 1982;31(1):101-10.

[36] Wu SY, Baeyens J. Effect of operating temperature on minimum fluidization velocity. Powder Technol 1991;67(2):217-20.

[37] Foka M, Chaouki J, Guy C, Klvana D. Gas phase hydrodynamics of a gas-solid turbulent fluidized bed reactor. Chem Eng Sci 1996;51(5):713-23.

[38] Shabanian J, Jafari R, Chaouki J. Fluidization of ultrafine powders. Int Rev Chem Eng 2012;4(1):16-50.

[39] Avrami M. Kinetics of Phase Change. I. General Theory. Chem Phys 1939, 7, 1103-12.

[40] Tasaka K, Furusawa T, Tsutsumim A. Steam gasification of cellulose with cobalt catalysts in a fluidized bed reactor. Energy Fuels 2007;21(2):590-5.

[41] Sornkade P, Atong D, Sricharoenchaikul V. Enhancement of cassava rhizome gasification using mono-metallic cobalt catalysts. Energy Procedia 2013;34:273-81.

[42] Botterill JSM. Fluid-Bed Heat Transfer. Academic Press 1975;145-277.

[43] Gronli MG. Theoretical and experimental study of the thermal degradation of biomass. Ph.D. thesis, Norwegian University of Science and Technology, Norway; 1996.

Appendix A

The main reactions taking place in the freeboard region are water gas shift (WGS) and reforming reactions (Table 5.9). The reaction rate constant for WGS can be neglected at temperatures below 400 °C and for reforming reaction it can be neglected if the temperature is below 600 °C (Figure 5.11).

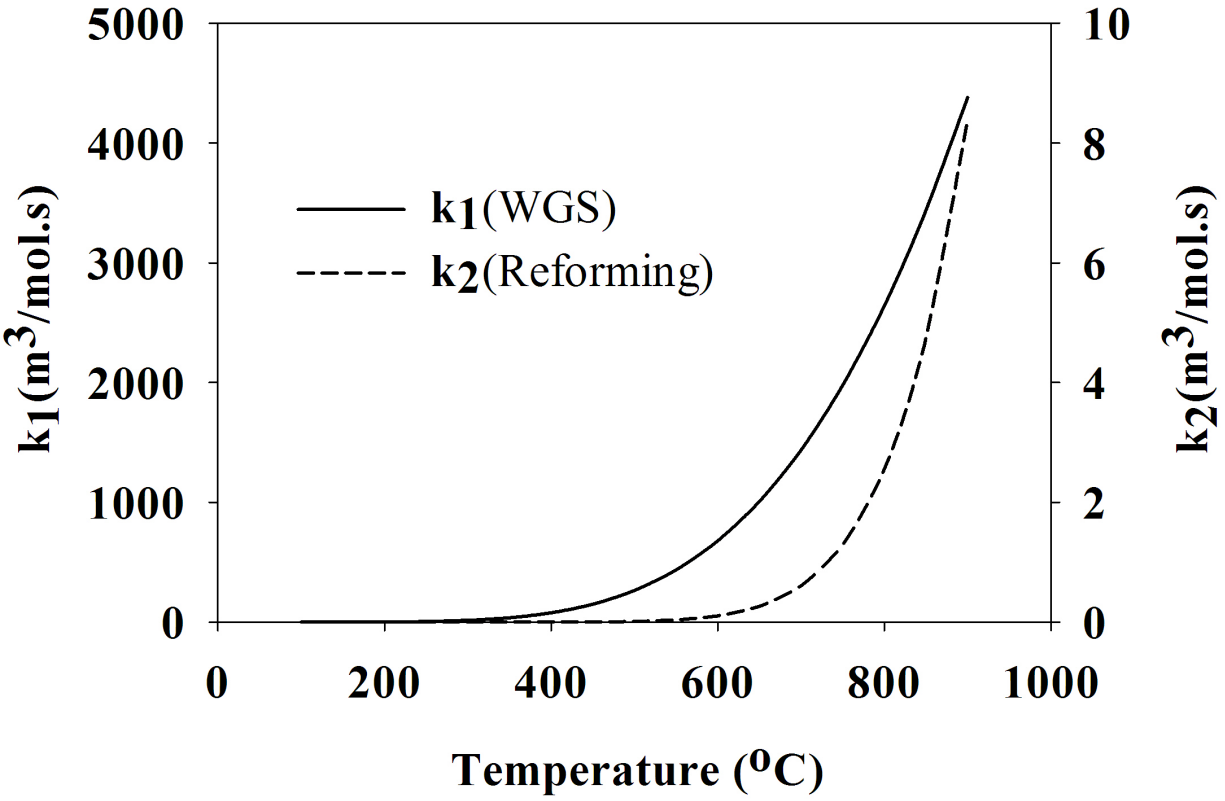

Figure 5.11 WGS and reforming reaction rate constant versus temperature [13]

Therefore, in disengagement zone where the temperature in below 230 °C, no reaction is taking place.

Appendix B

There are three main mechanisms by which heat is transferred to an object in a fluidized bed: convection from gas, contact with bed material and radiation. The radiation can be neglected if the object is in the dense bed. Considering that the particle temperature is only a function of time (T_p=$f(t)$), Eqs. 5.10-5.13 demonstrate the heat balance for a single biomass particle neglecting the reaction inside the particle, shrinkage of biomass and heat transfer in the injection line.

$$m_p \frac{d(C_p T_p)}{dt} = S(h_g + h_{bed})(T_\infty - T_p) \tag{5.10}$$

h_g is the convection coefficient of the gas phase and h_{bed} is the apparent convection coefficient of the bed material. "S" is the area of the biomass particle. Botterill [42] presented a correlation for h_g and h_{bed} of group D particles:

$$h_g = 0.86 \frac{k_g}{D^{0.5}} Ar^{0.39} \quad Wm^{-2}K^{-1} \tag{5.11}$$

$$h_{bed} = 0.843 \frac{k_g}{D} Ar^{0.15} \quad Wm^{-2}K^{-1} \tag{5.12}$$

The numerical constant 0.86 has the dimension of $m^{-0.5}$ and "D" is the characteristic length of the particle and was considered as the diameter of the biomass pellet (6 mm). The heat capacity of the particle changes with temperature. Gronli et al. [43] presented a correlation for the specific heat of wood in the range of 273-1273 K:

$$C_p = 0.42 + 2.09 \times 10^{-3} T + 6.85 \times 10^{-3} T^2 \quad kJ/kgK \tag{5.13}$$

Solving the energy balance equation shows that the biomass particle reaches the bed temperature (e.g., 850 °C) in around 2 seconds (Figure 5.12).

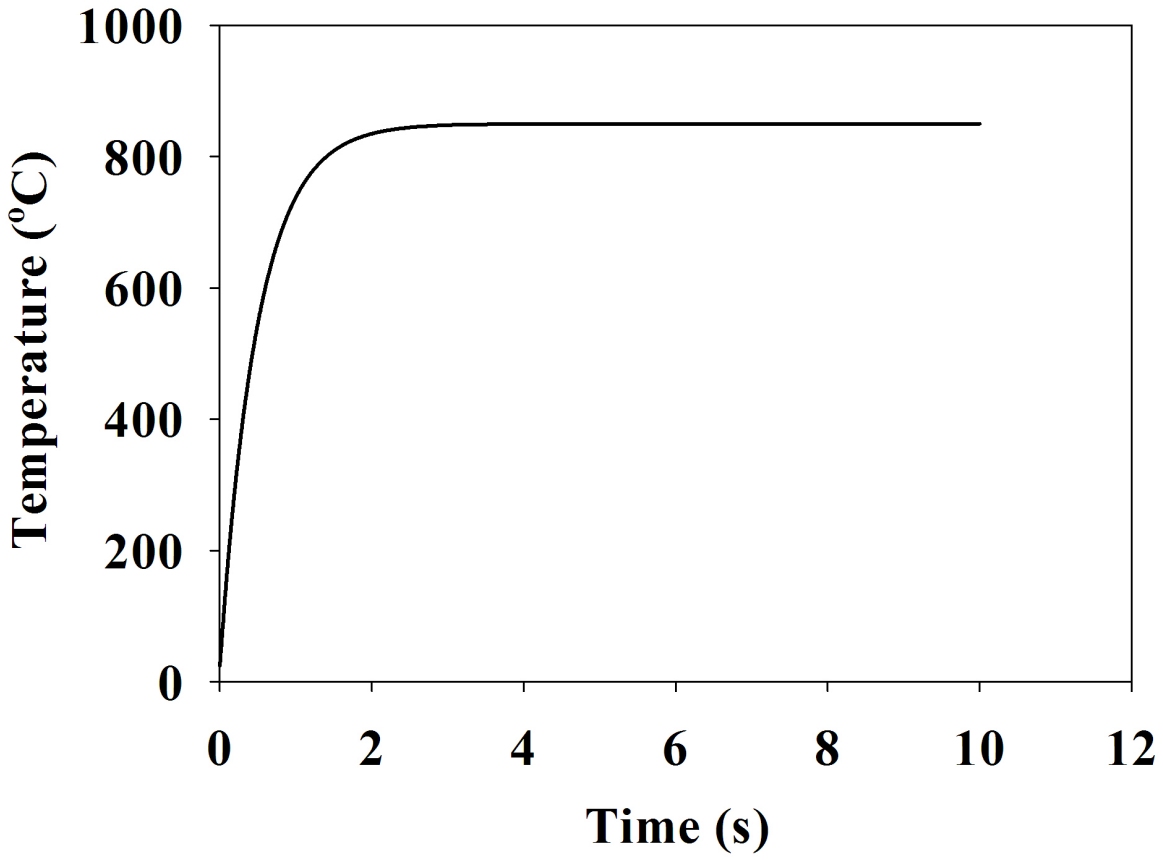

Figure 5.12 Variation of biomass particle temperature upon entering to the bubbling fluidized bed operating at 850 °C

The biomass particle should spend a longer time in the bed to reach the operating temperature if the pyrolysis is taken into account. However, the biomass shrinkage and preheating in the injection line help the heat transfer to the particle and can neutralize the endothermicity effect of pyrolysis.

CHAPTER: 6

ARTICLE 3: TECHNO-ECONOMIC COMPARSION OF A 7 MW_{th} BIOMASS CHEMICAL LOOPING GASIFICATION UNIT WITH CONVENTIONAL SYSTEMS

Milad Aghabararnejad, Gregory S. Patience, Jamal Chaouki

Department of Chemical Engineering, Polytechnique Montréal, C.P. 6079, Succ. CV Montréal, H3C 3A7 Québec, Canada

This work was submitted to the journal: *Chemical Engineering & Technology* (2014)

Abstract

Gasification is a process by which biomass is converted into carbon monoxide, hydrogen, and carbon dioxide through exposure to oxygen and/or steam. Conventional gasification (CG) systems use air, steam, and carbon dioxide as an oxygen source. Besides air, the chemical looping process is an alternative method to provide the system with the required oxygen. The syngas produced using the chemical looping has a higher calorific value than that produced using a conventional process with air. For comparison purposes, a conventional gasification unit with pure oxygen (CGPO) and a chemical looping gasification (CLG) system were simulated using Aspen Plus to treat 86 t/d biomass, with an economic analysis comparing the operating and capital costs of the two systems. The two systems were identical except for the reactor configuration. The "CGPO" reactor consisted of a bubbling fluidized bed (ID=1.8 m and H=6.6 m) as gasifier and sand as bed material with oxygen supplied via a pressure swing adsorption unit. The CLG consisted of a bubbling fluidized bed gasifier (ID=1.8 m and H=6.6 m) working in parallel with a fast fluidized bed oxidizer (ID=1 m and H=10 m). Co_3O_4(8 %)/Al_2O_3 with a circulation rate of 44.6 kg/s between gasifier and oxidizer supplied the oxygen for the CLG system. The total capital investment (TCI) of the CGPO and CLG units were $6.3M and $9.7M, respectively. However, the annual operating cost of the CLG was $0.58M less than that of the CGPO which repays the difference in TCI in less than 6 years.

Keywords: *Biomass Gasification, Conventional Gasifier, Design, Economic analysis, Simulation.*

6.1 Introduction

Biomass is principally composed of carbon, hydrogen, oxygen, nitrogen, and small quantities of heavy metals. Besides its abundance and low-cost, the sulfur content of biomass is lower compared to other fossil fuels and therefore, produces less acid gases such as SOx [1]. Furthermore, it is

carbon neutral with respect to CO_2. These characteristics make biomass an attractive source of renewable energy. Although biomass from plants was the first fuel used by mankind to meet its energy demands, converting biomass to a convenient energy form remains challenging.

Among the various technologies available to convert biomass into energy, thermo-chemical processes have received the most attention, particularly combustion, gasification, and pyrolysis. We focus on gasification because of its superior efficiency. Gasification is environmentally friendly and produces a high heating value gas which is predominantly H_2 and CO (syngas). Syngas is used as a building block for Fischer Tropsch (FT) and in the production of synthetic natural gas, hydrogen, and methanol, and may also be used as a direct fuel source. In conventional gasification (CG), air and/or steam are the gasification agents. Air dilutes the syngas with N_2 so steam is used whenever a high purity of H_2 is required. Steam gasification however, is an endothermic process and the H_2:CO ratio is superior to 4 [2]. One way to decrease the H_2:CO ratio which favours FT synthesis or methanol production, and supplies the required energy is to partially combust part of the biomass feed.

In the chemical looping gasification (CLG) process, instead of air, a metallic oxide which circulates between two vessels, provides the oxygen. In one vessel, the reduced metal is oxidized by air and carried to the fuel reactor. The oxygen then desorbs from the metal oxide and together with the steam reacts with the biomass to form syngas. The most common design configuration for a chemical looping process is based on a low velocity bubbling fluidized bed gasifier and a high velocity oxidizer [3]. Controlling the solid circulation rate, adjusting solid residence time, and avoiding gas leakage between the two vessels, are the major challenges of this configuration. Different materials ranging from ilmenite to oxides of iron, nickel, and manganese have been used as oxygen carriers. A 10 kW_{th} and a 1 MW_{th} are the smallest and largest chemical looping processes, respectively, which have been documented in the literature (Tab. 6.1).

Table 6.1 Design of the chemical looping processes

Process	Reactor configuration	Fuel	Oxygen carrier	Capacity	Reference
Combustion	MB+FB	Coal	Fe_2O_3	25 kW_{th}	Kim et al. [4]
Combustion	FB+FB	Coal	N.A.	1 MW_{th}	Strohle et al. [5]
Combustion	Two interconnected FB	Coal	Ilmenite	10 kW_{th}	Berguerand et al. [6]
Combustion	Dual circulating FB	Natural gas	NiO	120 kW_{th}	Kolbitsch et al. [7]
Combustion	Double loop CFB	Methane	Manganese	150 kW_{th}	Bischi et al. [8]
H_2 Prod.	MB+MB	Syngas	Fe_2O_3	25 kW_{th}	Sridhar et al. [9]

MB: Moving bed, FB: Fluidized bed, CFB: Circulating fluidized bed, N.A.: Not applicable

Kim et al. [4] designed a 25 kW_{th} moving bed+fluidized bed coal chemical looping combustion. The coal is injected as solid fuel from the side and Fe_2O_3 as oxygen carrier is entered to the combustor from the top and flows to the bottom. The gas velocity (u_0) in the combustor should always be less than the minimum fluidization velocity of the oxygen carrier; while u_0, on the other hand, should be bigger than the minimum fluidization velocity of the coal particles to ensure that no coal enters the oxidizer. Low velocity in the reactor results in a huge diameter. Kim et al. [4] assumed that the oxygen carrier particles move individually in the oxidizer and therefore, the particle velocity is the difference between superficial gas velocity and terminal velocity. Kolbitsch et al. [7] presented a procedure to design a 120 kW_{th} chemical looping combustion (CLC) of natural gas. They considered the fuel reactor as a turbulent fluidized bed operating at a velocity greater than the turbulent velocity (u_c) and lesser than the critical velocity (u_{se}) which is the point where solids begin to be entrained significantly. Also, the superficial gas velocity at the oxidation reactor is 2 times greater than u_{se} to ensure proper solid circulation [7]. The effects of devolatilization (increase in gas velocity) and solids returning to the bed were not discussed in their work.

Although the design procedures for chemical looping systems have been relatively well documented, as yet there has not been a rigorous economic analysis comparing chemical looping systems to conventional gasification systems. Olaleye and Wang [10] are among the few who analyzed the economics of the CLC. They compared the feasibility of a conventional combustor to a CLC unit. Their analysis indicates that the CLC process has a lower payback period and consequently higher commercialization potential.

Aghabararnejad et al. [11] developed an oxygen carrier based on a cobalt and alumina support,

which has superior oxygen transport capacity, as well as thermal and mechanical strength. They showed by further experiments in a TGA that the cobalt oxide performance was not affected by the presence of biomass [12].

The objective of this paper is to present three biomass gasification scenarios to produce high concentrated syngas including: A conventional gasification unit (CG) with air; a conventional gasification unit with pure oxygen (CGPO); and a chemical looping gasification (CLG) process. Only the design of the reactor (as the main operating unit) has been discussed in detail; however, the simulation of all three systems were performed with ASPEN PLUS. It is assumed that the CGPO unit receives pure oxygen from a pressure swing adsorption system. Finally the capital and operating costs of the three systems were compared.

6.2 Design and simulation of the CG unit

86 t/d biomass (48 %wt C, 6.2 %wt H, 45 %wt O, 0.2 %wt N, 0.6 %wt S) is fed to a bubbling fluidized bed gasifier and gasified with steam and air at 850 °C. This might be considered as a small scale gasification unit compared to a typical gasification system with 1000 t/d [13]. However, since biomass transformation costs are the dominant price of the raw material, small scale gasification units which can be operated at the harvesting site, have received more attention. Assuming the steam to carbon molar ratio (λ=S/C), the steam flow rate was calculated by knowing the biomass feed rate. A value in the range of 2-2.5 is suggested for "λ" [13]. Steam gasification is an endothermic process and the required energy can be achieved by the partial combustion of biomass using oxygen via the following reactions:

$$C + 0 \cdot 5\,O_2 \longrightarrow CO - 111\ (kJ/\text{mol}) \tag{6.1}$$

$$C + O_2 \longrightarrow CO_2 - 394\ (kJ/\text{mol}) \tag{6.2}$$

The second reaction consumes twice as much O_2 as the first reaction. Therefore, in an oxygen

deficient atmosphere (e.g., gasifier), the first reaction is more likely to take place. The ratio of the oxygen required to gasify the biomass to the oxygen required for complete combustion is known as the equivalent ratio (ER). Considering λ=2, as ER increases, the gasifier duty decreases indicating less energy is required and at ER=0.076 the gasification is auto thermal (Fig. 6.1). The ER is normally in the range of 0.2-0.3 [13]. Lower ER is due to the higher oxygen content in the biomass feed. Furthermore, the gasifier was considered to be adiabatic whereas the heat loss from the entire system is inevitable. A larger portion of the biomass should be combusted to compensate for the heat loss which requires more oxygen and results in a higher ER. The gasifier model was "RGibbs reactor" which was operating at T=850 °C.

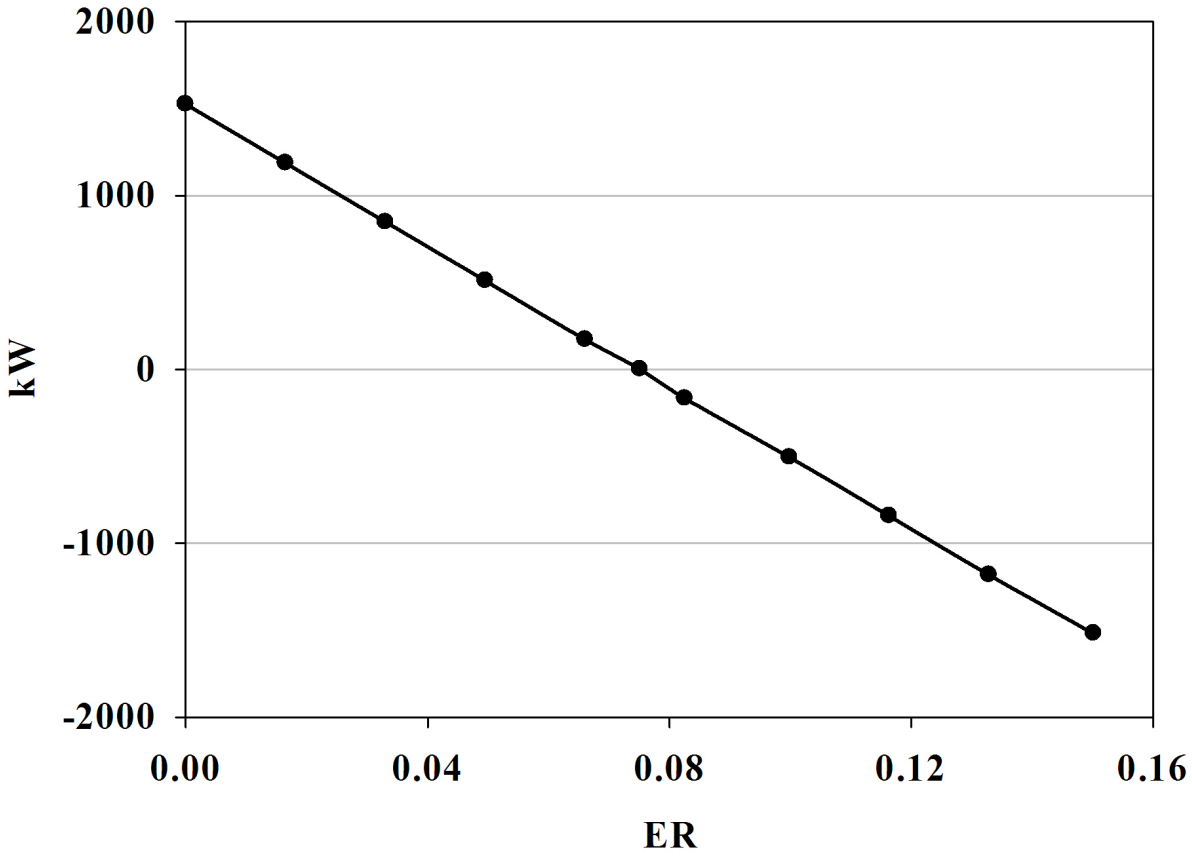

Figure 6.1 Gasifier duty vs. ER, 86 t/d biomass, λ=2

The battery limits of this process is to produce a concentrated syngas which can be used as a feed stock for production of synthesis fuels. The ash particles are separated from the produced gas in a cyclone and the fine particles are removed with a hot gas filter. The hot gas is cooled in a heat exchanger where its energy can be used to generate steam. The exit temperature should not be lower than the dew point of the stream to avoid condensation and blockage. The syngas is then washed with water to remove impurities in a scrubber. The oil phase and the aqueous phase can be further separated using a decanter (Fig. 6.2).

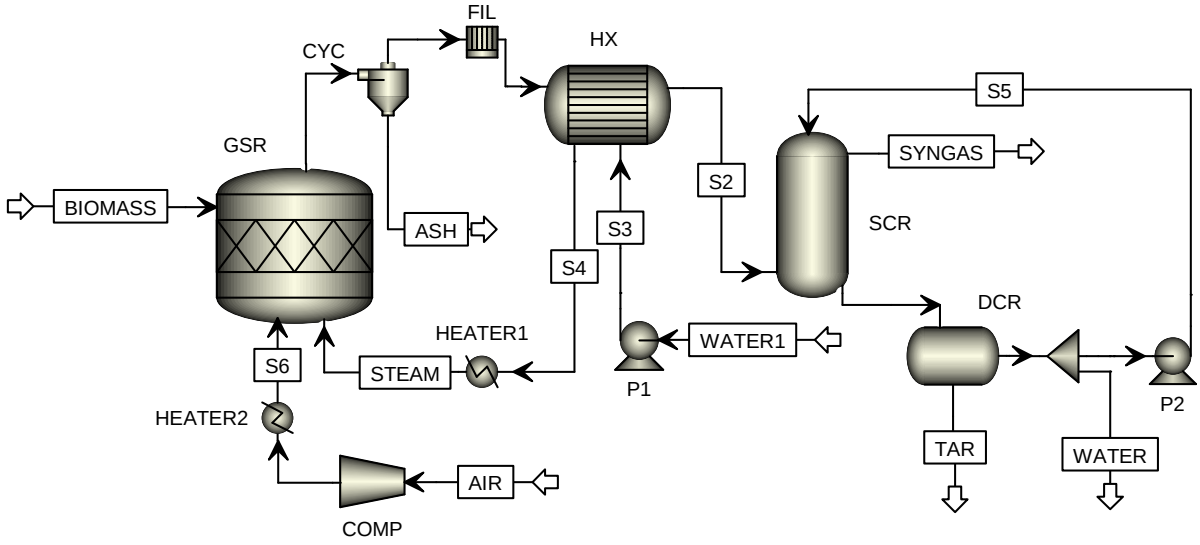

Figure 6.2 Simulation of the CG unit, GSR: Gasifier, CYC: Cyclone, FIL: Filter, HX: Heat exchanger, SCR: Scrubber, DCR: Decanter, P: Pump, COMP: Compressor

The syngas has 14 % CO_2 (Tab. 6.2) which can be separated from the syngas using an amine absorption process. The sulfuric components which were absent in this process can also be removed in the amine absorber.

Table 6.2 Mass balance of the CG unit, Aspen plus V. 7.2

Component	Stream										
	BIOMASS	AIR	S6	STEAM	ASH	S2	S4	SYNGAS	TAR	WATER	S5
y_{H_2}						0.23		0.32			
y_{CO}						0.17		0.23			
y_{CH_4}						0.07		0.09			
y_{CO_2}						0.10		0.14			
y_{O_2}		0.21	0.21								
y_{N_2}		0.79	0.79			0.13		0.18			
y_{H_2O}				1		0.26	1	0.04	0.04	1	1
$y_{Biomass}$	1				0.54						
y_{Tar}						0.056			0.99		
y_{Ash}					0.46						
Mass flow (kg/s)	1	0.43	0.43	1.44	0.322	2.55	1.44	1.37	0.784	0.399	0.7
T (^oC)	25	25	850	850	850	200	133	30	30	30	30
P (bar)		1	3	3		1.5	3	1	1	1	1.5

The syngas contains 18 % N_2 which is considered as a diluent for the downstream facilities. One possible option to remove N_2 from the produced syngas is to use a conventional gasification unit with pure oxygen (CGPO) instead of the air. Pure oxygen is provided from an air separation unit (ASU). The ASU can use cryogenic distillation, pressure swing adsorption (PSA), or membrane technologies. The PSA technology is the most appropriate option for the present system based on the required oxygen capacity and level of purity [14]. The syngas from CGPO is more concentrated in H_2 and CO (Tab. 6.3).

Table 6.3 Mass balance of the CGPO unit, Aspen plus V. 7.2

	Stream										
Component	BIOMASS	O2	S6	STEAM	ASH	S2	S4	SYNGAS	TAR	WATER	S5
y_{H_2}						0.26		0.39			
y_{CO}						019		0.28			
y_{CH_4}						0.07		0.11			
y_{CO_2}						0.12		0.17			
y_{O_2}		1	1								
y_{H_2O}				1		0.3	1	0.04	0.04	1	1
$y_{Biomass}$	1				0.54						
y_{Tar}						0.06			0.99		
y_{Ash}					0.46						
Mass flow (kg/s)	1	0.1	0.1	1.44	0.322	2.22	1.44	1.035	0.784	0.399	0.5
T (^oC)	25	25	850	850	850	200	133	30	30	30	30
P (bar)		1	3	3		1.5	3	1	1	1	1.5

The AIR stream is replaced with O2

The energy consumption of two units are very close to each other (2670 kW for CG vs 2607 kW

for CGPO). It is assumed that the feeding streams are at 850 °C except for the biomass (Tab. 6.4).

Table 6.4 Simulation description of CG and CGPO units

Unit	Function	Aspen Model	Outlet T(^oC)	Duty (kW)	
				CG	CGPO
GSR	Gasifier	RGibbs	850		
CYC	Cyclone	Cyclone	850		
FIL	Filter	Plate	850		
HX	Heat exchanger	HeatX	133-200		
P1	Pump	Pump	25	0.38	0.38
P2	Pump	Pump	25	0.13	0.11
HEATER1	Heater	Heater	850	2281	2522
HEATER2	Heater	Heater	850	324.4	71.18
SCR	Scrubber	Extract	30		
DCR	Decanter	Decanter	30		
COMP	Compressor	Compressor	110	63.48	13.29
Total				2670	2607

For simplicity, we have just presented the design procedure of the CGPO unit. However, the gasifier dimensions of both units (CG and CGPO) were compared ultimately (Tab. 6.5). The gasifier is a bubbling fluidized bed reactor (T=850 °C) with sand as inert material (d_p=300 μm, ρ_p=2650 kg/m^3). The superficial gas velocity (u_0) should be higher than the minimum fluidization (u_{mf}) and lower than the critical velocity (u_{se}), where the solid entrainment is significant. The gas velocity increases by injecting biomass. Therefore, the gas velocity varies along the bed height. The diameter of the bubbling bed (D_b) is chosen with respect to u_0. The total gasifier height is the sum of the bubbling bed (dense bed) height (H_b) and freeboard height (H_f). The bubbling bed should be high enough to provide sufficient gas residence time to reach the desired biomass conversion. The limiting step during steam gasification is the char-steam reaction.

$$C + H_2O \longrightarrow CO + H_2 \tag{6.3}$$

Since Reaction 6.3 takes place in the bed, a proper hydrodynamic model (e.g., two phase) is required for the reactor design. However, as the first step (preliminary design), a completely mixed flow model with known hydrodynamics, is used to calculate the reactor volume.

$$F_{C_0} - F_C - (-r_C)V = 0 \tag{6.4}$$

$$F_C = F_{C_0}(1 - X_C) \tag{6.5}$$

The Reaction 6.3 rate expression is [15]:

$$-r_C = k[C][H_2O] \tag{6.6}$$

$$k = 2 \times 10^5 e^{\frac{-6000}{T}} \tag{6.7}$$

By substituting Eqs. 6.5 and 6.6 in Eq. 6.4:

$$F_{C_0} X_C = k[C][H_2O]V \tag{6.8}$$

where

$$[C] = [C]_0(1 - X_C) \tag{6.9}$$

$$[H_2O] = [H_2O]_0 - [C]_0 X_C = [C]_0(\lambda - X_C) \tag{6.10}$$

Where $[C]_0$ is the initial molar concentration of carbon in the mixed feed stream. By substituting Eqs. 6.9 and 6.10 in Eq. 6.8, the dense bed volume and consequently D_b is calculated as:

$$V = \frac{\pi}{4} D_b^2 H_b = \frac{F_{C_0}}{k[C]_0^2} \frac{X_C}{(1 - X_C)(\lambda - X_C)} \tag{6.11}$$

The energy of the bubble eruption at the bed surface tosses the particles up and separates them from the bed. The heavier particles fall down to the bed but the lighter particles are entrained because of the gas-solid drag force. To decrease the bed elutriation, an empty zone, so-called "freeboard" was considered between the bed and reactor outlet. Usually the freeboard diameter has to be more than the bubbling bed diameter to reduce gas velocity and consequently drag force. On

the other hand, the gas velocity in the freeboard region should be high enough to entrain the ash particles. Therefore:

$$u_{se}(Ash) < u_0(Freeboard) < u_{se}(Bed\ material) \tag{6.12}$$

By keeping the same diameter as the dense bed for the freeboard region, the gas velocity in the freeboard is 2.3 m/s which is more than the critical velocity of ash particles (see Appendix A). The particle flux from the surface decays exponentially with height [16]:

$$E_p = E_{pf} + E_{p0}exp(-4H) \tag{6.13}$$

$$E_{p0} = 9.6A(u_0 - u_{mf})^{2.5} g^{0.5} \rho_g^{3.5} \mu_g^{-2.5} \tag{6.14}$$

The particle flux converges to E_{pf} as H increases. The final solid flux is only a function of the particle and flow properties [17]:

$$\frac{E_{pf} d_p}{\mu_g} = Ar^{0.5} exp[6.92 - 2.11F_g^{0.303} - \frac{13.1}{F_d^{0.902}}] \tag{6.15}$$

where

$$F_g = g d_p(\rho_p - \rho_g) \quad and \quad F_d = C_D \rho_g u_0^2/2 \tag{6.16}$$

By choosing E_p=1.1E_{pf}, H_f=2.4 m (Fig. 6.3).

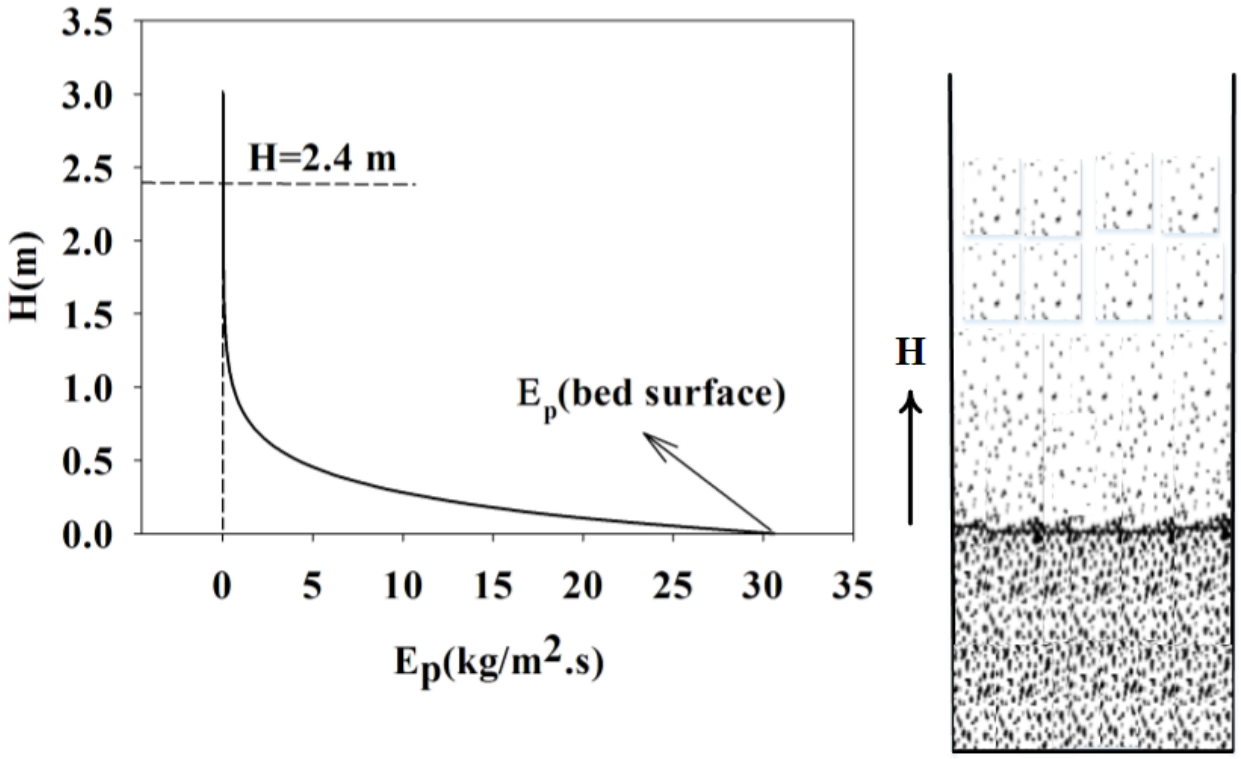

Figure 6.3 Particle flux (E_p) versus freeboard height (H)

Therefore, the gasifier has a unique diameter of 1.8 m and a total height of 6.55 m (Tab. 6.5; see Appendix A for details).

Table 6.5 CG and CGPO gasifier design results

Input			Output	
			CG	CGPO
$u_0(bed), m/s$	1.5	D_b, m	1.94	1.8
$F_{C_0}, mol/s$	40	H_b, m	3.57	4.15
$[C]_0, mol/m^3$	0.18	D_f, m	1.94	1.8
X_C	0.9	H_f, m	3.2	2.4
$T, {}^oC$	850			

The reactor dimensions for the CG unit is also presented in Tab. 6.5. Since the gas flowrate in the CG process is more than CGPO, D_b of CG unit is greater to keep the same gas velocity in the

dense bed as CGPO.

6.3 Design and simulation of the CLG unit

In CLG the oxygen is provided from the oxidation-reduction cycles of cobalt oxide rather than air (Fig. 6.4). The oxygen is released from Co_3O_4 in a gasifier and the reduced CoO is transferred to the oxidizer for regeneration.

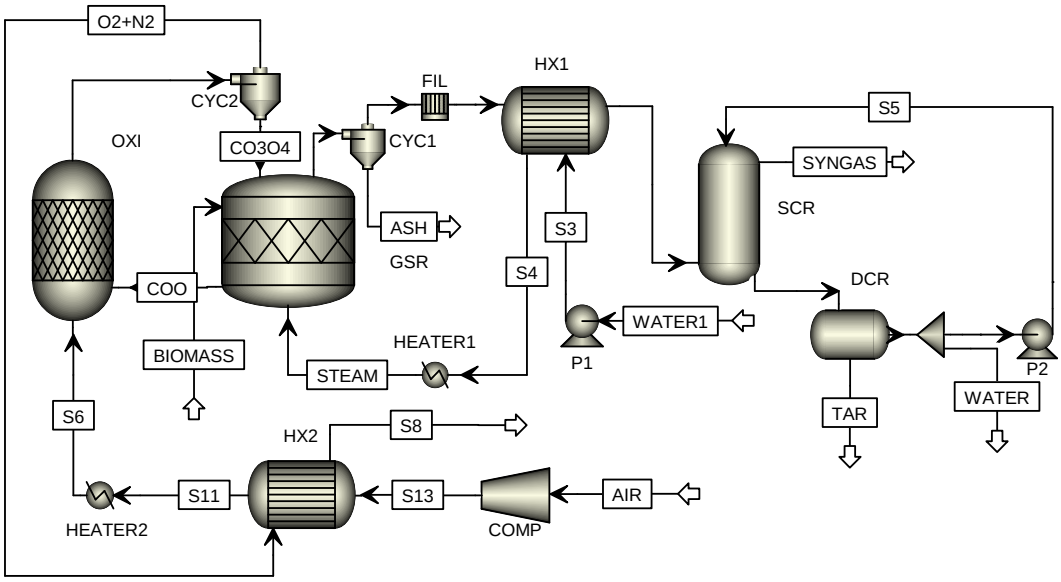

Figure 6.4 Simulation of the CLG unit; oxygen is supplied via transformation of Co_3O_4 to CoO in the gasifier, GSR: Gasifier, OXI: Oxidizer, CYC: Cyclone, FIL: Filter, HX: Heat exchanger, SCR: Scrubber, DCR: Decanter, P: Pump, COMP: Compressor

The oxidizer is a Rstoic reactor operating at 825 °C. Tab. 6.6 represents the mass balance of some of the main stream of the CLG unit.

Table 6.6 Mass balance of the CLG, Aspen plus V. 7.2

	Stream							
Component	Air	S13	O2+N2	S11	S8	S6	*COO*	*CO3O4*
y_{CoO}							0.68	
$y_{Co_3O_4}$							0.32	1
y_{O_2}	0.21	0.21	0.14	0.21	0.14	0.21		
Mass flow (kg/s)	1.16	1.16	1.06	1.16	1.06	1.16	44.5	44.6
T (^oC)	25	214	825	434	600	825	850	825
P (bar)	1	4	1.5	3	1	3		

The oxidation of CoO to Co_3O_4 is exothermic. However, the reverse reaction in the gasifier is endothermic. Therefore, the net energy of the cyclic oxidation-reduction of cobalt oxide is zero. The required air in the oxidizer has to pass through a compressor and a heater to reach the operating conditions. The "N2+O2" stream at the exit of the oxidizer (T=825 °C) can be used to supply a part of the required energy. The total duty of the CLG is 3260 kW (Tab. 6.7).

Table 6.7 Simulation description of CLG system

Unit	Function	Aspen Model	Outlet T (^oC)	Duty (kW)
GSR	Gasifier	RGibbs	850	
OXI	Oxidizer	Rstoic	825	
CYC1	Cyclone	Cyclone	850	
CYC2	Cyclone	Cyclone	825	
FIL	Filter	Plate	850	
HX1	Heat exchanger	HeatX	133-200	
HX2	Heat exchanger	HeatX	433-600	
P1	Pump	Pump	25	0.38
P2	Pump	Pump	25	0.11
HEATER1	Heater	Heater	850	2522
HEATER2	Heater	Heater	825	513
SCR	Scrubber	Extract	30	
DCR	Decanter	Decanter	30	
COMP	Compressor	Compressor	214	225
Total				3260

The reactor design consists of two elements: the gasifier and the oxidizer.

6.3.1 Gasifier

Instead of using air in the gasifier, we propose replacing sand used in the conventional systems with cobalt oxide ($d_p = 300\ \mu m$, ρ_p=3200 m^3/kg). The fresh cobalt oxide (Co_3O_4) flows to the gasifier and supplies the required oxygen by reducing to CoO. The gasifier design from the conventional gasifier can be retained if the oxygen carrier provides the same amount of oxygen. If $\dot{m}_{O_2}$ is the required oxygen for the gasification, the oxygen carrier circulation rate ($\dot{m}_{oc}$, kg/s) to supply this quantity is:

$$\dot{m}_{oc} = \frac{\dot{m}_{O_2}}{R\alpha X_{Red}} \tag{6.17}$$

Where α is the active percentage of oxygen carrier and R=0.07 is the maximum oxygen transport capacity of Co_3O_4. X_{Red} is the conversion of Reaction 6.18:

$$Co_3O_4 \longleftrightarrow 3\,CoO + \tfrac{1}{2}\,O_2 \tag{6.18}$$

The solid inventory (m, kg) in the bubbling bed is:

$$m = \frac{\pi}{4} D_b^2 H_b \rho_p (1-\varepsilon_b) = \tau_{oc} \dot{m}_{oc} \tag{6.19}$$

Where τ_{oc} is the oxygen carrier residence time in the gasifier. Combining Eqs. 6.17 and 6.19:

$$X_{Red} = \frac{\dot{m}_{O_2}}{\frac{\pi}{4} D_b^2 H_b \rho_p (1-\varepsilon_b) R} \times \frac{\tau_{oc}}{\alpha} \tag{6.20}$$

On the other hand, X_{Red} and τ_{oc} are related to each other according to the reaction rate expression [11]:

$$ln(X_{Red}) = ln\left(1 - \frac{1}{exp(k_{Red}\tau_{oc}^{1.5})}\right) \tag{6.21}$$

At operating temperature (850 °C), $k_{Red} = 7.5 \times 10^{-5}\ s^{-1}$ [11]. Assuming X_{Red} is 40 % and

using Eq. 6.21, the oxygen carrier residence time in the gasifier should be 6 min. Consequently, α is calculated from Eq. 6.20 as 0.08 and finally $\dot{m}_{oc}$ is calculated from Eq. 6.17 as 44.6 kg/s. Therefore, by retaining the conventional gasifier configuration (CGPO) and replacing sand with Co_3O_4(8 %) with a circulation rate of 44.6 kg/s, the gasifier can operate without pure oxygen and the system performance will remain comparable to that of the conventional gasifier (see Appendix B). Although the oxygen desorption rate from the oxygen carrier is slower than the steam gasification rate, it is not a limiting step during chemical looping gasification.

6.3.2 Oxidizer

The reduced cobalt oxide is transferred to the oxidizer for regeneration. The solid circulation rate between gasifier and oxidizer is controlled by a pneumatic L-valve as it is simple to design, easy to operate and to maintain, and performs efficiently in solid flow control. Solid flow can be adjusted by varying the gas flow rate in the horizontal section of L-valve for Geldart group B particles [18]. The solid circulation rate imposes the particle velocity in the oxidizer by:

$$\dot{m}_{oc} = \frac{\pi}{4} D_o^2 u_p \rho_p (1 - \varepsilon_o) \tag{6.22}$$

Patience et al. [19] developed a model which describes the relationship between particle velocity and superficial gas velocity in a riser of a circulating fluidized bed:

$$\frac{u_0}{\varepsilon_o u_p} = 1 + \frac{5.6}{Fr} + 0.47 Fr_t^{0.47} \tag{6.23}$$

The ratio of $(u_0/\varepsilon_o u_p)$ is called the slip factor and converges to 2 at gas velocities more than 6 m/s. The oxidation of CoO to Co_3O_4 happens according to:

$$3\,CoO + \tfrac{1}{2}\,O_2 \longleftrightarrow Co_3O_4 \tag{6.24}$$

With the conversion as [11]:

$$ln(X_{Oxi}) = ln\left(1 - \frac{1}{exp(k_{Oxi}\tau_{oc}^2)}\right) - k_{Red}\tau_{oc}^2 \tag{6.25}$$

At the oxidizer temperature (T=825 °C), $k_{Oxi} = 6 \times 10^{-5}\ s^{-1}$ and $k_{Red} = 4.3 \times 10^{-5}\ s^{-1}$. It is supposed that 40 % of Co_3O_4 is converted to CoO in the gasifier. The oxidation of CoO is very fast and only 10 s are sufficient to regenerate according to Eq. 6.25. It is assumed that the unconverted Co_3O_4 does not affect the reaction rate. The oxidation rate decreases with temperature. Therefore, the oxidizer temperature was set slightly lower than gasifier temperature (825 °C compared to 850 °C). Considering the solid residence time in the oxidizer ($\tau_{oc}(oxidizer) = 10\ s$), the oxidizer height is:

$$H_o = u_p \times \tau_{oc} \tag{6.26}$$

The oxidizer diameter (D_o) was calculated via trial and error method (Fig. 6.5) and $\dot{m}_{oc}$ was derived by considering a value for D_o. D_o was substantiated by comparing $\dot{m}_{oc}$ with the required oxygen carrier circulation rate in the gasifier (Eq. 6.17).

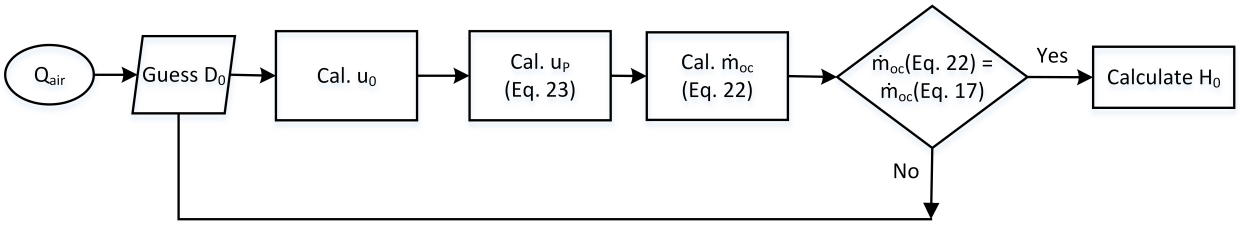

Figure 6.5 Oxidizer design algorithm

Considering higher X_{Red} results in higher α and consequently lower $\dot{m}_{oc}$ which decreases the oxidizer diameter. However, to reach the same oxidation state, a higher reactor is required. Since the oxidizer height is restricted due to the space limitation, a vessel with a bigger diameter is preferred to one with a greater height. The oxidizer diameter and height were designed as 1 m and 10 m respectively and the Co_3O_4 circulation rate was 44.6 kg/s to supply the required oxygen for the gasifier (Tab. 6.8; see Appendix B for calculations).

Table 6.8 Oxidizer design results (CLG unit)

Input		Output	
$Q_{Air}, nm^3/s$	1.01	$u_p, m/s$	0.97
D_o, m	1	$u_o, m/s$	4.7
X_{Red}	0.4	H_o, m	10
$T, {}^oC$	825	$\dot{m}_{oc}, kg/s$	44.6
ε_o	0.98		

6.4 Economic analysis of CG, CGPO, and CLG units

There are several methods for capital cost estimation ranging from the less accurate (order of magnitude estimate) to very accurate (detailed estimate) methods. Method selection depends on the amount of detailed information available and the desired accuracy. We used the factored estimate method which is based on the knowledge of major equipment ($\pm$ 30 accuracy) to estimate the capital cost [20].

6.4.1 Capital cost

In factored estimate method, the first step is to determine the total purchase equipment delivered costs (E). We estimated "E" from "Plant Design and Economics for Chemical Engineers" [20]. The costs associated with the total capital investment (installation, piping, engineering and supervision, etc.) are percentages of E (see Appendix C). The total capital cost of the CLG unit is \$9.66M which is \$3.39M and \$1.18M more than the capital cost of a CGPO and CG units respectively (Tab. 6.9).

Table 6.9 Total capital investment (TCI)

Item	CGPO(k$)	CG(k$)	CLG(k$)
Gasifier	653	832	653
Oxidizer			211
Heaters and Heat exchangers	143	214	309
Pumps	88	88	88
Compressor	126	246	422
Cyclone	32	43	58
Filter	43,400	62,700	43,400
Scrubber	133	168	133
Decanter	73	93	73
Total purchased equipment cost (E)	1,292	1,748	1,989
Total direct cost (D=300 %E)	3,888	5,261	5,988
Total indirect cost (I=66 %E)	852	1,154	1,313
Fixed capital investment (FCI=115 %(D+I))	5,451	7,376	8,397
Working capital cost (5%FCI)	273	369	420
Start up cost (10%FCI)	545	738	840
Total capital investment (TCI)	6,269	8,483	9,656

Updated on Aug. 2013

For a small chemical plant which does not have many operating units, the total capital cost can be also estimated from the cost of the reactor itself. Applying the scale factor of 8 (proposed by Godefroy et al. [21]) to the reactor cost, the capital costs of the CGPO, CG, and CLG systems are \$5.22M, \$6.7M, and \$6.9M respectively, which have 21 %, 17 %, and 28 % error compared to the estimates presented in Tab. 6.9.

6.4.2 Total production cost (TPC)

The production costs are classified into fixed and variable costs. The fixed costs are principally due to the depreciation (5 %FCI), taxes (4 %FCI) and insurance (0.6 %FCI). The variable costs include mainly raw materials, utilities, and labor. The utilities include water, steam, and electricity and the raw materials are oxygen, biomass, and oxygen carrier. The cost of oxygen was assumed to be \$300/t [14] and the cost of biomass was \$10/t [22]. The cost of oxygen carrier (Co_3O_4/Al_2O_3) was assumed to be \$30,000/t [23]. Labor costs were estimated to be 10 % of the total operating costs [20]. The annual production costs of the CGPO, CG, and CLG units are \$1.9M, \$1.14M, and

$1.32M respectively (Fig. 6.6).

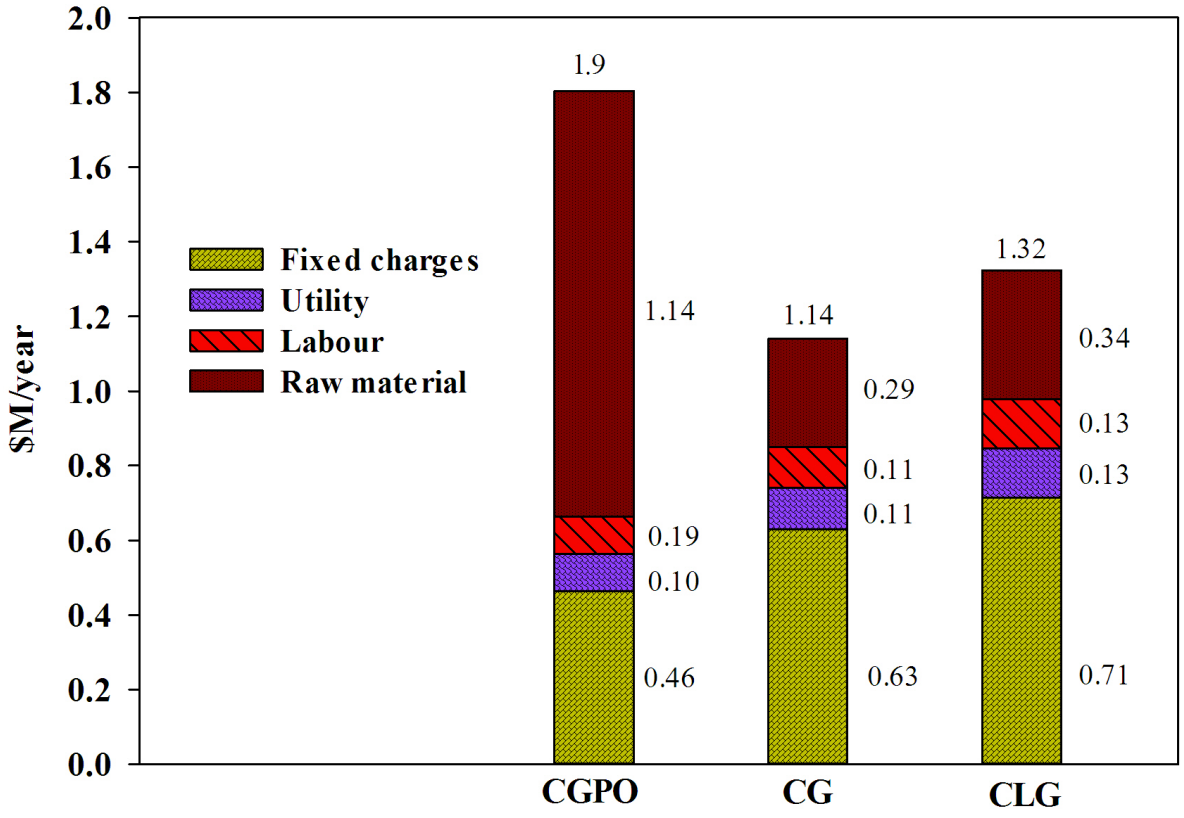

Figure 6.6 Operating cost breakdown

The main difference between the operating costs of the units is related to the cost of raw materials. Specifically the CGPO unit uses pure oxygen which increases its operating cost. On the other hand, the CLG unit uses the oxygen carrier as oxygen supplier with a life time of two years. The following assumptions were considered for cost estimation:

1. The plant location for both cases is the United States (US);
2. The plant is designed to have the capacity to process 86 t/d biomass;

3. The plant is open for 330 working days per year;
4. All the cost estimations are carried out in US dollars ($);
5. The lifetime of the oxygen carrier is 2 years.

The operating cost of the CG unit is less than two other systems. However, the produced syngas from the CG is diluted with nitrogen which requires further conditioning in order to be used in downstream processes. Therefore, the CG systam is not economically comparable with two other systems because the purification costs have not been considered in its capital and operational costs. The annual production cost of the CLG is $0.58M less than the cost of the CGPO which repays the difference between TCI of CLG and CGPO ($3.39M) in less than 6 years. Furthermore, over 10 years of project life, the CLG unit earns $2.41M more than the CGPO unit. For sensitivity analysis a comparison index "γ" is defined as:

$$\gamma = \frac{TCI_{CLG} - TCI_{CGPO}}{TPC_{CGPO} - TPC_{CLG}} \tag{6.27}$$

The lower the γ is, the more profitability the CLG has over CGPO. The range over which the parameters for the sensitivity analysis vary, are ± 30 % of the designed value. The total capital investment has the most significant effect on the profitability of CLG (Fig. 6.7).

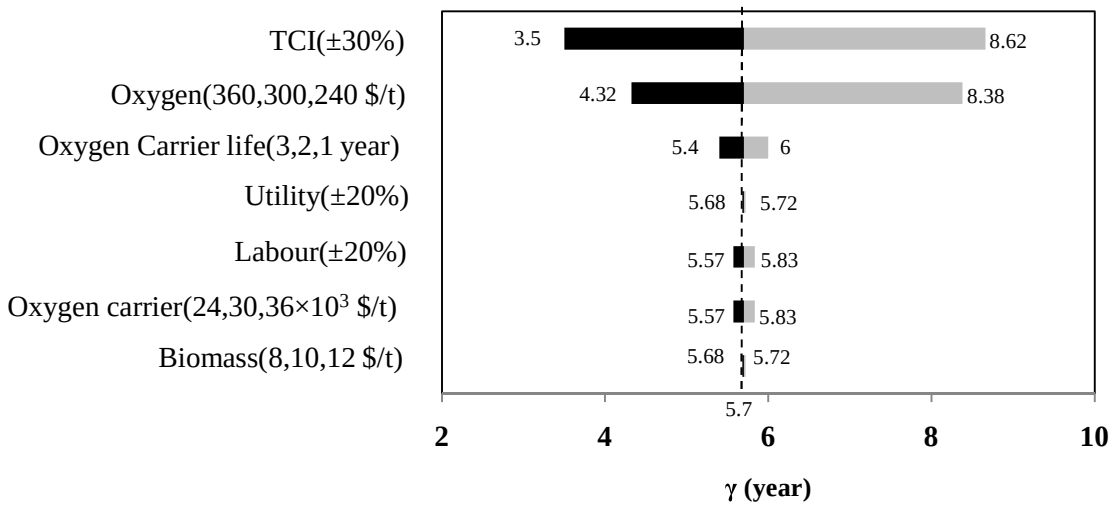

Figure 6.7 Sensitivity analysis of the CLG and CGPO units

The CLG has more benefits if the price of pure oxygen increases. Furthermore, this analysis shows that the biomass price does not affect the total production costs. The economical analysis reveals that, the chemical looping technology is a promising alternative for gasification of biomass especially when the oxygen price increases.

6.5 Conclusions

A 7 MW_{th} CLG unit with a bubbling bed gasifier coupled with a fast fluidized bed oxidizer was designed to treat 86 t/d biomass. The bubbling bed consists of two regions: a dense bed and a freeboard. The gas velocity in the dense bed was assumed to be 1.5 m/s which is greater than the minimum fluidization and lesser than the critical velocity of bed materials. The dense bed height was calculated as 4.15 m which gives enough gas-solid contact time to reach 90 % biomass conversion at T=850 °C. To return the entrained particles to the bed, a 2.5 m height freeboard region was designed on the top of the bubbling bed. The oxygen carrier (Co_3O_4(8 %)/Al_2O_3) circulation

rate should be 44.6 kg/s to provide auto thermal conditions in gasifier. The oxygen carrier is re-oxidized in a riser (ID=1 m, H=10 m) working at u_0=4.7 m/s and T=825 °C. Although the capital cost of CLG unit is $3.4M more than that of the CGPO, the annual operating cost is $0.58M less. This confirms that the CLG process is a feasible alternative to CGPO for biomass gasification. The total capital investment and the price of oxygen have the most significant effects on the total production costs, while the cost of biomass as raw material and cobalt oxide as oxygen carrier do not significantly influence the total capital costs.

Appendix A: CGPO reactor system

Calculation of dense bed diameter - D_b:

Considering that the bed contains sand (d_p=300 μm, ρ_p=2650 kg/m^3) and char (d_p=200 μm, ρ_p=1200 kg/m^3);

At T=850 °C and using $Re_{mf} = \sqrt{27.2^2 - 0.0408Ar} - 27.2$ [24] and $Re_{se} = 1.53Ar^{0.5}$ [25]:

u_{mf}(sand)=0.03 m/s, u_{mf}(char)=0.006 m/s;

u_{se}(sand)=7.63 m/s, u_{se}(char)=4.2 m/s;

Therefore, u_0 should be within: 0.03<u_0<4.2;

u_0 is chosen as 1.5 m/s;

Steam flow rate=$\lambda \times C = 2 \times \frac{(1000\ g/s) \times (0.48\%wt)}{(12\ g/mol)} = 80\ mol/s = 1.44\ kg/s$;

Oxygen flow rate=0.1 kg/s based on simulation with Aspen plus (Fig. 6.1);

Reactants: 1 kg/s biomass + 1.44 kg/s steam + 0.1 kg/s oxygen;

At T=850 ^oC and P=2 bar, Q_{in}=3.88 m^3/s;

$D_b = \sqrt{\frac{4Q_{in}}{\pi u_0}} = 1.8\ m$**;**

Calculation of dense bed height - H_b:

$F_{C_0} = \frac{1000(g/s) \times (0.48)}{12(g/mol)} = 40\ mol/s$;

From Eq. 6.7: $k = 956\ m^3 mol^{-1} s^{-1}$;

From Eq. 6.11:

$V = \frac{40}{956 \times 0.18^2} \frac{0.9}{(1-0.9)(2-0.9)} = 10.56\ m^3$;

$H_b = \frac{4V}{\pi D_b^2} = 4.15\ m$;

Calculation of freeboard diameter - D_f:

Ash particles (d_p=40 μm, ρ_p=1600 kg/m^3);

u_{se}(ash)=2.1 m/s;

Q_{in}=3.88 m^3/s and the flow rate increased to Q_f=5.95 m^3/s;

Retaining the same diameter of the dense bed for the freeboard region, u_0 in freeboard is 2.3 m/s which is more than u_{se} (ash) and less than u_{se}(char and sand);

D_f is kept constant at 1.8 m;

Calculation of freeboard height - H_f:

The freeboard height was calculated to minimize the entrainment of char particles. The ash entrainment is preferable compared to char and sand particles. If the freeboard height is high enough to minimize char entrainment, it will also minimize sand entrainment because of the greater density and particle size of sand.

From Eq. 6.14, $E_{p0} = 30.59\ kg/m^2.s$;

From Eq. 6.15 and 6.16, $E_{pf} = 0.02\ kg/m^2.s$;

Letting 10 % of the particles leaving the system to optimize the reactor height:

$E_p = 1.1E_{pf}$;

Conversely, from Eq. 6.13:

$E_p = E_{pf} + E_{p0}exp(-4H)$;

Therefore,

$H_f = -0.25ln(\frac{0.1E_{pf}}{E_{p0}}) = 2.4\ m$;

And the total gasifier height is:

$H(gasifier) = H_b + H_f = 4.15 + 2.4 = 6.55\ m.$

Appendix B: CLG reactor system

Gasifier:

The gasifier dimensions and configuration from the CG unit are maintained. The required oxygen carrier circulation rate to supply the oxygen was calculated using Eq. 6.17. At gasifier temperature T=850 °C, $k_{Red} = 7.5 \times 10^{-5}\ s^{-1}$. The required residence time in the gasifier to reach 40 % conversion was calculated by Eq. 6.21:

$\tau_{oc} = 359\ s$;

From Eq. 6.20 and considering $\varepsilon_b = 0.6$,

α=0.08 and consequently from Eq. 6.17:

$\dot{m}_{oc} = 44.64\ kg/s$.

Oxidizer:

The oxidizer diameter (D_o) was calculated through trial and error.

D_o=1 m;

Considering 250 % excess air: $Q_{Air} = 3.63\ m^3/s$

$u_0 = \frac{Q_{Air}}{\frac{\Pi}{4}D_o^2} = \frac{3.63}{\frac{\Pi}{4}(1)^2} = 4.7\ m/s$;

Considering $\varepsilon_o = 0.98$ and using Eq. 6.23, $u_p = 0.97\ m/s$;

And from Eq. 6.22, $\dot{m}_{oc} = 44.78\ kg/s$.

Which is in agreement with the required oxygen carrier circulation rate from Eq. 6.17;

To recover the 40 % conversion, the oxygen carrier residence time in the oxidizer should be $\tau_{oc} = 10\ s$ (using Eq. 6.25), and consequently the oxidizer height (H_o) is:

$H_o = u_p \times \tau oc = 0.97 \times 10 = 9.7\ m$;

Appendix C: Estimation of fixed capital investment of CGPO unit

Purchased equipment delivered, E=1,292

Purchased equipment installation, 39 %E=504

Instrumentation (installed), 28 %E=362

Electrical (installed), 10 %E=130

Piping (installed), 31 %E=401

Buildings including services, 22 %E=159

Yard improvement, 10 %E=129

Service facilities installed, 55 %E=710

Land, 6 %E=78

Total direct cost, D=3,888

Engineering and Supervision, 32 %E =413

Construction expenses, 34 %E=439

Total Indirect cost, I=852

Contractors fees, 5 % of (D+I)=237

Contingency, 10 % of (D+I)=474

Fixed capital investment, FCI=5,451

Working capital cost, 5 %FCI=273

Start up cost, 10 %FCI=545

Total Capital investment, TCI=6,269

Symbols

A	Surface area, m^2
Ar	Archimedes number, $\frac{d_p^3 g(\rho_p - \rho_g)\rho_g}{\mu^2}$
C_D	Drag force coefficient, $Nkg^{-1}ms^{-2}$
D	Reactor diameter, m
d_p	Particle diameter, μm
E	Activation Energy, $kJmol^{-1}$
E_p	Particle flux, $kgm^{-2}s^{-1}$
E_{pf}	Final particle flux, $kgm^{-2}s^{-1}$
E_{p0}	Particle flux at the bed surface, $kgm^{-2}s^{-1}$
F	Molar flowrate, $mols^{-1}$
Fr	Froude number, $\frac{u_0}{(gD)^{0.5}}$
Fr_t	Froude number at terminal velocity, $\frac{u_{tr}}{(gD)^{0.5}}$
H	Height, m
$[i]$	Molar concentration of component i, $molm^{-3}$
K	Reaction rate constant, $m^3 mol^{-1}s^{-1}$
$\dot{m}$	Mass flow rate, kgs^{-1}
Q	Volume flowrate, m^3
R	Oxygen carrying capacity of oxygen carrier
r_C	Reaction rate, $mols^{-1}m^3$
u_0	Superficial gas velocity, ms^{-1}
u_{mf}	Minimum fluidization velocity, ms^{-1}
u_p	Particle velocity, ms^{-1}
u_{se}	Critical velocity, ms^{-1}
V	Reactor volume, m^3
X	Conversion
y	Molar fraction
α	Percentage of active phase on the oxygen carrier
ε	Voidage
λ	Steam to biomass molar ratio
μ_g	Gas viscosity, Nsm^{-2}
ρ	Density, kgm^{-3}
τ	Gas solid contact time, s
Subscript	
b	Bubbling bed
f	Freeboard
o	Oxidizer
oc	Oxygen carrier
Oxi	Oxidation
Red	Reduction

References

[1] K. Kuramoto, K. Matsuoka, T. Murakami, H. Takagi, T. Nanba, Y. Suzuki, S. Hosokai, J. Hayashi, Ind. Eng. Chem. Res. **2009**, 48(6), 2851-2860. DOI: 10.1021/ie800760s

[2] J. D. Martinez, K. Mahkamov, R. V. Andrade, E. E. Silva Lora, Renew. Energ. **2012**, 38(1), 1-9. DOI: 10.1016/j.renene.2011.07.035

[3] M. M. Yazdanpanah, A. Hoteit, A. Forret, A. Delebarre, T. Gauthier, Oil Gas Sci. Technol. **2011**, 66(2), 265-275. DOI: http://dx.doi.org/10.2516/ogst/2010025

[4] H. R. Kim, D. Wang, L. Zeng, S. Bayham, A. Tong, E. Chung, M. V. Kathe, S. Luo, O. McGiveron, A. Wang, Z. Sun, D. Chen, L. Fan, Fuel **2013**, 108, 370-384. DOI: http://dx.doi.org/10.1016/j.fuel.2012.12.038

[5] J. Ströhle, M. Orth, B. Epple, Appl. Energ. **2014**, 113, 1490-1495. DOI: 10.1016/j.apenergy.2013.09.008

[6] N. Berguerand, A. Lyngfelt, Fuel **2008**, 87(12), 2713-2726. DOI: 10.1016/j.fuel.2008.03.008

[7] P. Kolbitsch, T. Proll, J. Bolhar-Nordenkampf, H. Hofbauer, Chem. Eng. Technol. **2009**, 32(3), 398-403. DOI: 10.1002/ceat.200800378

[8] A. Bischi, Ø. Langørgen, I. Saanum, J. Bakken, M. Seljeskog, M. Bysveen, J.X. Morin, O. Bolland, Int. J. Green. Gas Con. **2011**, 5(3), 467-474. DOI: 10.1016/j.ijggc.2010.09.005

[9] D. Sridhar, A. Tong, H. Kim, L. Zeng, F. Li, L. Fan, Energ. Fuel **2012**, 26 (4), 2292-2302. DOI: dx.doi.org/10.1021/ef202039y

[10] A. Olaleye, M. Wang, Fuel **2014**, 124, 221-231. DOI: 10.1016/j.fuel.2014.02.002

[11] M. Aghabararnejad, G. S. Patience, J. Chaouki, Can. J. Chem. Eng., 2014, DOI: 10.1002/cjce.22046.

[12] M. Aghabararnejad, G. S. Patience, J. Chaouki, Fuel, 2014, in press.

[13] P. Basu, Biomass Gasification and Pyrolysis: Practical Design and Theory, Academic Press, **2010**.

[14] H. H. Gunardson, Industrial Gases in Petrochemical Processing: Chemical Industries, Taylor & Francis, **1997**.

[15] A. Inayat, M. M. Ahmad, M. I. A. Mutalib, M.K. Yunus, Int. Conf. for Technical Postgraduates, Kula Lumpur **2009**.

[16] C. Y. Wen, L. H. Chen, AIChE J. **1982**, 28(1), 117-128. DOI: 10.1002/aic.690280117

[17] J. H. Choi, I.Y. Chang, D.W. Shun, C.K. Yi, J.E. Son, S.D. Kim, Ind. Eng. Chem. Res. **1999**, 38(6), 2491-2496. DOI: 10.1021/ie980707i

[18] D. Geldart, P. Jones, Powder Technol. **1991**, 67(2), 163-174. DOI: 10.1016/0032-5910(91)80153-A

[19] G. S. Patience, J. Chaouki, F. Berruti, R. Wong, Powder Technol. **1992**, 72(1), 31-37. DOI: 10.1016/S0032-5910(92)85018-Q

[20] M. Peters, K. Timmerhaus, R. West, Plant Design and Economics for Chemical Engineers, 5th ed., McGraw-Hill, Boston **2003**.

[21] A. Godefroy, G. S. Patience, T. Tzakova, D. Garrait, J. L. Dubois, Chem. Eng. Technol. **2009**, 32(3), 373-379. DOI: 10.1002/ceat.200800309

[22] U.S. Department of Energy. **2011**. U.S. Billion-Ton Update: Biomass Supply for a Bioenergy and Bioproducts Industry. R.D. Perlack and B.J. Stokes.

[23] A quote from Haldor Topsoe, Feb **2014**.

[24] G. Hetsroni, Handbook of multiphase systems, Hemisphere Pub. Corp. **1982**.

[25] H. T. Bi, J. R. Grace, Int. J. Multiphase Flow **1995**, 21(6), 1229-1236. DOI: 10.1016/0301-9322(95)00037-X

CHAPTER: 7

GENERAL DISSCUSSION

Gasification is a promising technology to convert low added fuels (e.g., biomass) to energy or value added chemicals. Biomass gasification faces three main issues: biomass pre-treatment, air separation unit, and syngas cleaning. The air separation units are costly and increase the capital and operating costs of the process. In this thesis the possibility of replacing the air separation unit with a chemical looping system has been studied.

Chemical looping technology is based on the separation of oxygen from air at high temperature using oxygen carriers. The high temperature operation makes it possible to integrate chemical looping with gasification, which also takes place at high temperature.

Chemical looping is limited in terms of oxygen supply. Although gasification requires less oxygen compared to combustion, the application of chemical looping has been widely ignored in gasification, whereas the chemical looping combustion, especially gaseous fuels, has been extensively explored.

The oxygen of the oxygen carrier is in lattice form, which is not readily available to react with biomass. However, if the oxygen is released from the oxygen carrier in the first step, it is available in gaseous form and can partially combust the biomass. Only copper, manganese, and cobalt have been reported to be able to release oxygen in gaseous form in an oxygen deficient atmosphere. The oxygen transport capacity and oxidation-reduction rates of Cu, Mn, and Co were measured using thermogravimetric analysis by switching the gas from air to argon at different temperatures. The oxygen transport capacity decreases from 10 % for copper to 7 % for cobalt and only 3 % for manganese.

The higher the oxygen transport capacity is, the less solid circulation rate will be required. A high solid circulation rate demands a large solid capturing-circulation system and high gas velocity. The high gas velocity increases the attrition rate. Therefore, using an oxygen carrier with a

high oxygen carrier capacity decreases the capital and operational expenses by lowering the cost associated with the cyclones, L-valve, and the oxygen carrier make up. Hence, many authors prefer copper over cobalt and manganese due to its higher oxygen transport activity. However, the transformation of CuO to Cu_2O starts at 900 °C and the reaction rate increases with the temperature. The operating temperature of copper oxide is close to its melting point, which may cause agglomeration and defluidization. The manganese and cobalt oxide transformations happen at 760 and 800 °C despite their melting points being higher than copper. They are therefore being considered as a potential candidates for biomass gasification.

The other parameter in the chemical looping systems that has to be taken into consideration during oxygen carrier selection is the oxidation-reduction rates. An oxygen carrier with a higher reduction rate needs less residence time to reach a certain conversion in the gasifier. A shallow bed, therefore, supplies sufficient residence time for the oxygen carrier to reach the desirable conversion. Consequently, using an oxygen carrier with a higher reduction rate results in a gasifier with a lower height. Also, the oxidizer height will be lower if the oxidation rate of the oxygen carrier is high. Although the reaction rate has the same importance as the oxygen transport capacity in designing a chemical looping system, it has not been considered in the literature as a crucial parameter in oxygen carrier selection. The results of the thermogravimetric analysis showed that cobalt has the highest oxidation and reduction rates compared to copper and manganese.

The oxygen carrier in the chemical looping process undergoes many reduction-oxidation cycles at high temperature. Therefore, it should have superior thermal and mechanical strength. The particles with low thermal strength agglomerate to each other and defluidize the bed. This decreases the gas-solid contact dramatically and affects the performance of the system. Pressure drop measurement across the bed is normally used to monitor the particle agglomeration. However, agglomeration does not always cause an increase in the pressure drop. In many cases, the gas channeling occurs with defluidization and the pressure drop across the bed does not change, and even decreases. Many authors have compared the SEM pictures of the sample before and after the reaction to confirm the presence or absence of agglomeration. This technique only represents a

small portion of the particles and to generalize it for the whole sample, many pictures have to be taken from different parts of the sample. The other method, which was used in this work, is to compare the bulk properties of the particles before and after the reaction, like average particle size and total surface area. The average particle size increases with agglomeration while the total surface area decreases. The surface area is mainly attributed to the internal pores. Particle agglomeration collapses the pores and, hence, the surface area decreases. The decline of the surface area in the first cycles was considerable (77 % Cu, 32 % Co, and 61 % Mn). After the 5^{th} cycle, however, it reaches a plateau.

To increase the reduction rate, the oxygen carrier should be subjected to an inert media, like argon. In gasification, steam is usually used as the gasifying agent. Unlike argon, steam is not a superior inert atmosphere, especially for copper oxide and can oxidize the reduced Cu_2O to CuO [70], which may decrease the oxygen desorption rate dramatically.

During the combustion of gaseous fuels with the oxygen carrier, the fuel reaches the surface of the particle and reacts with the lattice oxygen of the metal oxide. In calcination, a part of the active phase (MeO) reacts with the support (Al_2O_3) to form a spinel structure ($MeAl_2O_4$). Therefore, a portion of the metal which appears as spinel, is no longer available to combust the fuel. The spinel of nickel ($NiAl_2O_4$) is very common as it is used itself as a support to prepare the oxygen carrier. In this work some trace of spinel formation during the oxygen carrier preparation has been observed by XRD. It did not, however, affect the oxygen transport capacity.

Various models have been applied for modeling the oxidation-reduction rates of the oxygen carrier in the presence of air and a reducing agent (e.g., CO, CH_4, and H_2). The nuclie growth model, which was developed by Awrami [77, 78], has been used frequently to predict the conversion of phase transformation. This model considers that the transformation of phase “A” to “B” is non-reversible. This assumption is true for the oxidation of metal oxide Me to MeO, where the reverse reaction is very slow, especially in the presence of excess air, and can be neglected. During the reduction, however, the released oxygen in gaseous form can react with Me and form MeO. The reverse reaction can affect the reduction rate and has to be considered in modeling. It is

clearly demonstrated that the modified nuclei growth model can satisfactorily predict the oxidation-reduction rate of the oxygen carrier.

Cobalt oxide is not preferred over copper and manganese, because it is more expensive and is not environmentally friendly. It has been shown, however, that although cobalt has the moderate oxygen transport capacity, its operating temperature is lower and oxidation-reduction rates are higher. Furthermore, its thermal stability is superior compared to other carriers. Due to these advantages, cobalt is being considered as a potential carrier in addition to copper and manganese.

To test the performance of the oxygen carrier in the presence of biomass, the gasification test has been performed in a fluidized bed reactor where the biomass injection into the reactor is possible. The original proposed configuration was to have a circulating fluidized bed consisting of a bubbling gasifier and a fast fluidized bed riser working in parallel. Unfortunately, time and financial limitations obliged us to go through a single 7.8 cm bubbling fluidized bed. The cyclic process of chemical looping was simulated by switching the carrier gas between air and a steam/argon mixture. The oxygen carrier was oxidized by air and when steam/argon was fluidizing the bed, it was reduced and the oxygen was released to the system. Ten grams of biomass were injected when the gas was switched to the steam/argon mixture. The injection line is connected to the reactor where the dense bed ends. The biomass particles stay at the bed surface due to the difference between biomass and bed material density and low gas velocity.

Transient and steady state modeling are two approaches for gasification modeling. Although we had to use the transient approach due to the reactor configuration, it is more difficult in terms of modeling. On the other hand, providing the steady-state conditions to carry on the gasification is problematic. A Pfeiffer Vacuum mass spectrometer (MS) was used to sample the produced gas from the reactor. The ideal situation was to have only steam as the fluidizing gas during reduction, but the MS became saturated if the steam composition of the gas was more than 18 %. Therefore, the steam percentage was kept below 18 % in all runs and argon was used as a balance component.

The effect of temperature, steam percentage and Co_3O_4 on the product gas composition were discussed in detail in the second article. In general, increasing temperature and steam percentage,

increases the biomass conversion and favours H_2 production. Also, Co_3O_4 increases the CO yield by deriving partial combustion of char. The increase in CO yield was less than 50 %. The biomass contains only 16 % char and 81 % converts to volatile gases by pyrolysis. To see the effect of the oxygen carrier on gasification, it would be better to use pure char.

Gasification, particularly biomass gasification contains impurities, such as tar and sticky materials, which can deactivate the oxygen carrier during the time. In a chemical looping process, however, the oxygen carrier undergoes a cyclic reduction-oxidation cycle. In other words, the oxygen carrier is regenerated in each cycle in the oxidation reactor and all the impurities are burnt in the air. The oxygen carrier deactivation has not been observed in the present experiments after 10 oxi-red cycles. The TGA test of the used oxygen carrier confirms that no carbon was deposited after oxidation.

The bubbling fluidized bed consists of two regions: dense bed and freeboard. The gas hydrodynamic in the dense region is completely different from the freeboard due to the presence of bubbles. The bubble motion is random and provides mixing and turbulency in the bed. Therefore, the gas hydrodynamic in the bed deviates from plug flow. Examining the gas phase in the bed in more detail, it splits into bubble and emulsion. The bubbles move faster than the emulsion phase and the gas hydrodynamic is different from emulsion. The radial dispersion was negligible due to low reactor diameter and, also, the high gas mixing in the radial direction in the bed. The proposed model accounted for 83 % of the variance in the experimental data.

The design and economic analysis of the chemical looping gasification are the last step of this thesis, which discusses a method to determine the reactor diameter and height. First, a conventional gasifier, which uses pure oxygen, was designed and the possibility of applying the same reactor as the reducer of a chemical looping gasifier was discussed. Finally, the capital and operational costs of two gasification units were compared. The design objectives are to calculate the size of the main equipment included in the process, which can be achieved by preliminary design. To construct the unit, though, a detailed design, including solid capturing, biomass feeding, distributor, steam supply system, and etc. must be considered.

The fluidization regime determines operating gas velocity. To operate at a bubbling fluidization regime, the superficial gas velocity should be between the minimum fluidization and the critical velocity of the particles. Having the properties of the bed material, the gas velocity in the bed can be determined. The gas velocity along the bed increases due to the devolatilization which will increase the particle elutriation. To return the particles back to the bed, there should be a freeboard region on top of the bubbling bed. The gas velocity in the freeboard, however, should be high enough to entrain ash to prevent the ash accumulation.

The limiting step during the biomass gasification is the steam-char reaction. Therefore, the bubbling bed should be high enough to provide sufficient gas-solid contact time to reach a certain biomass conversion. The freeboard height was calculated to minimize the solid entrainment. The solid entrainment is at its maximum at the bed surface and decreases exponentially with height and at a certain height it emerges and remains at a constant value. This height is referred to as the transport disengagement height and is the most economical reactor height that can be chosen.

In the next step the possibility of conserving the same reactor configuration as a reducer of a chemical looping system was tested. The previous design was for a conventional steam gasification unit, which receives oxygen from a pressure swing adsorption (PSA) process. Cobalt oxide was chosen as the potential oxygen carrier. The first step was to calculate the required oxygen carrier circulation rate to deliver the same amount of oxygen as a PSA unit. Although the oxygen desorption rate was smaller than the steam-char reaction rate, the bubbling bed height supplied sufficient residence time for the oxygen carrier to reach the desired conversion. Therefore, the same gasifier design can be used as the reducer of the chemical looping gasification. This enables the existing gasification units to integrate with the chemical looping technology to be independent of the air separation unit.

The oxidizer is designed to work at 825 °C, which is slightly less than the operating temperature of the gasifier (850 °C). This is because the oxidation rate of cobalt oxide is higher at lower temperatures. The oxidation of the oxygen carrier with oxygen in the air reactor is exothermic. This energy, however, is consumed in the gasifier when the oxygen is released from the metal oxide.

Therefore, the net produced energy from reduction-oxidation of the oxygen carrier is zero. The oxidation of combustible components in the gasifier is the only source of energy in the reactor and the required energy can be controlled by adjusting the solid circulation rate.

The gas velocity in the oxidizer should be high enough to provide a sufficient solid circulation rate in the gasifier. The correlation developed by Patience et al. [79], which relates the gas velocity to the particle velocity is used. By calculating the particle velocity, and the sufficient particle residence time in the oxidizer, the oxidizer height can be determined. The economic analysis showed that the capital cost of the chemical looping gasifier is 35 % more than the conventional gasifier, but the operational cost of the conventional gasifier is 34 % greater than the CLG.

CHAPTER: 8

CONCLUSIONS AND RECOMMENDATIONS

8.1 Conclusions

The chemical looping concept is a promising technology, which can supply the required oxygen for combustion and gasification processes. Having no N_2 in the produced gas, the CO_2 can be easily removed from the steam through condensation (in combustion) or the produced synthesis gas during gasification has a higher calorific value. The oxygen is separated from air at high temperature using solid particles, which serve as the oxygen carrier. The oxygen carrier is oxidized with air in the oxidizer and circulated to the fuel reactor where its lattice oxygen is available to combust or gasify the fuel. The reaction between the solid fuel and the lattice oxygen of the carrier is impossible or very slow. One way to overcome this issue is to apply a specific kind of oxygen carrier, which is able to release oxygen at high temperature in the gaseous form. Among various materials proposed as oxygen carriers for a conventional chemical looping process, only manganese, copper, and cobalt are able to release oxygen at high temperature in an inert media.

In the first step the performance of copper, manganese, and cobalt as a proper oxygen carrier for the gasification of biomass as solid fuel has been tested in a thermogravimetric analyzer. Although copper has the highest oxygen transport capacity, the temperature at which it releases oxygen is 100 °C more than cobalt and manganese. This might affect the fluidization behaviour considering the low melting point of copper. Manganese is less expensive and the most environmentally friendly choice. The oxygen transport capacity, however, is very low, which demands a high solid circulation rate to supply the required oxygen in the gasifier. On the one hand, cobalt has not been seriously considered as a potential carrier in the combustion and gasification of solid fuels due to its high cost and toxicity. On the other hand, its moderate oxygen transport capacity, low operating temperature, high oxidation-reduction rates and high thermal and mechanical strength were

excellent reasons to consider it as a proper oxygen carrier for biomass gasification.

Various kinetic models have been proposed for the oxidation and reduction of the oxygen carrier in the presence of a reducing agent. Little effort, though, was made to model the reduction rate (e.g., of cobalt oxide) in an inert atmosphere. Using the nuclei growth model with some modifications, it was possible to model the oxidation-reduction rate of cobalt in air-nitrogen media, respectively. The modified model is able to predict the reduction and oxidation rate of cobalt oxide in the temperature range of 825-875 °C and different oxygen concentrations.

Based on the first phase of the thesis, cobalt oxide has been chosen as a superior oxygen carrier for chemical looping gasification of biomass. The performance of cobalt in the presence of wood pellets has been tested in a 7.8 cm ID bubbling fluidized bed reactor. Produced gases from the injection of 10 g of wood pellets were monitored and recorded at the top of the reactor with a mass spectrometer. Increasing temperature had a positive effect on the production of hydrogen and the biomass conversion. Furthermore, increasing the steam percentage increased the hydrogen selectivity due to the water gas shift reaction. The CO selectivity increased by replacing sand as bed material with Co_3O_4. This is due to the presence of oxygen in the reactor. The oxygen is only available to partially combust the char in the bed. Therefore, the selectivity of carbon dioxide remained unchanged.

In addition, a comprehensive model has been proposed which is able to predict the produced gas composition versus time. It was assumed that the biomass pyrolysis instantaneously upon being injected into the bed and the produced char formed a thin layer, which remained at the bed surface. The fully oxidized cobalt, subjected to an inert atmosphere when the fluidizing gas was switched from air to argon, released oxygen in the gas phase. The oxygen together with steam reacted with the char at the bed surface. A two phase model was considered as the gas phase hydrodynamic in the bubbling bed. Furthermore, the solids were considered to be completely mixed in the entire bed. The proposed hydrodynamic model was verified with the argon blank test. The radial dispersion was negligible and the axial dispersion increased with temperature, which was due to higher turbulency in the bed. The reaction rates were chosen from the literature and our

first paper. The model accounted for 83 % of the variance in the experimental data.

In the last step the experimental data and kinetic models which had been found in the first two phases, were applied to simulate and design a 86.4 t/d steam biomass gasifier. A conventional stem gasification unit and a chemical looping gasification system were simulated with ASPEN PLUS. To achieve the autothermal gasification, the equivalent ratio had to be 0.076 for the conventional gasifier. The design of all individual operating units was not on the framework of the present work. However, the gasifier design as the main operation unit was planned in detail. The steam gasification reaction is the limiting step during conventional gasification and a bubbling fluidized bed (ID=1.8 m, H=6.6 m) can provide enough residence time for the biomass to reach 90 % conversion.

In a chemical looping system by using the conventional gasifier as the fuel reactor, the oxygen carrier circulation rate and active percentage were determined in order to reach the same reactor performance as the conventional gasifier. The Co_3O_4(8 %)/Al_2O_3 with the circulation rate of 44.6 kg/s can supply the required oxygen for autothermal operation. To regenerate the reduced oxygen carrier an oxidizer with ID=1 m and H=10 m is working in parallel with the gasifier. Although the oxygen release from the oxygen carrier is slower than the steam gasification reaction, it is not the limiting step. The residence time of the biomass in the gasifier is less than the oxygen carrier. Therefore, a conventional gasifier can provide sufficient residence time for oxygen carrier to release oxygen.

The capital cost of the conventional gasification unit is $3.4M less than the chemical looping gasification unit. The annual production cost of the chemical looping gasification system, however, is $0.58M less. Therefore, the chemical looping system can repay the difference in total capital investment in less than 6 years. The performed economic analysis is an estimation with a $\pm$30 % error, which is acceptable for comparison reasons. However, a comprehensive economic analysis is essential for the construction of the unit.

One of the main drawbacks of the cobalt oxide over other oxygen carriers is its high cost. However, the sensitivity analysis reveals that the oxygen carrier cost and life time had little effect on the total production cost. On the other hand the total capital investment and the oxygen price had

the most significant effect on the profitability of the chemical looping gasification over conventional gasification.

8.2 Recommendations

- The oxygen carriers were prepared by incipient wetness impregnation. Yet, other methods of preparation, like mechanical mixing, precipitation, and freeze granulation, can be used to prepare the oxygen carrier. Furthermore, using a spinel structure as the support of the oxygen carrier is recommended;
- The oxygen carrier is subjected to many reduction-oxidation cycles. Therefore it should have high mechanical strength to resist attrition. In this thesis the impregnated cobalt oxide over alumina was used as the oxygen carrier and it was assumed that the oxygen carrier had the superior mechanical strength. However, the attrition rate of the oxygen carrier can be found experimentally to support this idea;
- The used biomass in the present work has only 16 % char and in chemical looping gasification the effect of oxygen-steam on char is very important. Therefore, using another fuel with a higher char content (e.g., coal) can better reveal the effect of the oxygen carrier on the char gasification. Furthermore, the used biomass had only 0.6 % sulfur. In order to see the effect of sulfur on the performance of the oxygen carrier, a fuel with a higher sulfur quantity is recommended;
- In the third article the chemical looping system for biomass gasification was designed and simulated. The performance of the proposed configuration, however, was not validated experimentally. To do so the first step is to construct a cold setup has to be constructed followed by a study of the gas hydrodynamic and the solid movement. In addition, the cyclone and the L-valve performances to control the solid circulation have to be checked ;
- In the second article it is assumed that the solids in the dense bed are completely mixed and biomass remained at the bed surface due to its lower density. Although these assumptions were refereed in the literature, it is recommended to study the solid behavior experimentally

using the radioactive particle tracking technique;

– After the cold study, the performance of the reactor has to be tested at high temperature. The objective is to have an autothermal gasifier in which cobalt oxide provides the required oxygen by circulating between the oxidizer and reducer. Operating the system continuously for hundred hours can validate the life time of the oxygen carrier.

REFERENCES

[1] International Enrgy Agency. *World Energy Outlook*, 2013.

[2] D.C. U.S. Department of Energy, Washington. *International Energy Outlook*. Energy Information Administration, 2011.

[3] B.M. Jenkins. Combustion Properties of Biomass. vol. 54 :pp. 17–46, 1998.

[4] P. Basu. *Biomass Gasification and Pyrolysis : Practical Design and Theory*. Elsevier Science, 2010.

[5] T. Werpy and G. Petersen. Top Value Added Chemicals From Biomass. *National Renewable Energy Laboratory*, vol. 1 :pp. 11–13, 2004.

[6] K. Waldron. *Bioalcohol Production : Biochemical Conversion of Lignocellulosic Biomass*. Woodhead Publishing Limited, 2010.

[7] A. Demirbas. Biorefineries : Current Activities and Future Developments. *Energy Conversion and Management*, vol. 50 :pp. 2782–2801, 2009.

[8] P. Basu. *Combustion and Gasification in Fluidized Beds*. Taylor and Francis, 2006.

[9] H. Boerrigter and R. Rauch. *Handbook of Biomass Gasification*. Biomass Technology Group (BTG), 2005.

[10] A. Drift, R. Ree, H. Boerrigter, and K. Hemmes. Bio-Syngas : Key Intermediate for Large Scale Production of Green Fuels and Chemicals. *Energy Research Centre of the Netherlands*, vol. 48, 2004.

[11] J. Rezaiyan and N. P. Cheremisinoff. *Gasification Technologies : A Primer for Engineers and Scientists*. Taylor and Francis, 2005.

[12] H. Hofbauer, G. Veronik abd T. Fleck, R. Rauch, H. Mackinger, and E. Fercher. The FICFB-Gasification Process. Banff, Canada, 1997.

[13] M. Mozaffarian and R. Zwart. Feasibility of SNG Production by Biomass Hydrogasification. In *12th European Conference and Technology Exhibition on Biomass for Energy, Industry and Climate Protection*, Amsterdam, The Netherlands, June 2002.

[14] M. Mozaffarian, E. P. Deurwaarder, and S. Kersten. Green Gas (SNG) Production by Supercritical Gasification of Biomass. 2004.

[15] R. A. Kalinenko, A. P. Kuznetsov, A. A. Levitsky, V. E. Messerle, Z. B. Mirokhin, L. S. Polak Sakipov, and A. B. Ustimenko. Pulverized Coal Plasma Gasification. *Plasma Chemistry and Plasma Processing*, vol. 13(no. 1) :pp. 141–167, 1993.

[16] A. N. Bratsev, V. E. Popov, A. F. Rutberg, and S. V. Shtengel. A Facility for Plasma Gasification of Waste of Various Types. *High Temperature*, vol. 44(no. 6) :pp. 823–828, 2006.

[17] A. C. Hoffmann and L. E. Stein. *Gas Cyclones and Swirl Tubes : Principles, Design, and Operation (Second Edition)*, volume vol. 6. Springer, 2008.

[18] P. J. Woolcock and R. C. Brown. A Review of Cleaning Technologies for Biomass-Derived Syngas. *Biomass and Bioenergy*, vol. 52 :pp. 54–84, 2013.

[19] C. Higman and M. Burgt. *Gasification*. Elsevier Science, 2008.

[20] D. A. Lloyd. *Gasification Precipitator Handbook*. Philadelphia, 1988.

[21] W. Torres, S. Pansare, and J. Goodwin JG. Hot Gas REmoval of Tars, Ammonia, and Hydrogen Sulfide from Biomass Gasification. *Catalysis Reviews : Science and Engineering*, vol. 49 (no. 4) :pp. 407–456, 2007.

[22] J. Seville. *Gas Cleaning in Demanding Applications (First Edition)*. Blackie Academic and Professional, 1997.

[23] J. Ciferno and J. Marano. *Benchmarking Biomass Gasification Technologies for Fuels, Chemicals and Hydrogen Production*. Energy USDo, 2002.

[24] A. V. Bridgwater. The Technical and Economic-Feasibility of Biomass Gasification for Power-Generation. *Fuel*, vol. 74(no. 5) :pp. 631–653, 1995.

[25] The ECN Tar Dew Point Site. Energy Research Centre of the Netherlands (ECN), 2009.

[26] J. Han and H. Kim. The Reduction and Control Technology of Tar During Biomass Gasification/Pyrolysis : an Overview. *Renewable and Sustainable Energy Reviews*, vol. 12(no. 2) : pp. 397–416, 2008.

[27] A. Tregrossi, A. Ciajolo, and R. Barbella. The Combustion of Benzene in Rich Premixed Flames at Atmospheric Pressure. *Combustion and Flame*, vol. 117(no. 3) :pp. 553–561, 1999.

[28] S. Phillips, A. Aden, J. Jechura, D. Dayton, and T. Eggeman. Thermochemical Ethanol Via Indirect Gasification and Mixed Alcohol Synthesis of Lignocellulosic Biomass. Technical report, 2007.

[29] A. Dutta and S. D. Phillips. Thermochemical Ethanol Va Direct Gasification and Mixed Alcohol Synthesis of Lignocellulosic Biomass. Technical report, 2009.

[30] A. Dutta, R. L. Bain, and M. J. Biddy. Techno-Economics of the Production of Mixed Alcohols from Lignocellulosic Biomass Via High-Temperature Gasification. *Environmental Progress and Sustainable Energy*, vol. 29(no. 2) :pp. 163–174, 2010.

[31] B. Dou, J. Gao, X. Sha, and S. W. Baek. Catalytic Cracking of Tar Component from High-Temperature Fuel Gas. *Applied Thermal Engineering*, vol. 23(no. 17) :pp. 2229–2239, 2003.

[32] D. Sutton, B. Kelleher, and J. R. H. Ross. Review of Literature on Catalysts for Biomass Gasification. *Fuel Processing Technology*, vol. 73(no. 3) :pp. 155–173, 2001.

[33] M. M. Yung, W. S. Jablonski, and K. A. Magrini-Bair. Review of Catalytic Conditioning of Biomass-Derived Syngas. *Energy and Fuels*, vol. 23(no. 4) :pp. 1874–1887, 2009.

[34] C. Xu, J. Donald, E. Byambajav, and Y. Ohtsuka. Recent Advances in Catalysts for Hot-Gas Removal of Tar and NH_3 from Biomass Gasification. *Fuel*, vol. 89(no. 8) :pp. 1784–1795, 2010.

[35] Z. Abu El-Rub, E. A. Bramer, and G. Brem. Review of Catalysts for Tar Elimination in Biomass Gasification Processes. *Industrial and Engineering Chemistry Research*, vol. 43 (no. 22) :pp. 6911–6919, 2004.

[36] J. P. A. Neeft, H. A. M. Knoef, and P. Onaji. *Behaviour of Tar in Biomass Gasification Systems : Tar Related Problems and Their Solutions*. Novem, 1999.

[37] D. Stevens. Hot Gas Conditioning : Recent Progress With Larger-Scale Biomass Systems. Technical report, 2001.

[38] T. E. Rufford, S. Smart, G. C. Y. Watson, B. F. Graham, J. Boxall, J. C. Diniz da Costa, and E. F. Maya. The Removal of CO_2 and N_2 from Natural Gas :A Review of Conventional and Emerging Process Technologies. *Journal of Petroleum Science and Engineering*, vol. 94-95 : pp. 123–154, 2012.

[39] J. L. V. Nichols, B. M. Friedman, A. L. Nold, S. McCutcheon, and A. Goethe. Processing Technologies for CO_2 Rich Gas. In *88th Annual Convention of the Gas Processors Association*, 2009.

[40] B. Burr and L. Lyddon. *A Comparison of Physical Solvents for Acid Gas Removal*. Bryan Research and Engineering, 2008.

[41] A. Kohl and R. Nielsen. *Gas Purification*. Gulf Publishing Company, 1997.

[42] J. Zhou, S. M. Masutani, D. M. Ishimura, S. Q. Turn, and C. M. Kinoshita. Release of Fuel-Bound Nitrogen in Biomass During High Temperature Pyrolysis and Gasification. In *32nd Intersociety Energy Conversion Engineering Conference*, 1997.

[43] W. F. Castle. Air Separation and Purification : Recent Developement and Prospects for the Beginning of the New Millennium. *International Journal of Refrigeration*, vol. 25 :pp. 158–172, 2002.

[44] D. R. Vinson. Air Separation Control Technology. *Computers and Chemical Engineering*, vol. 30 :pp. 1436–1446, 2006.

[45] C. C. K. Beh and P. A. Webley. The Dynamic Response and Characteristics of an Oxygen Vacuum Swing Adsorption Process to Step Perturbations. Part 1. Open Loop Responses. *Adsorption Science and Technology*, vol. 21(no. 4) :pp. 319–347, 2003b.

[46] L-S Fan. *Chemical Looping Systems for Fossil Energy Conversions*. John Wiley and Sons, Inc, Hoboken, New Jersey, 2010.

[47] L. F. de Diego, F. Garcia-Labiano, J. Adanez, P. Gayan, A. Abad, B. M. Corbella, and J. M. Palacios. Development of Cu-Based Oxygen Carriers for Chemical-Looping Combustion. *Fuel*, vol. 83(no. 13) :pp. 1749–1757, 2004.

[48] M. Johansson, T. Mattisson, and A. Lyngfelt. Investigation of Fe_2O_3 with $MgAl_2O_4$ for Chemical-Looping Combustion. *Industrial and Engineering Chemistry Research*, vol. 43 (no. 22) :pp. 6978–6987, 2004.

[49] I. E. Achouri, N. Abatzoglou, C. Fauteux-Lefebvre, and N. Braidy. Diesel Steam Reforming : Comparison of Two Nickel Aluminate Catalysts Prepared by Wet-Impregnation and Co-Precipitation. *Catalysis Today*, vol. 207 :pp. 13–20, 2013.

[50] W. K. L. Newton and E. R. Gilliland. Production of Pure Carbon Dioxide, 1949.

[51] S. Y. Chuang, J. S. Dennis, A. N. Hayhurst, and S. A. Scott. Development and Performance of Cu-Based Oxygen Carriers for Chemical Looping Combustion. *Combustion and Flame*, vol. 154(no. 1-2) :pp. 109–121, 2008.

[52] T. Mattisson, F. Garcia-Labiano, B. Kronberger, A. Lyngfelt, J. Adanez, and H. Hofbauer. Chemical Looping Combustion Using Syngas as Fuel. *International Journal of Greenhouse Gas Control*, vol. 1(no. 2) :pp. 158–169, 2007.

[53] Y. Cao, B. Casenas, and W. P. Pan. Investigation of Chemical Looping Combustion by Solid Fuels : 2. Redox Reaction Kinetics and Product Characterization with Coal, Biomass, and Solid Waste as Solid Fuels and CuO as an Oxygen Carrier. *Energy and Fuels*, vol. 20(no. 5) : pp. 1845–1854, 2006.

[54] H. T. Leion, Mattisson, and A. Lyngfelt. Solid Fuels in Chemical-Looping Combustion. *International Journal of Greenhouse Gas Control*, vol. 2(no. 2) :pp. 180–193, 2008.

[55] A. Rubel, K. L. Liu, J. Neathery, and D. Taulbee. Oxygen Carriers for Chemical Looping Combustion of Solid Fuels. *Fuel*, vol. 88(no. 5) :pp. 876–884, 2009.

[56] H. Zhao, L. Liu, B. Wang, D. X u, L. Jiang, and C. Zheng. Sol-Gel Derived $NiO/NiAl_2O_4$ Oxygen Carriers for Chemical-Looping Combustion by Coal Char. *Energy and Fuels*, vol. 22 (no. 2) :pp. 898–905, 2008.

[57] J. Adanez, A. Abad, F. Garcia-Labiano, and P. Gayanand L. F. de Diego. Progress in Chemical-Looping Combustion and Reforming Technologies. A Review. *Progress in Energy and Combustion Science*, vol. 38 :pp. 215–282, 2012.

[58] T. Mattisson, A. Lyngfelt, and H. Leion. Chemical-looping with oxygen uncoupling for combustion of solid fuels. *International Journal of Greenhouse Gas Control*, vol. 3 :pp. 11–19, 2009.

[59] I. Adanez-Rubio, P. Gayan, A. Abad, F. Garcia-Labiano, L. F. de Diego, and J. Adanez. CO_2 Capture in Coal Combustion by Chemical-Looping with Oxygen Uncoupling (CLOU) with a Cu-Based Oxygen-Carrier. In *Proceeding of the 5th International Conference on Clean Coal Technologies (CCT2011)*, Zaragoza, Spain, 2011.

[60] A. Lyngfelt and H. Thunman. *Construction and 100 h of Operational Experience of a 10-kW Chemical Looping Combustor*. Elsevier Science, 2005.

[61] L. F. de Diego, F. Garcia-Labiano, P. Gayan, J. Celaya, J. M. Palacios, and J. Adanez. Operation of a 10 kW_{th} Chemical-Looping Combustor During 200 H with a CuO-Al_2O_3 Oxygen Carrier. *Fuel*, vol. 86(no. 7-8) :pp. 1036–1045, 2007.

[62] P. Kolbitsch, J. Bolhar-Nordenkampf, T. Proll, and H. Hofbauer. Design of a Chemical Looping Combustor Using a Dual Circulating Fluidized Bed (DCFB)Reactor System. In *9th International Conference on Circulating Fluidized Beds*, 2008.

[63] T. Proll, K. Rupanovits, P. Kolbitsch, J. Bolhar-Nordenkampf, and H. Hofbauer. Cold Flow Model Study on a Dual Circulating Fluidized Bed (DCFB) System for Chemical Looping Processes. In *9th International Conference on Circulating Fluidized Beds*, 2008.

[64] H. J. Ryu, Y. Seo, and G.-T. Jin. Development of Chemical - Looping Combustion Technology : Long - Term Operation of a 50 kW_{th} Chemical- Looping Combustor with Ni-and Co-Based Oxygen Carrier Particles. In *Proceedings of the Regional Symposium on Chemical Engineering*, 2005.

[65] N. Berguerand and A. Lyngfelt. Design and Operation of a 10 kW_{th} Chemical-Looping Combustor for Solid Fuels-Testing with South African Coal. *Fuel*, vol. 87(no. 12) :pp. 2713–2726, 2008.

[66] N. Berquerand and A. Lyngfelt. The Use of Petroleum Coke as Fuel in a 10 kW_{th} Chemical-Looping Combustor. *International Journal of Greenhouse Gas Control*, vol. 2(no. 2) :pp. 169–179, 2008.

[67] L. Shen, J. Wu, Z. Gao, and J. Xiao. Reactivity Deterioration of NiO/Al_2O_3 Oxygen Carrier for Chemical Looping Combustion of Coal in a 10 kW_{th} Reactor. *Combustion and Flame*, vol. 156(no. 7) :pp. 1377–1385, 2009.

[68] L. Shen, J. Wu, and J. Xiao. Experiments on Chemical Looping Combustion of Coal with a NiO Based Oxygen Carrier. *Combustion and Flame*, vol. 156(no. 3) :pp. 721–728, 2009.

[69] L. Shen, J. W u, J. Xiao, Q. Song, and R. Xiao. Chemical-Looping Combustion of Biomass in a 10 kW_{th} Reactor with Iron Oxide as an Oxygen Carrier. *Energy and Fuels*, vol. 23 : pp. 2498–2505, 2009.

[70] F. X. Chiron and G. S. Patience. Kinetics of Mixed Coppereiron Based Oxygen Carriers for Hydrogen Production by Chemical Looping Water Splitting. *Hydrogen Energy*, vol. 37 : pp. 10526–10538, 2012.

[71] P. Chiesa, G. Lozza, A. Malandrino, M. Romano, and V. Piccolo. Three-Reactors Chemical Looping Process for Hydrogen Production. *International Journal of Hydrogen Energy*, vol. 33 :pp. 2233–2245, 2008.

[72] H. Hofbauer, H. Stoiber, and G. Veronik. Gasification of Organic Material in a Novel Fluidization Bed System. In *Proceeding of the 1st SCEJ Symposion on Fludization*, Tokyo, pages pp. 291–299, 1995.

[73] A. Zschetzsche, H. Hofbauer, and A. Schmidt. Biomass Gasification in an Internally Circulating Fluidized Bed. In *Proceeding of the 8th European Conference on Biomass for Agriculture and Industry*, volume vol. 3, pages pp. 1771–1777, 1994.

[74] S. T. Chaudhari, S. K. Bej, N.N. Bakhshi, and A. K. Dalai. Steam Gasification of Biomass-Derived Char for the Production of Carbon Monoxide-Rich Synthesis Gas. *Energy and Fuels*, vol. 15(no. 3) :pp. 736–742, 2001.

[75] R. J. Lancee, A. I. Dugulan, P. A. C. Thune, H.J. Veringa, J. W. Niemantsverdriet, and H. O. A. Fredriksson. Chemical looping capabilities of olivine, used as a catalyst in indirect biomass gasification. *Applied Catalysis B : Environmental*, vol. 145 :pp. 216–222, 2014.

[76] L. Fan, F. Li, and S. Ramkumar. Utilization of Chemical Looping Strategy in Coal Gasification Processes. *Particuology*, vol. 6 :pp. 131–142, 2008.

[77] M. Awrami. Kinetics of Phase Change. I. General Theory. *Jornal of Chemical Physics*, vol. 7 (no. 12) :pp. 1103–1112, 1939.

[78] M. Awrami. Kinetics of Phase Change. II. Transformation-Time Relations for Random Distribution of Nuclei. *Journal of Chemical Physics*, vol. 8(no. 2) :pp. 212–224, 1940.

[79] G.S. Patience and J. Chaouki. Scaling considerations for circulating fluidized bed risers. *Powder Technology*, vol. 72(No. 1) :pp. 31–37, 1992.